UNIVERSITY OF MICHIGAN
Department of Mechanical Engineering
Cavitation and Multiphase Flow Laboratory

Report No. UMICH 014456-7-I

BUBBLE DYNAMICS OF CAVITATION AND BOILING

by

F. G. Hammitt

Supported by ONR contract No. NOOO14-76-C-0697

January, 1977

Chap. IV - Bubble Dynamics of Cavitation and Boiling

A. Cavitation Bubble Growth and Collapse

1. General Background

Cavitation flow regimes are by definition multiphase flow regimes. Two phases are most importantly involved, i.e., a liquid and its own vapor. However, in almost all real cases, at least a trace quantity of non-condensable gas such as air, is also involved significantly in both bubble collapse and inception, but particularly inception. Thus cavitation is generally a 3-phase, 2-component flow.

The non-liquid portion in general can be either in the form of quasi-fixed cavities or "travelling" bubbles*. It is generally agreed today that it is the collapse of these latter to which cavitation erosion can be attributed. Semi-fixed cavities are usually found in cases of relatively low cavitation "sigma" **. Consider, eg, a cavitating hydrofoil, propellor blade, or similar component. For sufficiently high sigma, cavitation will not be present. However, for very much lower sigma for the same component, a large relatively fixed cavity will be formed. In the extreme case, the flow regime will become that of "super-cavitation", i.e., the cavity termination will be downstream of the cavitating body (hydrofoil, etc.). If sigma is then raised from the super-cavitating condition, the cavity length will be reduced so that its termination point will move upstream. Cavity attachment will then exist along the body. A further increase in sigma will cause the fixed cavity to disappear completely. However, after complete disappearance of the fixed cavity, there will still remain small cavitation "bubbles" in the region of minimum pressure. These generally will exist entrained in the flow, and hence are "travelling" cavities. It is the collapse of these which presumably produces cavitation damage.

---

*Nomenclature introduced by Knapp, et al (1).

**"Cavitation Sigma", $\sigma = (p_\infty - p_v)/\rho V^2$.

Even for those cavitation regimes dominated by a fixed, or semi-fixed cavity, it is generally true that "travelling" bubbles exist in the interface region between the cavity and the main liquid flow. One important cavitation damage flow regimes studied originally by Knapp (1,2, eg.) is that of the travelling bubbles penetrating the region of stagnation pressure sometimes found at the closing end of a semi-static cavity along a submerged body such as an ogive. This flow regime is shown schematically in Fig. 4-1, repeated for convenience from ref. 1. The collapse in the region of cavity termination of the travelling bubbles is presumed responsible for the cavitation damage observed in this region. Thus, in most cases, it appears that travelling bubbles, the dynamics of which are the main subject of this chapter, are responsible for the cavitation damage which often occurs with such flows.

Other possibilities for damaging mechanisms exist. For example, the partial collapse of large semi-fixed cavities, i.e., not travelling bubbles, can create large forces, even if insufficient local instantaneous pressures for "pitting" are created. These forces can cause damage to adjacent structures, possibly through damaging vibrations. However, this is not the typical cavitation pitting mechanism, which in general must involve bubble collapse. A flow regime, such as that shown in Fig. 4-1, can be responsible for such large and possibly damaging vibrational forces. High-speed motion pictures by Knapp (1,2) indicated that the cavity in the particular case studied (Fig. 4-1) was by no means steady-state. Rather, it exhibited a cycle of growth and partial collapse due to the action of a re-entry liquid jet, penetrating into the cavity periodically from the stagnation region at the downstream termination point. The time-period of this cavity collapse is much greater than that associated with the collapse of small individual travelling bubbles, so that the vibration frequencies thereby induced have a much greater period than that associated with the collapse of individual bubbles.

It is the growth and collapse of individual bubbles which is the primary subject of this chapter. This subject can be considered from many viewpoints, depending upon the degree of complexity desired in the mathematical models. The following sections will consider these various possible analytical approaches commencing with the most simple.

2. Ideal Treatment

a. General-Rayleigh and Besant

Historically the earliest analyses of bubble growth and collapse considered mathematical models idealized to the maximum extent possible. The earliest of these was that by Besant (3) and was published in 1859. However, this work considerably predated the appearance of bubble dynamics as an important engineering problem, and was merely a mathematical textbook treatment of an interesting and tractible mathematical problem. Hence it was not followed up until Lord Rayleigh's analysis (4) in 1917, which laid the foundation for much of the analytical work to follow up to the present day. Lord Rayleigh (J. W. Strutt), associated with the British Admiralty at that time, was concerned with the first important engineering manifestations of liquid "cavitation" (so named in that era). The engineering problem was associated with new and prematurely high-speed marine propellors used, essentially because of the earlier shift from reciprocating steam engine to steam turbine marine drives. Rayleigh quoted Besant's 1859 formulation (3) of the problem of the dynamics and kinematics of an empty spherical cavity in a constant density liquid with constant pressure at infinity: "An infinite mass of homogeous incompressible fluid acted upon by no forces is at rest, and a spherical portion of the fluid is suddenly annihilated; it is required to find the instantaneous alteration of pressure at any point of the mass, and the time in which the cavity will be filled up, the pressure at an infinite distance being supposed to remain constant."

Rayleigh then proceeded to solve the problem using an energy balance method whereas Besant had used a straight-forward application of the spherically symmetric equations of conservation of mass and momentum. However, Besant did not elaborate upon his solution and apply it to the cavitation case, as did Rayleigh. Full details of the Rayleigh analysis are given in Ref. 1 and are generally well-known to cavitation researchers. Hence they will not be repeated here, except in brief summary. However, it is important to note that in many ways Rayleigh "solved" a most significant portion of the overall cavitation bubble dynamics problems. However, various aspects, which at first glance might appear relatively minor, and which were definitely beyond the scope of his "ideal" approach, have assumed considerable later day importance, and have been the subject of numerous much more complex analyses continuing to the present time. Since it is not so well known, and since its more conventional approach, utilizing the conventional fluid momentum and mass conservation relations, forms the basis for many of the later more complete analyses, the Besant solution will be included in this chapter.

The foregoing discussion illustrates the meaning in this context of "ideal treatment". Both the Rayleigh and Besant solutions assumed "ideal fluid" conditions, i.e., incompressible, inviscid liquid, neither of which assumption is entirely valid. In addition, it was assumed at first that the cavity was empty or contained a fluid (presumably vapor) which remained at constant pressure (less than liquid pressure) throughout the bubble collapse. Such a "constant vapor pressure" assumption is fully equivalent to that of an empty cavity. Also surface tension was neglected. Rayleigh did (4) extend his solution to consider a perfect gas within the cavity, which could be assumed to be compressed during the collapse either isothermally or adiabatically. However, the coupled heat transfer problem, generated by the adiabatic compression

of such a gas, or by the necessary condensation of the vapor within, if the vapor pressure were to remain constant, was not considered.

In addition, to the "ideal fluid" assumptions discussed above, there are also important questions relating to the geometry of the problem, which were not considered in these "ideal treatments". The most important of these is the lack of spherical symmetry, if bubble collapse is to occur near a solid object and thus cause damage. Spherical symmetry is also destroyed in many real cavitation flow regimes by the existence of velocity and pressure gradients, and also the presence of other nearby bubbles. The consequences of these assumptions will be discussed in this chapter along with the research investigations leading to their evaluation. First, however, the Besant solution will be presented and the Rayleigh results summarized.

b. Besant Analysis

Historically, the earliest analysis of the growth or collapse of a vapor or gas bubble, or void, in a continuous liquid medium known to the authors is that of Besant[3]. This is included here in detail because of its simplicity and general applicability. The same result, but using a different approach, was also obtained by Lord Rayleigh [4] as discussed already.

Consider the case of an expanding or contracting spherical bubble in an inviscid fluid. The basic equations of motion and continuity can be written in polar coordinates, for spherical symmetry, as follows:

$$\frac{\partial u}{\partial t} + u \frac{\partial u}{\partial r} = -\frac{1}{\rho}\frac{\partial p}{\partial r} \qquad (4\text{-}1)$$

and:

$$\frac{\partial}{\partial r}(r^2 u) = 0 \qquad (4\text{-}2)^*$$

where: u is the radial component of the velocity
r is the radius measured from the center of the bubble
ρ is the liquid density
p is the pressure.

From (4-2): $r^2 u = \text{constant} = R^2 U = R^2 \dot{R}$

or: $$u = \frac{\dot{R} R^2}{r^2} \qquad (4\text{-}3)$$

where the capital letters refer to the same quantities as measured at the liquid-void interface, i.e., the bubble wall, and the dot indicates time derivatives. The last version of (4-3) is of course directly obvious from physical considerations for incompressible, spherically-symmetric flow.

*This form of the conservation of mass equation for spherical symmetry with an incompressible fluid is obvious if one considers that $4\pi\rho r^2 u$ is the mass flow rate for a source or sink.

By substitution of (4-3) into (4-1):

$$\frac{\partial}{\partial t}\left(\frac{\dot{R}R^2}{r^2}\right) + \frac{\dot{R}R^2}{r^2}\frac{\partial}{\partial r}\left(\frac{\dot{R}R^2}{r^2}\right) = -\frac{1}{\rho}\frac{\partial p}{\partial r}$$

or:

$$\frac{R^2\ddot{R}}{r^2} + \frac{2R\dot{R}^2}{r^2} - \frac{2\dot{R}^2R^4}{r^2} = -\frac{1}{\rho}\frac{\partial p}{\partial r}$$

Integrating between r = r and r = ∞ :

$$R^2\ddot{R}\int_r^\infty \frac{dr}{r^2} + 2R\dot{R}^2\int_r^\infty \frac{dr}{r^2} - 2\dot{R}^2R^4\int_r^\infty \frac{dr}{r} = -\frac{1}{\rho}\int_p^{p_\infty} dp$$

or:

$$\frac{R^2\ddot{R}}{r} + \frac{2R\dot{R}^2}{r} - \frac{\dot{R}^2R^4}{2r^4} = -\frac{1}{\rho}(p_\infty - p) \qquad (4\text{-}4)$$

At the bubble wall, r = R and p = P, so that (4-4) becomes:

$$R\ddot{R} + 2\dot{R}^2 - \frac{\dot{R}^2}{2} = -\frac{1}{\rho}(p_\infty - P)$$

or:

$$R\ddot{R} + \frac{3}{2}\dot{R}^2 = \frac{1}{\rho}(P - p_\infty) \qquad (4\text{-}5)$$

which is sometimes called the extended Rayleigh equation for the bubble wall motion.

c. Significant Results - Rayleigh Analysis (4,eg.)

The Rayleigh analysis, essentially solving the equations earlier formulated by Besant and discussed in the previous section, leads to various highly significant results from the viewpoint of cavitation damage. Essentially, the Rayleigh analysis makes plausible the idea that cavitation damage is primarily a result of fluid-mechanical, rather than corrosive effects. In most cases this is apparently true, though sometimes corrosion also makes a significant contribution. Due to its "ideal" nature, it is not able to show in detail the mechanisms by which mechanical cavitation pitting may occur. However, it does show the potential for the generation of very high fluid pressures and velocities by cavitation bubble collapse. In fact, according to the Rayleigh model, these would become infinite at the completion of bubble collapse, when the originally finite bubble has become a mathematical point. Infinite energy is then ascribed to zero mass, so that no violation of the energy conservation law is involved. The existence of pressures within the liquid during collapse much higher than the "stagnation pressure" for the process is possible, since the essence of the collapse problem is its non-steady nature. In a sense, such bubble collapse provides a very good mechanical amplifier, due primarily to the spherical geometry. The low intensity energy, originally spread throughout the liquid and related to p_{∞} , is concentrated by the collapse into a much smaller mass and exists then at much higher levels of intensity. While the Rayleigh model demonstrates the potential for very high, local, and transient pressures and velocities in the liquid as a result of bubble collapse, it does not provide a plausible mechanism for the transmission of the pressures and velocities to an eroded surface. It is the search for such mechanisms which has been the subject of much of the cavitation damage research since Rayleigh.

Figure 2 (reprinted from Ref. 1 for convenience) shows the essentials concerning the pressure distribution in the liquid during bubble collapse according to the Rayleigh analysis. While the pressure at large distances remains p_∞ during the collapse, and that at the bubble wall zero (if vapor pressure, internal gas, surface tension, and viscosity are neglected), there is an increasing rise in liquid pressure near the bubble wall as the collapse proceeds. The radial position of this pressure peak approaches 1.56 x (bubble wall radius), as the collapse proceeds toward completion. The amplitude of the pressure peak approaches infinity at this time, as does the wall velocity of the bubble. However, as will be shown in a later section, if the existence of either liquid compressibility or viscosity is assumed, these "infinities" vanish as would be expected.

The Rayleigh analysis also allows calculation of the time of collapse (1) in the form of a dimensionless time,

$$\tau = 0.91468 \; R_o \sqrt{\rho/p} \qquad \text{-------} \qquad (4\text{-}6)$$

Table 4-1 (reprinted from ref. 1 for convenience, and originally from calculations of ref. 5) shows precise values of the non-dimensional time as the collapse proceeds in terms of $\beta = R/R_o$. Figure 3 (reprinted from ref. 1 for convenience) shows the collapse curve of Rayleigh compared with photographic results of Knapp and Hollander (6). The slight disagreement as the collapse proceeds toward completion may be due to the lack of complete symmetry of the experimental bubble and/or to a small quantity of air entrapped within the bubble. The fact that the experimental bubble commences a "rebound" at the completion of collapse tends to confirm the probable existence of an important amount of air, from the viewpoint of bubble collapse, within the bubble.

However, Fig. 3 was not introduced here primarily to illustrate the approximate experimental confirmation of the Rayleigh collapse model, but rather to illustrate the form of radius vs. time curve there generated. For an appreciable part of the total collapse time the radius remains approximately constant, but then the collapse accelerates rapidly toward completion. Since the high velocities and pressures also occur only during this final portion of the collapse, its detailed study becomes extremely important in attaining an understanding of cavitation damage mechanisms. As noted from Fig. 3, the duration of complete collapse for a bubble of initial radius of 3.5 mm., in $\sim$ 1 atm. pressure field, is $\sim$ 0.7 millisec. However, the final portion of the collapse, important from the viewpoint of detailed damage mechanisms, requires only a few microseconds, in a typical case such as that shown in Fig. 3. Since the time duration is extremely short and the bubble very small during this final collapse period, it is extremely difficult to obtain precise experimental information for this portion of the bubble collapse process. For this reason primarily there is still room for doubt concerning detailed collapse mechanisms in various cases, so that substantial research efforts continue in the cavitation damage field.

d. Inclusion of Internal Gas and Surface Tension in Rayleigh Model

The basic Besant-Rayleigh differential equation for bubble collapse (Eq. 4-5) can be easily modified to include both surface tension and the effect of an internal gas in addition to vapor pressure:

$$\ddot{R} - \frac{3}{2}\dot{R}^2 = \frac{P_1 - P_\infty}{\rho} \qquad \text{----------} \qquad (4\text{-}7)$$

where:

$$P_1 = P_v - \frac{2\sigma}{R} + \frac{NT}{R^3} \qquad \text{----------} \qquad (4\text{-}8)$$

In the original Besant and Rayleigh formulations, it was assumed that a "void" in the liquid was suddenly annihilated. From this classical problem, the differential equation (4-7) results, but $P_1 = 0$ for this case, as previously shown. In all cases the pressure term making up the right-hand side of the equation is actually the pressure differential between the liquid pressure at a large distance, p_∞ , and that within the bubble, i.e., the liquid pressure at the bubble wall, P_1. In the classical Besant-Rayleigh problem, $P_1 = 0$.

It is obvious that this model can be easily generalized to include the effects of internal bubble pressure and surface tension. The simplest model, beyond the original formulation, is the assumption of a constant pressure within the bubble such as, eg., the vapor pressure, p_v. Then $P_1 = p_v$ in Eq. (4-7 and 4-8), and the solution of the differential equation is in no way complicated from the version in which $P_1 = 0$.

The next simplest version, which was in fact also considered by Rayleigh (4), is the assumption of an ideal gas within the bubble, which is compressed according to the ideal gas laws as the bubble collapses. Rayleigh solved this problem for the isothermal case, introducing the 3rd term in Eq. 4-8 , i.e., NT/R^3, to represent internal gas pressure. This formulation obviously follows Boyle's law for isothermal compression. For most cases of bubble collapse or growth, it is a reasonably good approximation for gas-filled bubbles. However, it does often lose its validity for the cavitation bubble collapse process near termination, where the bubble wall velocities are too great, and the time too short, for adequate heat transfer to occur. The final portion of the collapse is then often modelled more closely by the adiabatic assumption. In this case the final term in Eq. 4-8 would become: NT^{γ}/R^3, where γ is the ratio of specific heats of the gas.

The second term on the right-hand side of Eq. 4- 8 represents the effect of surface tension. For the static case, we have:

$$(P_l - p_i) = 2\sigma/R \qquad \text{---------} \quad (4\text{-}9)$$

where $2\sigma/R$ is the pressure differential between inside and outside of a static bubble, and p_i is the pressure within the bubble. It will be noted that this equation also applies for the stress in a thin-walled spherical pressure vessel, i.e., the stress and the surface tension play identical roles in these two different physical situations. Eq. (4- 9) is derived by a static force balance between pressure forces acting on the projected area of the spherical surface and surface tension, or stress, acting on the circumference.

It will be noted from Eq. (4- 7 and 4-8) that the term representing internal gas pressure and vapor pressure are simply additive. Both then act to restrain collapse, and to accelerate growth. The term representing surface tension, Eq. (4-A-X+1), is of the opposite sign to the terms representing gas and vapor pressure. Since these latter act to restrain collapse, the surface tension effect will be to accelerate collapse. However, it will restrain (or prevent, in many cases) growth. Thus surface tension always acts opposite to gas and/or vapor pressure effects. Note that all the terms in Eq. (4- 8) always must have the signs indicated externally, since all the parameters included in these terms are inherently positive.

It should be noted at this point that the original differential equations (4- 7 and 4-8) apply equally well to either collapse or growth, though bubble collapse was the problem for which it was originally generated. These equations have been used in fact to study growth and collapse for the case of a cavitation bubble subjected to an oscillating pressure field. Of course the use of an oscillating pressure in an incompressible liquid presents no special problem

at least in the formulation, rather than solution, stage, since simply $p_{\infty} = p_{\infty}(t)$. Of course, if internal gas pressure or surface tension are included, P is already P (t). The problem of an oscillating pressure at "infinity", presents no special problem for an incompressible liquid, since the speed of sound therein is infinite. The problems involved with the introduction of compressibility and viscosity will be considered later.

While Eq. (4-7 and 4-8)are equally applicable to either bubble collapse or growth, as explained in the foregoing, they are essentially applicable to "cavitation" rather than "heat transfer" bubbles. They apply to cases of either growth or collapse wherein the principle restraints against bubble wall motion are inertial, i.e., the conventional case of cavitation. If instead, conventional boiling is considered, the restraints against bubble growth are of thermal rather than inertial nature, i.e., bubble growth can accurately be considered as limited to the rate of evaporation of liquid to fill the growing bubble, and maintain an internal pressure equal to vapor pressure. The fact that this internal pressure is larger than the pressure at large distances is of course the mechanism by which the bubble will grow. However, the controlling differential equation is that of heat transfer rather than momentum conservation, as in the Besant-Rayleigh formulation. The inertial resistance to the growth of the "heat transfer" bubble is essentially negligible, so that it will grow as rapidly as the inward supply of heat for evaporation of the necessary vapor will permit. Thus the Besant-Rayleigh differential equation is pertinent to neither growth nor collapse for a "heat transfer" bubble. Formulations suitable for such heat transfer bubbles will be treated in a different section of this chapter.

Of course there are many cases of interest where both inertial and heat transfer effects are important. In the cavitation literature, such a combined case is termed one in which "thermodynamic effects" are important. These cases will be treated in the section under that title. Such a case is that of cavitation in

"hot" water vs. conventional cold water cavitation. Another case is that of cavitation in cryogenic liquids such as liquid hydrogen or oxygen, important from the viewpoint of liquid propellant rocket pumps.

A case of boiling in the intermediate range, where both inertial and thermal effects must be considered is "sub-cooled" boiling. In fact, highly-subcooled boiling and "thermodynamic-effect" cavitation are essentially identical from the viewpoint of bubble dynamics, if not from their method of generation.

3. Real Fluid Parameters

a. General

The "real fluid" effects in probable order of importance from the viewpoint of bubble collapse are: thermal effects, liquid compressibility, viscosity, and surface tension. From the viewpoint of bubble growth, the order might be: thermal effects, surface tension, and viscosity. For growth, compressibility is no longer an important parameter, since the bubble wall velocities, or more appropriately the liquid Mach numbers, are not sufficient to make liquid compressibility an important effect. On the other hand, in the fluid stages of collapse, if spherical symmetry were maintained and bubble gas content not large, velocities and Mach numbers would become quite large. In this case, the collapse velocities would be limited primarily by compressibility effects, or by viscosity, if very viscous liquids, such as e.g., lubricating oils were involved.

In collapse, surface tension is not of major importance if it is of the range of that for ordinary water. On the other hand, surface tension can be of controlling importance in bubble growth and nucleation, as indicated by the static balance relation between surface tension and pressure differential effects (Eq. 4-9), which controls commencement of growth, i.e., nucleation.

In collapse, in most typical cases of cavitation damage interest, when the radius becomes sufficiently small for the surface tension term to become important, wall velocities are very large and the inertial term dominates. Of course for the collapse of sufficiently small bubbles, surface tension would dominate, but such bubbles are too small to be of interest in the study of cavitation damage.

Thermal effects, i.e., "thermodynamic effects" according to the cavitation literature, can be of major importance in either growth or collapse in certain instances, and in other cases they are entirely negligible. They are essentially negligible for most cases of cavitation in cold water, which was the physical situation considered by Besant and Raleigh in their original formulations. On the other hand, for "hot water" the thermal effects can become predominent in both collapse and growth, i.e., they substantially affect both cavitation damage rate and the other effects of cavitation upon component performance. These questions will be discussed in much greater detail in a later section. At this point it is difficult to delineate more precisely the relative importance of "thermodynamic" effects compared to the other "real fluid" effects already discussed, since as yet there is no generally accepted parameter grouping by which the "thermodynamic effects" can be evaluated, and there is no generalized comprehensive mathematical study which can be utilized for this purpose. The thermal effects differ in kind from other pertinent real fluid parameters such as compressibility, viscosity, and surface tension, eg., in that these involve only single, easily describable, fluid properties, the variation of which have been studied in the cavitation literature. This has not been done for thermodynamic effects, since the parameter groups, the variation of which must be studied, is not as yet fully known.

b. Viscosity

In general, the effect of viscosity is clear in that it must at least to some extent reduce rates of growth or collapse compared to those attained in an inviscid liquid, for otherwise identical problem parameters. The effect of viscosity can be considered as a damping effect, and provides a degradation of mechanical energy to thermal energy. The rate of such energy degradation in a given case can be computed by integrating the "dissipation function" over the liquid region. Since viscosity varies over a very wide range, as compared to other liquid properties such as surface tension or density, between liquids of interest, or for the same liquid within the temperature range of interest, its effect in cavitation bubble dynamics can vary from negligible to very important in some instances. Table 4-2 reprinted for convenience from ref. 1, lists typical values of viscosity and other pertinent fluid properties for some liquids of interest over a range of pertinent temperatures.

The introduction of the viscosity effect into the analysis is surprisingly easy, in that it appears only as a "boundary condition" in the description of the liquid pressure at the bubble wall, Eq.(4-8) with an additional term, so that the original Besant-Rayleigh differential equation, Eq. (4-6) still applies, as first pointed out in 1952 by Poritsky (7).
This work resolved what might have been termed previously the "viscosity paradox". The basic Navier-Stokes momentum balance equation for an incompressible fluid under conditions of spherical symmetry can be so arranged that no term involving viscosity is present. It would thus appear at first glance that viscous effects do not influence the bubble dynamics problem, but the simple energy consideration of degradation of mechanical energy through viscous effects, indicates that this is not a tenable hypothesis. Poritsky pointed out in his analysis of the problem (7) that the viscous effects do alter the pressure at bubble wall, and thus act to reduce the effective pressure

differential in such a way as to reduce rates of either bubble growth or collapse. Thus though not realized earlier, the Besant-Rayleigh formulation is not limited to the inviscid case. These points are developed in more detail in the following.

The "viscosity paradox" mentioned above arises from the fact that viscosity can be eliminated from the equation of motion for an incompressible source or sink flow such as that describing spherically symmetric bubble collapse or growth. In its simplest and most conventional form this is Eq. (4-1). It is shown as Eq. (23) of Goldstein's classical book (8), and presented below for convenience in the form here pertinent.

$$\frac{\partial \vec{V}}{\partial t} - \vec{V} \times \vec{\omega} = - \text{grad}(p/\rho + \Omega + 1/2\vec{V}^2) - \nu \, \text{curl} \, \vec{\omega} \quad \text{----} \quad (4\text{-}10)$$

$\vec{\omega}$ is vorticity, i.e., curl $\vec{V}$, Ω is the body force potential, and ν is the kinematic viscosity. For source or sink flow of an incompressible fluid it can easily be shown that curl $\vec{V} = 0$. Therefore, the equation of motion for this case reduces to Eq. (4-11) even for a viscous fluid, if body force is neglected, which is certainly appropriate for most cases of bubble collapse or growth.

$$\frac{\partial \vec{V}}{\partial t} = - \text{grad}(p/\rho + \vec{V}^2/2) \quad \text{------} \quad (4\text{-}12)$$

Eq. (4-12) can of course easily be reduced to the form of Eq. (4-1). Hence the bubble dynamics "viscosity paradox", since it seems intuitively obvious that bubble growth or collapse rates must depend to some extent upon the viscosity of the liquid.

The "paradox" was resolved initially by Porisky (7), by noticing that the normal stresses in both liquid and gas (or vapor) at the bubble wall must be balanced rather than the pressures. The essentials of the analysis are given below. Refer to Fig. 4-4 for the appropriate force balance for a "pill-box" control volume cut from the bubble wall. The thickness of the control

volume, b, is arbitrarily thin so that shear forces acting upon its circumference can be neglected. However, its radius is finite, so that the normal stresses in the X-direction acting thereon must be balanced. For this simple one dimensional incompresible case, the pertinent relations between normal stresses and pressure are given below:

$$\sigma_x = -p + \mu(2\ \partial u/\partial x) \qquad \text{--------} \qquad (4\text{-}13)$$

where $-p = \bar{\sigma} = 1/3\ (\sigma_x + \sigma_y = \sigma_z)$

If the gas or vapor viscosity are neglected for simplicity, assuming that they are typically small compared to the liquid viscosity, then

$$p_g = -\sigma_x = P - \mu_L\ (2\ \partial u/\partial x) \qquad \text{-------} \qquad (4\text{-}14)$$

where P is pressure in liquid at bubble wall. Continuity (Eq. 4-2) gives:

$$\frac{\partial}{\partial r}\ (r^2 u) = 2\ ru + r^2\ \partial u/\partial r = 0, \text{ so that } \partial u/\partial r = \frac{\partial u}{\partial x} = -2u/r \quad \text{-- (4-15)}$$

Combining these relations:

$$P = p_g + 2\mu_L\ (-2u/r)_R, \quad \text{or}$$

$$P = p_g = 4\ \mu_L\ \dot{R}/R.$$

Since $\dot{R}$ is negative for a collapsing bubble, if we use the absolute value of $\dot{R}$, and also include the surface tension term*, we obtain:

$$P = p_g - 2\sigma/R + 4\ \mu_L[\dot{R}]/R \qquad \text{----------} \qquad (4\text{-}16)$$

where p_g is total pressure within the bubble, whether gas, vapor, or both. It is thus seen that for a collapsing bubble the effect of viscosity is opposite to that of surface tension as would be expected. Since surface tension increases collapse velocity, viscosity decreases it, as intuitively expected. For bubble growth, the sign of $\dot{R}$ is reversed so that both surface tension and viscosity restrain growth, as also would be intuitively expected.

---

*To be discussed in detail in a later section.

If the effect of the vapor or gas viscosity within the bubble is also considered, in an analogous manner, the resultant equation is as below:

$$P = p_g - 2\sigma/R + 4(\mu_L + \mu_g)\,\dot{R}/R \qquad \text{------} \qquad (4\text{-}17)$$

The energy dissipation due to viscous liquid effects in bubble growth or collapse can also be easily evaluated (7) through application of the "dissipation function" for the fluid. In this case:

$$P_{diss.} = \int_R^\infty \underline{\Phi} \cdot 4\pi r^2 \, dr = 48\pi\mu_L \int_R^\infty u^2 \, dr \qquad \text{-----} \qquad (4\text{-}18)$$

where $\underline{\Phi}$ is the dissipation function, and $P_{diss.}$ the power dissipated by viscosity. Substituting the continuity relation Eq. (4-2) into (4-18) and integrating, one obtains:

$$P_{diss.} = 16\,\mu_L \pi \dot{R}^2 R \qquad \text{------} \qquad (4\text{-}19)$$

From this it is obvious that the Rayleigh energy balance analysis (4) could not be applied correctly to a viscous fluid unless $P_{diss.}$ were included in the energy balance.

Numerical calculations by Ivany (9) show that, as predicted by Poritsky's pre-computer analysis (7), the effect of viscosity in bubble collapse is essentially negligible for fluids such as cold water, but reduces collapse velocity to virtually zero for fluids such as lubricating oils ($\sim$1470 x cold water viscosity) for a "standard bubble" collapsing under a pressure differential to infinity of 1 atm. (Fig. 4-5).

c. Compressibility, Viscosity, and Surface Tension Effects and Results

1) General

The effects of liquid compressibility are important, as for all fluid flow problems, only when the Mach number is appreciable. Since the sonic velocity in water is $\sim$1500 m/s, this is not likely to be the case except in relatively unusual circumstances. For example, it is certainly not in general a consideration in bubble growth problems, except perhaps in cases involving actual underwater explosions. The World War II investigations of underwater explosion problems (10,11,eg.), are perhaps the first instance when it was necessary to consider liquid compressibility effects. The Kirkwood-Bethe approximation there developed did in fact lead to the earliest relatively comprehensive and accurate consideration of liquid compressibility effects in cavitation bubble collapse, i.e., the study of Gilmore (12). This model has since been utilized in various computerized numerical studies of bubble collapse.

As is well known, the original ideal-fluid incompressible Rayleigh analysis leads to an infinite bubble wall collapse velocity as the radius approaches zero. However, the liquid Mach number remains zero, since sonic velocity is infinite in an incompressible fluid. If spherical symmetry were maintained, as assumed by Rayleigh (4), for the entire collapse, it is clear that liquid Mach number in a liquid such as water would also achieve very large (supersonic) values as the collapse proceeded toward zero radius. Thus it appears intuitively probable that liquid compressibility effects would become important for such a collapse, as it proceeded towards completion. More recent research shows that in most cases spherical symmetry is not maintained through a sufficient radius ratio for such large velocities to be obtained, and this feature is discussed in detail in a later section. However, to obtain a realistic evaluation of the collapse behavior for hypothesized spherical symmetry, it is necessary to investigate the effects of both liquid viscosity and compressibility. The viscosity effect was discussed in the previous section, and that of compressibility will be summarized here.

2) Analysis

The general Navier-Stokes equations of motion and the conservation of mass equation are of course the basic tools for the bubble collapse (or growth) analysis considering liquid compressibility. These were most suitably arranged for that purpose by Gilmore (12), and his approach, also used by Ivany (9,13), will be followed here. Related material is also presented in Cavitation (1). The pertinent version of the Navier-Stokes equation is:

$$\frac{D\vec{V}}{Dt} = -\ 1/\rho\ \text{grad}\ p + 4/3\ \mu/\rho\ [\text{grad}\ (\text{div}\ \vec{V})] \qquad \text{-----} \qquad (4\text{-}20)$$

If this is combined with the conservation of mass relation, the result is:

$$\frac{D\vec{V}}{Dt} = -\ 1/\rho\ \text{grad}\ p + 4/3\ \mu/\rho\ [\text{grad}\ (-1/\rho\ \frac{D\rho}{Dt})] \qquad \text{-----} \qquad (4\text{-}21)$$

At this point several assumptions were made by Gilmore and also by the others who followed the same procedure. First the viscous effect is assumed to be small as is the compressibility effect, so that their product, which is represented by the last term of Eq. (4-21) is assumed to be negligible. However, the compressibility effect is still included through the continuity relation (Eq. 4-22) in its most important aspect.

$$\frac{1}{\rho}\frac{D\rho}{Dt} + \text{div.}\ \vec{V} = 0 \qquad \text{----} \qquad (4\text{-}22)$$

The major effect of viscosity can still be included through the boundary condition at the bubble wall, as explained in the previous section, following the pioneering Poritsky analysis (7). This effect was not computed by Gilmore, or any of the subsequent investigators to my knowledge, with the expection of Ivany (9,13).

Another assumption made by Gilmore and followed by various later investigators was the assumption that the liquid was "barotropic", i.e.,

the density is a function only of pressure. Perhaps the most suitable liquid equation of state is that of Tait (14). This form, shown below, has been used by most investigators in this field.

$$\left[\frac{p + B}{p_r + B}\right] = \left[\frac{\rho}{\rho_r}\right]^n \qquad \text{---- (4-23)}$$

where p_r and ρ_r are any reference pressure and density. For cold water B = 3000 bar and n = 7.

The consequence for this analysis of the assumption of a "barotropic" liquid is that then:

$$1/\rho \ \text{grad}\ p = \text{grad}\ (p/\rho)$$

simplifying substantially the analysis. Gilmore now defines a new quantity h, which may be thought of simply as a form of enthalpy pertinent to the barotropic fluid assumed, i.e.,

$$h\ (p) = \int_{p_\infty}^{p} dp/\rho \qquad \text{----(4-24)}$$

Then:

$$\text{grad}\ p/\rho = \text{grad} \int_{p_\infty}^{p} dp/\rho = \text{grad}\ h \qquad \text{---- (4-25)}$$

Eq. (4-21) is now written neglecting the last term involving the cross-product of viscous and compressible effects as previously explained, and Eq. (4-25) substituted for the pressure term. Converting to spherical coordinates:

$$\frac{D\vec{V}}{Dt} \quad \frac{\partial h}{\partial r} = -\partial h/\partial r \qquad \text{---- (4-26)}$$

The compressibility effect is now introduced through substituting the sonic velocity, i.e.,

$$c^2 = dp/d\rho, \text{ and } dh/dp = 1/\rho$$

Then the equation of motion becomes:

$$\frac{D\rho}{Dt} = \frac{d\rho}{dh} \quad \frac{Dh}{Dt} = \frac{Dh}{Dt} \frac{d\rho}{dp} \frac{dp}{dh} = \frac{Dh}{Dt} \frac{\rho}{c2} \qquad \text{---- (4-27)}$$

and the continuity equation becomes:

$$-\frac{1}{c^2} \quad \frac{Dh}{Dt} = \text{div}\ \vec{V} \qquad \text{---- (4-28)}$$

There are now two partial differential equations (4-27) and (4-28), with three dependent variables, V,h, and C, and two independent variables, r and t.

By using the Tait equation of state (4-23), c and h can be reduced to one variable, leaving two equations with two dependent and two independent variables, which can be solved simultaneously.

Various solutions to these equations exist in the literature, prior to that of Ivany and Hammitt (9,13) here discussed. Flynn (15) presented an approximate analytical solution using a computed table of values of pressure and density rather than an explicit equation of state (such as Eq. 4-23). Mellen (16,17) computed the bubble wall velocity using Gilmore's method, and used this to compute the pressure in the liquid at a fixed distance far from the point of bubble collapse. He computed the propagation of the shock resulting from the complete collapse of an empty bubble to zero radius. He included the shock pressure as a function of distance from the center of collapse, with some experimental verification from spark-induced cavitation bubbles of 1-2 cm initial radius. Schneider (18) used the method of characteristics in a hand calculation to obtain a graphical solution of the compressible flow equations. Brand (19,20) made a similar calculation to that of Schneider, except that a computerized finite difference computation of the characteristics was made rather than a graphical solution. As did Schneider, he found the shock waves resulting from collapse upon a rigid sphere. Hickling and Plesset (21) present the most thorough solutions to the compressible equations for bubbles collapsing and rebounding upon contained gas, which is assumed to be compressed adiabatically. The computer solution was continued to the point where a shock wave formed from the rebound pressure wave. They did not use the Kirkwood-Bethe approximation (11) as

did Gilmore (12) and other subsequent investigations. Since the results agree closely with the other investigations, the validity of this approximation for the bubble collapse problem is thus verified. The key results of Hickling and Plesset (21) are presented in Figs. 4-A-6 -4-A-8, repeated from Cavitation (1) for convenience.

All of the above previous investigations did not include the effect of viscosity. However, it was included in the work of Ivany(9,13) here discussed, through the boundary condition at the bubble wall.

The resulting relation at the bubble wall is as below:

$$P(R) = P_i(R) - 2\sigma/R - 4\,\mu U/R - \frac{4\mu U}{3c^2}\,\frac{dH}{dR} \qquad \text{----} \quad (4\text{-}29)$$

where the capital letters signify values at the bubble wall, small letters having been used used for the same parameters within the liquid. P_i is the total vapor and gas pressure within the bubble. The effects of gas viscosity are assumed to be negligible compared to those in the liquid. According to Gilmore (12), the last term is of the same order of significance as the term involving the cross-product between compressibility and viscous effects earlier neglected. Hence this term also was neglected in the Ivany analysis (9,13).

3) Results

As already mentioned Figs. 4-A-6 through 4-A-8 present the key results of the Hickling-Plesset study (21), which is much more comprehensive in scope than the preceeding primarily pre-computer, studies mentioned in the foregoing. Hickling and Plesset show the effects of different quantities of entrapped permanent gas. Such gas inevitably causes a "rebound" since time for its solution in the liquid is not available. It thus prevents the collapse from going to completion. In almost all real cases with almost any fluid, the presence of some entrapped permanent gas seems inevitable, since the cavitation bubbles are generally supposed to nucleate originally from gas micro-bubbles. In addition, it is quite probable that vapor would

act as a permanent gas during the final phases of collapse, since time for its condensation and removal of the resultant latent heat would not be possible in the final phases of collapse. In typical cases time durations for this phase are $\sim$ 1 μs. Later numerical studies by Hickling (22) and Mitchell (23) as well as various others tend to confirm this conclusion, as does the experimentally observed "sono-luminescence", which is generally subscribed to very high temperatures (22, eg). This phenomenon will be described in greater detail elsewhere.

The Hickling-Plesset results (Figs. 4-A-6 - 4-A-8) also indicate the expected existence of bubble wall liquid Mach numbers between 10 and 100, if spherical symmetry could be maintained through radius ratios of the order 10^3-10^4. This certainly verifies the necessity for the consideration of compressibility effects. Significant resultant reductions in wall velocity from the Rayleigh case are shown in the figures. However, as previously indicated, this maintenance of symmetry appears to be most unlikely in real cases. This point will be discussed in full detail in the section concerning asymmetrical bubble collapse.

Figure 4-A-7 shows the envelope of maximum pressure within the liquid during rebound. This is generally considerably greater than the liquid pressure during collapse at distances from the center of collapse greater than the initial radius, R_o. Assuming as a first approximation that the bubble center remains stationary during collapse, R_o would be the closest possible distance to an adjacent material surface which might be damaged by the collapse. Of course a symmetrical collapse would be out of the question in such close proximity to a wall. However, it can easily be shown for ideal fluid considerations (10, eg.) that the bubble collapse center would approach a solid wall during collapse and conversely be repelled from a free surface. Since an analysis of this situation assuming maintenance of spherical symmetry would obviously not be physically meaningful, these questions will only be

discussed in detail in the section considering asymmetrical collapse phenomena.

As shown in Fig. 4-A-7, the maximum pressure at a distance of R_o from the collapse center is 500 bar for a typical case. The maximum pressure decreases approximately as r^{-1}. Obviously this pressure would not be sufficient to damage most structural materials of the sort, which are in fact known to be readily damagable by cavitation. Fig. 4-A-9 from Ivany's study (9,13) shows the maximum pressure envelope around the bubble at various distances during collapse. In this case, the maximum pressure at a distance R_o is only $\sim$ 10 bar, which of course also is not damaging to most materials. Hence, it would appear from these results that while the pressure wave upon rebound may be an important contributory factor in the damage mechanism, that upon collapse is not, and other contributing factors must also be involved, as, eg., the high-velocity microjet resulting from asymmetric bubble collapse and discussed in a later section, as well as the migration of the bubble center toward the wall.

Figure 4-A-5 , already mentioned concerning viscosity, from Ivany (9,13) summarizes his results concerning the effects of viscosity and compressibility. As in the Hickling-Plesset study, the existence of highly supersonic liquid bubble wall Mach numbers upon collapse, if spherical symmetry is maintained through large radius ratios, is verified. The effect of surface tension and viscosity are included in these calculations, as opposed to the Hickling-Plesset study. The effect of variation of surface tension was not included, but rather a surface tension value pertinent to cold water was used. It was found, however, that the surface tension effect was not important in any portion of the collapse, even though it approaches infinitey as collapse approaches completion, since the inertial term grows faster. Surface tension effects are of course important in nucleation, and are discussed in more detail elsewhere.

The effects of liquid compressibility in strongly reducing collapse velocities as compared to the ideal fluid Rayleigh analysis (1) for radius ratios below $\sim 10^{-2}$, also shown by the Hickling-Plesset analysis, are confirmed (Fig. 4-A-5).

The effects of viscosity are also shown in Fig. 4-A-6. The effects for viscosities similar to that of cold water become significant only for radius ratios of 10^{-3}-10^{-4}, and are more important for liquid Mach number than velocity. For a viscosity of $\sim$ 100 x that of cold water, the effect becomes significant for radius ratios in the range 10^{-2} - 10^{3}. For the critical viscosity predicted by Poritsky (7), i.e., 1468 x cold water viscosity, the collapse is brought to a virtual standstill. This is a viscosity about equivalent to that of a residual crude oil.

The effects of various quantities of entrapped gas, studied in the Hickling-Plesset analysis (21), were investigated also by Ivany (9,13) and shown in Fig. 4-A-3. The results are essentially in agreement with those of Hickling and Plesset.

In brief summary of the results from Hickling-Plesset (21) and Ivany-Hammitt (9,13), it can be stated that for cavitation bubble collapse.

1) The effects of surface tension are probably never of substantial significance in bubble collapse for any liquid of engineering importance.

2) The effects of viscosity can only be substantial for liquids with viscosities in the range of lubricating oils.

3) The effects of liquid compressibility for liquidswith bulk moduli of the range of water are important only if spherical symmetry is maintained through very large radius ratios which present knowledge indicates is not probable for engineering applications. The effects of liquid compressibility are thus probably negligible for such fluids as liquid metals (sodium, mercury, etc.). However, to my knowledge, no investigation has been made for highly

compressible liquids of engineering importance such as, eg., petroleum products and other organic liquids. It is conceivable that for such liquids the effects of both compressibility and viscosity would be substantial in some engineering applications.

d) Surface Tension, Gas Content and Miscellaneous

The effects of very small permanent gas content within the bubble upon bubble collapse are shown in Figs. 4-A-5 - 4-A-9 already discussed, and also in 4-A-10 from Ivany (9,13). As indicated in all these cases the collapse is stopped at a finite radius ratio by the compression of this internal gas, assumed adiabatically compressed in all these cases. The minimum radius ratio attained decreases as would be expected for greater initial gas contents. Initial internal gas pressures of 10^{-1} - 10^{-4} bar were investigated in these studies.

Internal gas contents of these general magnitudes were investigated, since it is believed that in most cases cavitation bubbles "nucleate" from either entrapped or entrained gas "micro-bubbles", the sizes of which depend primarily upon surface tension effects, as discussed in detail in the chapter on nucleation. While, as stated above, surface tension is not of substantial importance directly in bubble collapse, it is of importance through its influence on nucleation in affecting the entire aspect of the cavitation field, and hence the initial size from which the bubble collapses.

The quantitative relation, sometimes called the "Rayleigh equation", particularly in the heat transfer literature, through which surface tension enters the bubble equation of motion has been already included (Eq. 4-8, eg.). Since its derivation is very simple, and also pertinent in other fields such as the calculation of wall stresses in a thin-walled spherical pressure vessel, it is included below.

See Fig. 4-A-11, and consider a static force balance applied to the hypothetical "free body" of the upper half of a typical bubble between the differential between internal gas pressure, P_i and external liquid pressure, P_L attempting to pull the bubble apart, and the surface tension σ applied to the circumference attempting to hold the bubble together.

Then,

$$\pi R^2 (P_i - P_L) = 2 \pi R \sigma \qquad \text{-----} \qquad (4\text{-}30)$$

so that

$$P_i - P_L = 2\sigma/R \qquad \text{-----} \qquad (4\text{-}31)$$

Capital letters are used since the quantities apply at the bubble wall rather than within the fluid.

4. Effects of Bubble Asymmetries

a. General Background

The most important "real fluid" deviation, especially from the viewpoint of cavitation damage, from the classical Rayleigh analysi is undoubtedly that of bubble asymmetries, which predominate particularly during the collapse process. This situation is discussed relatively briefly in Cavitation (1), but more recent and important information will be added here. In general, it has been shown theoretically (24), that the collapse process of an initially spherical bubble is basically unstable, so that small perturbations may grow into major asymmetries, while the growth process is essentially stable. The physical mechanisms involved are somewhat similar to those of the classical Taylor instability, involving the acceleration of a lighter fluid away from the interface between lighter and heavier fluids. However,in the bubble case the instability occurs in the opposite sense because of the controlling effects of the spherical geometry. Photographic information in general confirms these theoretical expectations (24), in that growing bubbles in most cases remain essentially spherical, while collapsing bubbles do not, in most engineering situations.

The asymmetries of major importance from the viewpoint of cavitation damage is obviously the necessary proximity of the wall to be damaged. However, pressure gradients or relative velocity ("slip"), or the presence of a body force such as gravity, produce relatively similar results in the actual shape of bubble collapse profiles. These results are in general confirmed both by high speed photographs and numerical analyses, as will be reviewed in the following.

b. Analytical Approaches

The numerical analysis computer problem is complicated by the fact that the moving boundary, of indeterminate shape at a given instant, between liquid and vapor must be followed mathematically during the progress of the bubble collapse. Procedures for doing this in various other similarly complex problems have been developed under various pseudonyms such as MAC ("Marker and Cell" technique), PIC ("Particle in Cell"), etc. (25-29,eg.). The former is written for incompressible fluids, and was hence adopted here (39,40,48,eg.) for the bubble collapse problem. The latter (PIC) is for highly compressible fluids only, and hence not applicable for the liquid regime in bubble collapse. Since MAC allows the inclusion of viscosity, its effect was also investigated here by Mitchell (39,40,48) who included the effects of pressure gradient and relative velocity as well as wall proximity. These were investigated in separate problems. No combined effect analysis has yet been reported. Spherical coordinates were used, since they were assumed to be least likely to lead to numerical instabilities.

During approximately the same time period as the Mitchell analysis here, the problem was also investigated at California Institute of Technology (CIT) by Chapman and Plesset (30,31, eg.). They used an entirely different numerical technique based upon potential flow assumptions, and hence were unable to include the effects of viscosity. These at least for water, are probably not of major importance. Since they only considered the wall proximity problem, of primary importance from the viewpoint of cavitation damage, they used cylindrical coordinates. This allowed them to

follow the progress of the microjet further than was possible in our own case with spherical coordinates, since in that case the numerical procedure must be terminated as the microjet approaches the initial bubble center. The results of these numerical studies, the only ones so far reported to my knowledge, are discussed later.

The general mechanism of collapse and microjet formation in a direction determined by the initial asymmetries is easily explicable from relatively simple arguments, involving the conservation of linear momentum (32). Assuming an initial linear momentum in some direction of the bubble virtual mass, i.e., including a portion of the surrounding liquid, this momentum must be conserved during collapse, since no external forces other than viscous are applied to the bubble during this period. Hence, as the collapse proceeds, and the bubble virtual mass decreases, its linear velocity must increase proportionately. As the bubble size approaches zero, this velocity would approach infinity. The initial linear momentum is a direct result of the initial asymmetry such as, eg., relative velocity, pressure gradient, gravity or other asymmetrical body force, wall proximity, etc. A simplified analysis considering this effect was also reported by Chincholle (33,34,eg.). Termed the "rocket effect", his investigation did not consider the actual bubble shape changes during collapse, but showed the trajectory of bubble centroid.

The wall effect, i.e., the "attraction" of a bubble toward a rigid wall, and also its repulsion from a free surface, was predicted by studies of underwater explosions during World War II (10), based on potential flow analyses and using the concept of "mirror images." Later work shows that a sufficiently flexible boundary (35) is similar to a free surface in this respect, thus partially explaining

the experimental observation of the remarkable cavitation damage resistence of soft rubbers, and other elastomeric materials, in some applications.

In very simple and naive terms, the wall attraction and free surface repulsion can be explained as follows. Consider a spherical bubble near a rigid wall, and starting to collapse. If the collapse were to be spherical, the radial liquid velocity in the inward direction would need to be uniform at all points of the bubble periphery. However, liquid "access" to the region between bubble and wall would be relatively restricted compared to that on the side away from the wall. Thus the radial wall collapsing velocity on the wall side would be less than that elsewhere, so that a motion of the bubble centroid toward the wall would be generated. Thus a linear motion of the bubble centroid in this direction would be created. Its necessary conservation (neglecting viscous effects) would lead to an acceleration of the bubble virtual mass toward the wall as the collapse continued, resulting in the formation of the eventual high-velocity microjet to which an important portion of cavitation damage is usually attributed.

In the case of a highly resilient wall or free surface, the above argument would apply in an inverse sense. Acceleration of the liquid on the side of the bubble away from such an interface is essentially restrained by the inertia of the liquid column extending theoretically from the bubble wall to infinity in that direction. Similar inward acceleration of the bubble wall near a free surface would involve only the inertia of the restricted liquid column between bubble wall and free surface, plus the inertia of the adjoining air

column, also, as a first approximation, considered to infinity, i.e., to a "long distance". Hence the inertial restraint for bubble collapse on the side toward the free surface would be much less than that on the opposite side, assuming that the bubble was in reasonable proximity to the free surface. Thus acceleration on the free surface side of the bubble would be greater, so that the bubble centroid would move away from the free surface. As the collapse proceeded, this acceleration of the bubble centroid would increase. Microjet formation would then occur away from the surface, rather than toward it as in the case of a rigid boundary. Precisely, the same arguments can be made for a highly resilient interface, (such as , e.g., a thin rubber diaphragm (36,37, eg.). Figures 12 and 13 show this effect for a study here involving spark-generated bubbles. Similar results were obtained in a more comprehensive study of this effect at Cambridge University (35). A sufficiently resilient surface would then be expected to repel collapsing bubbles, which is consistent with the already observed good cavitation damage resistance of various elastomeric materials (37,38,eg.).

During bubble growth the opposite effects occur for entirely analogous reasons, ie., a growing bubble is repelled from a solid surface, and attracted toward a highly resilient or free surface.

c. Specific Cases

1) Wall Proximity - Simplified Analyses

a) Double-Bubble and Other Cases

As previously indicated, wall proximity is the most important asymmetry from the viewpoint of cavitation damage. Also as previously discussed the problem of bubble centroid motion was

initially approximately solved (10) without considering the details of asymmetric bubble collapse profiles. This type of solution also has been applied much more recently (33,34,eg.). Since the original solution (10, eg.) relied upon a method of mirror images, considering a hypothetical "mirror image" bubble behind the wall. The wall was then considered a plane of symmetry for a double-bubble problem. This model is essentially exact, if the effects of viscosity are neglected, and hence it seems reasonable to investigate the double-bubble problem as being of interest in itself as well as shedding light on the single-bubble wall proximity problem. This has been done (36, 37,eg.) photographically here (Figs.12 and 13), and the results are in fact very similar to the wall problem with microjet formation along the axis connecting the bubbles, and in the direction toward the system centroid.

2) Comprehensive Wall Proximity Numerical Analyses

a) Chapman-Plesset (30,31,eg.)

The most complete numerical investigation of the wall-proximity bubble collapse problem, in terms of following the collapse to completion, is that of Chapman and Plesset (30,31). Their results, showing the initial substantial collapse of the sides normal to the wall, followed by the accelerating collapse of the side away from the wall, and the development of the expected microjet are shown in Figs. 14 and 15.

b) Mitchell-Hammitt (39,40, eg.)

Somewhat similar but less complete results in terms of the microjet development were obtained by Mitchell and Hammitt (27-29)

as previously mentioned. Figure 16 illustrates the computer output bubble collapse profiles from this study. Careful comparisons show that they are entirely similar to those of Chapman-Plesset, even though viscosity and wall roughness were included in that study. It is thus indicated that these effects are only of secondary importance in this particular bubble collapse problem, presumably because the bubble wall velocities attained in a typical case with water for such a collapse are not sufficiently large. The microjet velocity may be considerably larger ($\sim$100 - $\sim$1000 m/s is indicated)*, but this factor does not influence the collapse behavior otherwise.

Wall roughness was necessarily included in the Mitchell-Hammitt study because of the form of the spherical-coordinate computing cells. This was not involved in the Chapman-Plesset case because of their use of cylindrical coordinates. The wall roughness used here was approximately that of a cast-steel wall for a $\sim$2mm bubble initial diameter, so that the roughness result is of practical significance.

c) Kling, Timm, and Hammitt (37,41,42,eg.)

The Chapman-Plesset and Mitchell-Hammitt computer results were confirmed during about the same time period by the high-speed cinematographic results of Kling and Hammitt (41,42,eg.), obtained in a venturi with spark-generated bubbles in water using framing rates $\sim 10^6$ Hz. Camera speeds of this order are necessary, since the final important portion of the bubble collapse in pertinent cases occurs in only a few microseconds. Figure 17 (reprinted for convenienc from Cavitation (1)) and Ref.(43) show bubble collapse in a venturi pressure gradient, indicating bubble flattening normal to the

*Plesset, Chapman (39,40) estimate 130 and 170 m/s for two typical cases with water.

pressure gradient. Figure 18 (reprinted from Cavitation (1) for convenience) shows schematically the various forms of bubble collapse expected, including the effect of pressure gradient (Fig. 17) and wall proximity. Figure 19 is a sequence of high-speed motion pictures (41,42) showing the collapse of a spark-generated bubble in a two-dimensional venturi near a thin flat plate which is aligned parallel to the flow along the venturi axis. The complete expected sequence of events is observed: first, flattening of sides normal to wall, then of side parallel to and distant from the wall, followed by microjet generation and its impingement upon the wall.

The final event is that of bubble "rebound", i.e., re-growth of the vapor and gaseous mass. Such rebounds are typical of bubble collapses in flowing water systems, perhaps being due primarily to entrained gas and non-condensing vapor in the short time available. These features are discussed in detail in the section concerning "thermodynamic effects". Rebound is important in the damage process, since the strength of pressure pulses in the liquid due to a growing bubble are considerably greater than those due to collapse, as already discussed concerning spherical bubble dynamics.

Figs. 20,21 show detailed experimental bubble collapse profiles from the Kling-Hammitt study taken from photographic enlargements of the individual frames of high-speed motion pictures (Fig. 19). These show all the details of intermediate bubble shapes predicted numerically (30,31,27-29),eg.) and discussed previously. From these photos, for an initial $\sim$ 4 mm diameter bubble, the eventual microjet diameter is $\sim$80 μm, and was estimated to have an impact velocity of $\sim$100 m/s. However, later work by Brunton (44) and his

colleagues at Cambridge University estimated velocities up to 1000 m/s were possible. An intermediate jet velocity was predicted by the Chapman-Plesset study (30,31), as previously stated.

The Kling-Hammitt study also allowed a one-to-one correspondence to be obtained between bubble collapses and craters in the soft aluminum wall. In normal cavitation (45,46, eg.) this ratio appears to range up to 10^6, so that the 1:1 correspondence here results only from nearly complete control of the bubble parameters achieved using spark-generated bubbles. Figure 22 shows details of a crater in soft aluminum so created, indicating that it is somewhat larger than the microjet diameter, as would be expected from consideration of liquid jet impact characteristics discussed in a later chapter.

The high speed bubble-collapse photos obtained by Kling (41,42, e.g.), and any others yet available to my knowledge, provide information from one viewing direction only, so that the three-dimensional form of the collapse profiles can only be assumed from considerations of symmetry. To investigate further the three-dimensional form of bubble collapse, Timm (36,37, e.g.) here obtained high-speed motion pictures of spark-generated venturi bubble collapse using the same flow geometry as that of Kling, for two perpendicular viewing directions simultaneously, i.e., side pictures were combined with top pictures of venturi bubble collapse adjacent to a wall (Fig. 23). These simultaneous pictures (Fig. 23) were obtained using the same high-speed camera employed by Kling, but using a mirror system to obtain pictures from perpendicular directions together on each frame. In general, the side-view bubble pictures (lower pictures in each frame) are quite similar to those of Kling (Fig. 19),

showing again the attraction of the bubble mass toward the wall, eventual impinging microjet, followed by "rebound" of the vapor-gas mass. The top view pictures are interesting in showing a rapid breakdown of the circular profile, but no pronounced systematic asymmetry, even though there is a significant axial pressure profile (toward right in pictures). The top view pictures indicate only slight rebound (regrowth). In the final picture, the bubble has virtually disappeared from both views. The total sequence, including initial collapse, rebound, and final disappearance requires only about 0.5 ms (500 μs).

3) Pressure or Velocity Gradient, Body Force, and Relative Velocity

a) General

The effects of pressure or velocity gradients, asymmetrical body force, and relative velocity between bubble centroid and external liquid are very similar to those of wall proximity, or a second identical bubble, already discussed. In all cases, an eventual microjet results, with intermediate profiles relatively similar to the wall-proximity case.

There is little precise experimental information on these effects, though Fig. 17 shows the effect of a venturi diffuser pressure gradient, causing bubble flattening in the plane normal to the pressure gradient, i.e., venturi axis, with presumably eventual microjet formation in the upstream direction. In this particular case, it is likely that relative velocity between liquid and bubble ("slip") is also involved. Presumably this slip would be negative in a rising pressure region such as the venturi diffuser,

so that both pressure gradient and slip would cause microjet to be in the upstream direction. This venturi case in particular was analyzed here using a linear small-perturbation technique (47). The possibility of microjet generation in either direction, depending upon the direction and strength of relative velocity and pressure gradient, was shown. The only comprehensive numerical analyses of the pressure gradient and relative velocity cases, even separately considered, to our knowledge is that of Mitchell and Hammitt (27-29,e.g.). No comprehensive analysis of the asymmetrical body force problem, such as gravity primarily, but also possibly imposed magnetic or electrostatic fields, which may be of interest for various fusion reactor concepts using liquid metal coolants. As a first approximation, however, it would seem that the problem of a bubble rising due to gravity in an otherwise static liquid would involve both a relative velocity and a pressure gradient, so that microjet formation in the upward direction would result. Some crude experiments have been mentioned involving the final "jumping" of the collapsing bubble above the free surface in a simple beaker test.

b) Mitchell Analyses (27-29,48,e.g.)

The Mitchell-Hammitt study of the wall proximity case has already been discussed (Fig. 16). In his dissertation (48), Mitchell also included the effects of different pressure gradients and relative liquid velocity (slip) in separate problems. The qualitative results have already been discussed. Figure 24 shows typical computer results for a typical pressure gradient about that pr duced by gravity with water , and Fig. 25 shows the effects of an imposed relative velocity. Unfortunately the computer outputs do not proceed far enough to show final microjet development

because of the necessary termination of the calculation as the microjet approaches the original origin of coordinates, as previously explained.

Figure 26 compares the effects of these various asymmetries upon bubble profiles during collapse, including the effects of two different pressure gradients, the stronger of which is about that of gravity with water. The effects of the relative velocity and the pressure gradients are qualitatively quite similar, but that of wall proximity causes initial bubble flattening in the opposite sense, i.e., the bubble initially flattens in planes normal to the wall (Fig. 16). Figure 26 shows the effects upon bubble centroid migration of these same asymmetries. Again they are similar, and in this case in the same direction. For relative velocity the eventual microjet is in the direction of the initial bubble velocity relative to the liquid (thus preserving initial linear momentum), and for the pressure gradients it is in the direction of decreasing pressure, essentially for the same reason.

Figure 27 compares the calculated jet velocities, i.e., maximum wall velocity, for two pressure gradients, with the bubble wall velocity from the classical Rayleigh spherical analysis (4) for the same radius ratios, R/R_o. The asymmetrical maximum wall velocities exceed those for the spherical Rayleigh collapse model for relatively high radius ratios ($R/R_o \leqq 0.35$), i.e., near start of collapse for these asymmetrical cases. However, for smaller radius ratios, i.e., near the end of collapse, the Rayleigh velocity exceeds the asymmetric jet velocities, i.e., maximum wall velocity. Although these results are available only for the pressure gradient

asymmetric collapse case, it is believed that qualitatively similar results would be found for the other cases. Even though the jet velocities are less than the Rayleigh wall velocities near end of collapse, they are still sufficient to provide possibly a major component of the damaging mechanism, as previously discussed.

4) Compliant Boundary Effects: (Gibson and Lauterborn Studies (49-5

The effects of compliant boundaries in the vicinity of a collapsing bubble can be provided either by other neighboring bubbles, which are certainly very often present in many real cases, or compliant boundaries such as free or resilient surfaces. These effects in general are probably the most important asymmetrical effects to which little comprehensive analysis has yet been applied. Presumably this is due to the extreme complexities involved, making straight-forward computer analyses highly expensive. Nevertheless, some pertinent information is available. The simplest cases have already been discussed (Fig. 12 and 13, and ref. 10 e.g.), but other pertinent information will be reviewed in the following.

The most comprehensive study to date of the compliant boundary problem known to the author is that of Gibson and Brunton (49 and 50) at Cambridge University. Both theoretical and photographic studies were made of spark-generated bubbles, collapsing near a soft rubber wall. The theoretical profiles were derived from a perturbation model, and hence may not be as accurate as the numerical studies of either Mitchell or Chapman discussed earlier. Bubble repulsion from the wall during its collapse was observed as expected and also as confirmed by the Timm photos (Figs. 12 and 13) obtained here and previously discussed. Very recent work (50-a.) also confirms this bubble behavior.

Gibson also confirmed in great detail the bubble collapse profiles in a pressure gradient, again using spark-generated bubbles in a static beaker. Figure 28 shows these results.

Some very recent and excellent results concerning single bubble behavior using laser-generated bubbles and high-speed cinematography have also been reported (51-52, eg.) by Lauterborn and colleagues at the University of Göttingen. The use of a concentrated laser beam for single-bubble generation for research purposes represents some improvement over the spark-bubble technique, in that the liquid field is not perturbed by the presence of the electrodes, and also there is no introduction of non-condensible electrolytic gases. Of course the high-power pulse laser equipment is also much more expensive than that required for spark-bubble generation.

As already indicated, multiple bubbles may provide the most general source of compliant boundary effects in most cavitation (or boiling) situations. However, due to the complexity of the problem, very little comprehensive research on this problem has yet been attempted. Also as previously indicated, the problem of the collapse of two identical bubbles in close proximity (Figs. 12 and 13) is essentially that of collapse of a single bubble near a rigid wall, and hence has already been solved to a major extent. Results similar to those of Timm (Fig. 12 and 13) have also been reported more recently by Lauterborn (51,52).

Comprehensive numerical analyses to consider multiple bubble effects, other than that of two identical bubbles in close proximity, have not yet been reported to the author's knowledge. This multiple bubble problem appears to be nearly beyond the state of the art, within reasonable costs limits, for present-day large computers. Of course, any asymmetrical collapse analysis so far has neglected most real fluid effects, except for viscosity (27,28,48),

which is relatively easy to include. These were included in spherically-symmetric collapse studies, such as those of Hickling-Plesset (21,22) and Ivany-Hammitt (9 and 13). The neglect of compressibility, which proved to be relatively most important in the spherical collapse analyses for low viscosity liquids such as water (9,13,21,22,eg.), in the asymmetrical analyses so far reported, is perhaps reasonably permissible, because liquid Mach numbers do not become significant (as opposed to spherical analyses) by the time the collapse is terminated by the microjet impact upon either the opposite bubble wall or adjacent material surfaces.

The effects of the growth or collapse of nearby bubbles during the collapse of a given bubble could be either primarily somewhat similar to the double-bubble case already discussed (Figs. 12 and 13) involving a mutual attraction between the collapsing "voids" (which are essentially "sink" flows), or alternatively the triggering of asymmetrical collapse in a given bubble by shock waves generated by the collapse or growth of adjacent bubbles. Bubble microjet formation could sometimes be triggered in this way, much like the formation of a "Monroe jet" in a shaped-charge explosive used in mining or such as the World War II "Bazooka" anti-tank weapon. This possibility was suggested and studied quantitatively by Kozirev in the USSR (53). This concept represents admittedly an over-simplfiied model, but nevertheless it may be physically quite instructive in explaining the otherwise rather mysterious microjet collapse behavior.

5) Rebound Phenomena

Bubble "rebound", or regrowth, is, as indicated by high-speed cinematography, quite common in cavitating flow regimes. It is the present general conception, in this author's opinion, that the liquid "shock waves" emanating from bubble rebound are one of the major mechanisms involved in mechanical cavitation damage, along with microjet impact, as already discussed. This conception is confirmed in numerical analyses (9,13,21,22, eg.) showing that the shock wave strength on rebound is much greater than that occurring during Rayleigh collapse (4), and appears in fact to be of sufficient magnitude to contribute importantly to the observed damage. Nevertheless, no comprehensive numerical analyses of asymmetrical bubble collapse have yet been carried (30,31) beyond the point of microjet impact. This appears then to be a "next logical step" which is probably not beyond the capability of present computer techniques.

Bubble rebound is presumably primarily due to the compression of non-condensable gases within the bubble. Since cavitation bubbles presumably nucleate in most cases from entrained gas micro-bubbles, the presence of some gas within the collapsing bubble is inevitable. However, in some cases the internal pressure, which eventually causes rebound, may be augmented by vapor compression near the end of collapse. This effect is further discussed in the section on "thermodynamic effects". In the case of asymmetric collapse, a toroidal vortex is typically formed, along the axis of which the high-velocity microjet passes. The fluid centrifugal

forces associated with the toroidal vortex, i.e., essentially a "smoke-ring", also provide a mechanism for rebound in addition to that from internal gas or vapor. This is not the case for a spherical collapse.

6) General Summarization of Asymmetrical Bubble Collapse Studies

Several general observations concerning the effects of various asymmetrical conditions, and consistent with the previous discussions, seem useful.

i) Bubble collapse in most engineering situations does not follow even approximately the spherical collapse model first proposed by Rayleigh (4). Rather the "microjet mode" of collapse seems relatively universal, whether the dominent asymmetry is that of wall or free surface proximity, relative velocity, pressure gradient, body force, or the presence of neighboring bubbles.

ii) On both theoretical and experimental grounds, bubble growth is much more symmetrical than is collapse, so that the assumption of spherical symmetry provides a reasonable model in that case.

iii) The direction of the eventual microjet is always in the direction of the original linear momentum caused by the asymmetry itself. In the case of wall or surface proximity, or neighboring bubbles, this initial force unbalance must be due to differences in forces upon the neighboring bodies as compared to that with the liquid in the directions where no intermediate bodies exist.

iv) Since linear momentum for the bubble virtual mass is preserved during collapse, the associated linear velocity increases as the bubble virtual mass decreases with collapse of the bubble volume. This results in the eventual high microjet velocity

existing within a very small fluid mass.

v) Rigid surfaces "attract" the bubble centroid during bubble collapse, i.e., cause migration of bubble virtual mass toward the surface, resulting sometimes in the eventual impingement of the liquid microjet thereon. Free surfaces, or sufficiently resilient solid surfaces, result in bubble virtual mass repulsion from the surface during collapse, and eventual microjet formation in the direction away from the wall. This bubble centroid motion away from a resilient surface may be partially responsible for the good cavitation resistance of some rubber and other elastomeric materials. Effects during bubble growth are essentially the inverse of those during collapse in this respect.

vi) One or several bubble mass "rebounds" are common in flow systems. The resultant shock waves in the liquid constitute an important damage mechanism probably ranking in importance with microjet impact.

vii) The collapse of two symmetrical bubbles in close proximity to each other is essentially the same problem as that of a single bubble near a rigid wall. Similarly the growth of two identical bubbles in close proximity is essentially the same problem as that of growth of a single bubble near a free surface.

viii) The multiple-bubble collapse (or growth) problems have not been solved in detail, even for "ideal-flow" assumptions.

5. Thermodynamic Effects for Bubble Collapse

a. General

The so-called cavitation "thermodynamic effect" (1, e.g.), can be extremely important in both cavitation performance and damage. It is commonly understood to encompass all those features by which bubble growth or collapse are affected by factors other than those encountered in ordinary flow problems governed by the Navier-Stokes equations of motion and the mass conservation relations, but neglecting conservation of energy considerations such as heat transport or transfer, and condensation or evaporation. Thus the "thermodynamic effect" could better be called a "thermodynamic, heat transfer effect". The original Rayleigh model (4) and subsequent improvements thereto, neglecting also these "thermodynamic effects", did not consider the restraints upon bubble collapse or growth imposed by changes in internal pressure due to heat transfer restraints. This neglect is relatively quite appropriate for liquids such as cold water, where the vapor density, and hence vapor mass within the bubble, is very small. For "hot water" or other similar liquids such as petroleum products, e.g., this rapidly ceases to be the case as temperature is raised, since vapor pressure, or density, is an exponential functi of temperature. If vapor density within the bubble is sufficient, the flow regime becomes simliar to that of sub-cooled boiling where, to a first approximation, the restraints upon bubble growth or collapse are those of heat transfer and transport of the latent heat component released or absorbed by condensation or evaporation. Thus there are many important cases lying between classical cavitation and boiling in this respect. This situation was first recognized for cavitation by Stepanoff (54, e.g.), and

many recent publications upon the problem have been provided by Bonnin (57-58, e.g.). These and later specific analyses will be discussed in the following.

b. Stepanoff and Other Approximate Analyses (54-58, eg.)

It had been generally observed industrially (54-56, eg.) that the classical scaling factors for pump cavitation, eg., such as suction specific speed, S or the Thoma parameter, σ_T based primarily upon NPSH modelling did not successfully model cavitation performance of turbomachines between liquids differing in the "thermodynamic" parameters, i.e., the design for hot water pumps could be considerably more aggressive from the viewpoint of satisfactory cavitation performance than that for cold water pumps, considering only the conventional modelling parameters such as S, σ_T, etc. The same was found to be the case for pumps handling petroleum products, cryogenic liquids, etc. These trends appeared to apply for cavitation damage as well as performance. This general industrial observation was first formalized in the open literature to my knowledge by Stahl and Stepanoff (54), in 1956. They formulated a "thermodynamic parameter", B, defined as:

$$B = V_v/V_L = v_v \Delta h_f/v_L h_{fg} \qquad \text{---} \qquad (4\text{-}32)^*$$

This parameter represents essentially the ratio of vapor volume formed under steady-state equilibrium conditions in a closed system analysis to the liquid volume from which it was formed for a given small decrease of suppression pressure. It is thus a fluid "property" which can be computed and tabulated for various liquids at various

*B = thermodynamic factor = B-Factor, V = fluid total volume,
v = fluid specific volume
Δh_f = increment of liquid enthalpy corresponding to a reduction of NPSH below saturation conditions.
h_{fg} = heat of vaporization of liquid.

saturation temperatures, and represents in a sense the cavitatability of the liquid. This tabulation was in fact made by Stahl and Stepanoff (54), and correlated with empirical data, hopefully to allow quantitative prediction of the attainable improvement in machinery cavitation design parameters for different liquids, as compared to cold water, due to their differences in B-factor. The details of these analyses (1, 54-56) are given elsewhere, so that it is not useful that they be repeated in greater detail here. However, much later experience and tests have shown that good quantitative predictions are not possible on the basis of this apparently over-simplified model. This may be primarily due to its assumption of equilibrium thermodynamics for determining the relative cavity size, and its effect upon machine performance.

Many relatively comprehensive, and sophisticated complex analyses have since been made to hopefully provide the framework for the desired quantitative predicting ability of "thermodynamic effects", both for damage and performance. These will be discussed in the following. In many cases, these investigators have developed modified B-factors designed to take into consideration various factors not considered in the original Stepanoff approach. One such approach is that of Bonnin (57,58,eg.), to be discussed next.

c. Bonnin (57-59,eg.)

Bonnin in France has attempted (57-59,eg.) to improve the predicting capability for machinery cavitation thermodynamic effects which, as already indicated, is not good in terms of the Stepanoff B-factor alone, or various proposed modifications thereto, by introducing a second B-factor to be used together with the Stepanoff factor to

better correlate existing experimental data than would be otherwise possible. He presumes, on the basis of dimensional analysis, that a single B-factor cannot be adequate, and thus he proposes two new parameters, B' and B". On the basis of these two independent B-factors, he maps the total regime of cavitating flows, dividing this into regions where inertial effects only are predominent as in the Rayleigh model (4), regions where only heat transfer restraints are important as in conventional boiling analyses, and regions where both inertial and heat transfer effects must be considered, i.e., highly sub-cooled boiling or cavitation where "thermodynamic effects" must be considered. Some improvement in correlating ability is certainly achieved by the addition of a second correlating parameter, but it is not clear at this time whether the two B-factors utilized in the Bonnin analyses are in fact those most appropriate.

d) Individual Bubble Collapse Analyses

Several basic analyses based upon individual bubble collapse dynamics, but investigating primarily those cases where thermodynamic as well as inertial restraints are involved, have contributed considerably to the understanding of and ability to utilize effectively "thermodynamic parameters" in the design of machinery subject to cavitation restraints. Some of the more significant of these will be reviewed in the following.

1) Florscheutz, Wittke and Chao (60,61, eg.)

Florscheutz and Chao (60,61) were one of the first to analyse theoretically the collapse of cavitation bubbles in cases where both inertial and thermodynamic restraints were important. They derived a new B-factor, B_{eff} which allowed delineation on a

theoretical basis of those flow regimes where thermodynamic effects could be neglected from those where they could not. This parameter contained time-dependent effects to reflect heat transfer rates of latent heat of condensation away from the bubble, as well as the steady-state thermodynamic equilibrium considerations which alone were reflected by the original Stepanoff parameter (54-56, eg.). Correlation of bubble collapse regimes in terms of this revised parameter with high-speed photographic observations of individual bubble collapse were made, so that a more precise basis for the correlation of thermodynamic effects in bubble collapse was provided.

2) Hickling and Plesset(21,22, 62-65, eg.)

The "thermodynamic effect" from a primarily macroscopic viewpoint was discussed in the foregoing. However, various microscopi studies of indiviudal bubble dynamics have contributed significantly to the understanding of the related phenomena. The work of Florscheut and Chao (60) was in that category. However, that of Hickling and Plesset (21,22, 62-65, eg.) discussed next, provides considerably more detail on individual collapse behavior in cases where gas or vapor effects within the bubble are important, i.e., cases where the "thermodynamic effect" is significant.

Hickling and Plesset in the referenced papers investigated the actual heat transfer rates occurring between bubble contents and surrounding liquid. In addition, they calculated the temperature profile within a collapsing bubble, confirming the existence of very high internal temperatures upon bubble collapse, sufficient to explain the existence of "luminescence", observed experimentally and discussed also elsewhere. Since this phenomenon has generally been observed in acoustically-induced cavitation, it has been called "sonoluminescer

in the cavitation literature (62,63,66,67, eg.). Various explanations for this phenomenon have been advanced in the past, including ionization effects, chemical reactions, and others. However, it now seems most probable that the luminescence is primarily the result of the very high temperatures induced by bubble collapse, particularly upon various impurities within the bubbles. Of course, this mechanism would require collapse through a relatively large volume ratio, which may not occur in most cases of flowing cavitation. This is consistent with the fact that the luminescence is much more intense in "ultrasonic cavitation" as opposed to cavitation in flowing systems, although it has been reported (67, eg.) in both cases.

The existence of high gas and vapor temperatures within collapsing bubbles might be thought to contribute in some way to cavitation damage and some observations (68, eg.) of damaged surfaces appear to indicate the previous existence there of high temperatures. For example, cavitation "bluing" of steels, similar in appearance to oxide-bluing at high temperature has been observed in this laboratory and elsewhere. However, it is probably due to oxide deposition due to effects other than bubble collapse. However, consideration of the presumed bubble collapse mechanisms, already discussed, indicates the lack of a plausible mechanism for sufficiently rapid heat transfer between the bubble contents and the wall, the lack of sufficient heat capacity of the gas and vapor within the bubble, and the difficulty of obtaining a sufficiently high material surface temperature to be damaging, considering the high thermal conductivity of the metals involved. Hence, in the opinion of the writer the existence of such localized high temperature damage effects is unlikely.

Of course, the high temperature and corresponding high pressure of the bubble contents is in fact instrumental in the reduction of bubble collapse wall velocities, generally associated with "thermodynamic effects", and thus cases an important reduction in damage in some cases.

3) Mitchell-Hammitt Investigations (48,69,eg.)

Numerical results relatively similar to those of Hickling and Plesset for the collapse of a spherical bubble of initial radius, R_o containing both non-condensable (and non-diffusing) gas and saturated vapor were obtained here (48,67,eg.). Gas diffusion effects were neglected in this study, as in that of Hickling, since there is insufficient time during such a collapse for diffusion effects to become important. Nonetheless this is an important consideration in ultrasonic cavitation through the mechanism of rectified diffusion (68). The problem to be considered, along with presumed temperature profiles within the bubble and in the liquid is shown schematically in Fig. 29.

Figure 30 shows the resultant temperature profiles for a typical case compared with those of Hickling (62). Approximate agreement between the two studies is noted. Maximum ratio of absolute temperatures computed is ~ 9, indicating a maximum temperature within the bubble at conclusion of collapse of $\sim 4200°F$ ($\sim 2400°C$) for bubble collapse in room temperature water. Thus the probability of luminescence due to high temperatures in such an event is confirmed.

The Mitchell-Hammitt study included the effect of "evaporation coefficient", α to evaluate the non-equilibrium temperature differenti at bubble wall due to possible impurities on the wall, etc. This factor was not included in the Hickling-Plesset work, but was studied

in considerable detail by Theofanous, etal (70,71), and Borhhorst, etal (72,73). Three values of the evaporation coefficient were investigated in the Mitchell analysis, ranging from 0.01 to the maximum possible theoretical value corresponding to zero thermal resistence at the bubble wall, i.e., α = 1.0. The theoretical analysis of Theofanous (69,70) indicates the most probable value for α lies between 0.05 and 0.1. The latter value was used in the calculations for Fig. 30. Figure 31 shows the effect of the condensation coefficient α upon the portion of original vapor mass remaining within the bubble at completion of collapse for α ranging from 0.01 to 1.0, indicating that for very low α the portion of vapor remaining is $\sim$ 60%, whereas it is virtually zero for α = 1.0. Thus for low α the vapor contributes significantly to the non-condensable gas compression effect in restraining bubble collapse and producing an early rebound, but for ideal condensation coefficient the vapor effect in this respect is negligible.

Figure 32 shows the effect of the full range of α upon bubble radius ratio (referred to R_o) as a function of time (referred to the classical Rayleigh collapse time (4), i.e., collapse velocity is the slope of this curve. In these terms, the assumed values of condensation coefficient have little effect until the radius ratio for ratios less than 0.9, i.e., this parameter would probably have only negligible effect for asymmetric bubble collapse, discussed before, since both photographic evidence and numerical analyses show that in most cases in flowing systems only relatively

moderate collapse ratios will be attained before the formation of the microjet.

Figure 33 shows the effect of condensation coefficient upon internal gas-vapor temperature, and Fig. 34 internal pressure. The effect of α upon internal pressure (Fig. 34) is substantial throughout collapse, but that upon temperature only near its completion (Fig. 33). Both effects are very substantial for radius ratios below $\sim$ 0.2.

Figure 35 shows the effect upon internal pressure of the assumption of constant liquid temperature outside the bubble as opposed to variable liquid temperature. This effect is relatively small though certainly not negligible.

Figure 36 shows the effect of initial bubble radius upon internal gas-vapor temperature indicating that maximum internal temperature is increased by a factor of $\sim$ x2 for the larger initial bubble radius, i.e., 50 mils vs. 5 mils (1.27 vs. 0.127 mm). For smaller initial bubble radii, the collapse process is expected to be more nearly isothermal, rather than adiabatic, since the ratio of surface area to volume becomes larger for smaller size, so that outward heat transfer to maintain constant internal temperature is enhanced. Thus the maximum internal temperature attained is less for the smaller initial radius bubble. However, the internal gas pressure is very little influenced by initial radius as shown in Fig. 37. The corresponding calculations (48, eg.) show that the polytropic exponent γ for the mixture of water vapor and air takes values between $\sim$ 1.10 and 1.20 during the earlier stages of collapse for the smaller bubble, but when R/R_o reaches 0.05, γ is $\sim$ 1.30.

Thus these collapses are essentially isothermal at first, but approach adiabatic near conclusion. However, the larger bubble approaches the adiabatic condition more quickly so that the gas-vapor temperatures therein are higher.

The effects of internal gas conductivity and liquid over-pressure, i.e., "sub-cooling" from the viewpoint of boiling analyses, were also investigated. The effect of gas conductivity was essentially as expected, i.e., higher gas conductivities decrease internal gas-vapor temperature. This effect was also investigated by Hickling (62,63) with approximately similar results. This effect is taken to explain the reduced sonoluminescence (62,63) for gases with higher thermal conductivity.

The effect of over-pressure upon internal gas-vapor pressure is shown in Fig. 38. It is shown that the proportional gas-vapor pressure within the bubble is less for increased over-pressure. Thus for these conditions, spherical collapse would proceed through a greater radius ratio before rebound commences, so that presumably damage would be increased. This is of course consistent with experimental observations in this respect.

4) Garcia, Bhatt, and Hammitt (75-79, eg.)

"Thermodynamic" effects with respect to cavitation damage are most easily demonstrated with a vibratory damage facility (discussed further in the chapter on Cavitation Damage). The specimen to be damaged is vibrated at high frequency but low amplitude, while submerged in the test liquid, so that the test is essentially "static" in that liquid velocities are small and unimportant, while accelerations are controlling. For this type of test it has been known for some

time, and probably first reported by Plesset (74,eg.), that there was presumably for any liquid a maximum damage rate temperature, lying (very roughly) midway between melting point and boiling point for the test static pressure. For any given type of system there is also presumably a maximum damage suppression pressure, ie, there is no damage for boiling or for too high a suppression pressure, which would suppress cavitation completely. This situation is discussed in more detail in the section on engineering effects.

Figure 39 illustrates the effects upon damage rate in our vibratory facility with water for changes in suppression pressure ($NPSH \cdot \rho$) and temperature (77). While the reason for the decrease in damage rate for decreasing temperature below the maximum damage temperature is not clear, that for temperature increase above the maximum damage temperature is presumably the "thermodynamic effect". In essence, it is due to the increase in gas-vapor pressure within the bubble at collapse temination due to increase in vapor pressure and density, as well as temperature of the bubble contents, due to inability of heat transfer mechanisms to maintain isothermal conditions, as discussed in detail in the previous section. This internal pressure increase terminates collapse sooner than would otherwise be the case, resulting in reduced collapse velocities and radiated shock waves, thus reducing cavitation damage rate.

A series of tests in this laboratory using a vibratory facility were conducted originally by Garcia (75,76, eg.), using water and also various liquid metals as test liquids. The Florscheutz-Chao parameter, $B_{eff.}$ (60,61), previously discussed,

was used to correlate the damage results. Our method of use of this parameter differed somewhat from the original intention of Florscheutz and Chao (60) in that it was necessary to use the static suppression pressure for simplicity rather than the oscillating pressure of the vibratory facility, since this was not accurately known. Also it was necessary to assume an initial bubble size (also actually unknown) and assume that it was the same for all tests. Nonethless, the initial liquid metal results (bismuth, lithium, sodium, and mercury) all correlated well against B_{eff} as so computed (Fig. 40), showing a large region where thermodynamic effects were not important ($B_{eff} \leq 10^3$), and a region for lower values of B_{eff} where damage depended strongly on the thermodynamic effect. The relatively lower temperature liquid metal results were in the region of non-dependence upon thermodynamic effects, as was also molten bismuth at all temperatures, because of its very low vapor pressure. Unfortunately the water data did not fall upon the same curve (Fig. 42), since thermodynamic dependence commenced for values of $B_{eff} \leq 10^{-1}$ (rather than 10^3 as for the liquid metals).

Later more comprehensive vibratory facility tests in sodium were conducted here (79, eg.) and elsewhere, and are also included in Fig. 40. Unfortunately, these also do not fall upon the original Garcia curve. From this disagreement of the later sodium data, as well as that of the water data, it must be concluded that B_{eff} as here used is not in itself a sufficient correlating parameter. This is no doubt partly due to the fact that test facility parameters (specimen size, frequency, and amplitude) differ to some extent between the data sets, making our previously mentioned assumption of a constant NPSH$\cdot\rho$, and fixed initial bubble size

for all cases, particularly incorrect. These results tend to confirm Bonnin's previously discussed hypothesis (57-59, eg.) that it is in fact impossible to correlate thermodynamic effects of this kind in terms of a single correlating parameter such as B_{eff}, and that two independent parameters are actually required.

5) Fixed Cavity Theories

a) General

The original published conception of the "thermodynamic effect" by Stahl and Stepanoff (54-56, eg.) assumed the formation of a relatively fixed cavity in the inlet region of a cavitating pump, eg., which influenced the flow pattern in such a manner as to reduce head, or other measurable parameter, by a prescribed amount, then defined as the "cavitation inception" condition. It was assumed that the same geometrical cavity would have been formed with other liquids, when the same head (or other parameter) decrease occurred. However, quantitatively different changes in inlet NPSH would be required to produce this result according to the B-factor for the liquid. Thus the concept of a relatively steady cavity in the sensitive region, responsible for the general cavitation effect upon the machine performance, is accepted as being valid at least in many cases (1,eg). Damage in such flow regimes is presumed due to the collapse of "travelling bubbles" which skirt the cavity region and are impelled into the wall region by the re-entry jet at the trailing edge of the cavity, the position of which often is found to oscillate at relatively high frequency (1,80).

Since the above described cavity model is reasonably valid and general, and also sufficiently simple for more detailed and

meaningful analysis, it has in fact been utilized by several groups for this purpose. A specially designed venturi geometry with very sharp inlet geometry, and hence well localized cavitation (Fig. 42), has been used by groups at NASA-Lewis Laboratory (81-83, eg.) with water and Freon-114 and at Bureau of Standards (BuStd), Boulder (84-86, eg.) under contract to NASA, and using the same cavitating venturi geometry,but with cryogenic liquids nitrogen and hydrogen. Hydrogen is one of the liquids for which thermodynamic effects appear to be most important.

Somewhat related investigations during the same general time period were carried out by Holl and colleagues (87-89, eg.) at Pennsylvania State University, using test bodies (ogives, etc.) submerged in a small tunnel with both water and freon as test liquids. Both groups proposed theoretical models to allow computation of the cavity pressure under various conditions, which is necessary for the à priori prediction of the thermodynamic effect in given machines. These studies will be reviewed in the following sections.

b) NASA Studies (81-83, eg.)

The NASA studies involved water and Freon-114, while those at BuStd used liquid nitrogen and hydrogen, all in the same venturi geometry (Fig. 42). Thus a full range of cavitation thermodynamic effect parameters was investigated. The tests did not include damage effects, but rather performance effects including inception. The results of work under this program, performed primarily during the 1960's, is summarized by Ruggeri (83). A method for predicting thermodynamic effects, i.e., changes in cavity pressure depressions relative to stream vapor pressure, is presented. The prediction

method accounts for changes in liquid, liquid temperature, flow velocity, and body scale, based upon theoretical and experimental studies. The method appeared (83) to provide good agreement between predicted and experimental results for geometrically-similar venturis over the range of test liquids. Use of the method requires geometrical similarity of the body and cavitated region, a known reference cavity-pressure depression at some operating condition. The method can be applied to rotating machines such as pumps and inducers (82) as well as to stationary devices such as venturis (83, eg.).

Figure 43 shows typical vapor head depression (feet) as a function of vapor-to-liquid volume ratio in the cavitating region for different liquid temperatures for (a) water, liquid nitrogen, and Freon-114, and (b) liquid hydrogen. These results cannot be included on the same curve because of the much larger Δh_v values obtained with hydrogen for the same volume ratios.

Figure 44 shows cavity head depressions for Freon-114 as a function of distance from position of minimum pressure for various velocities and liquid temperatures, showing the effect of cavity size on head depression, whereas Fig. 45 shows the effects of venturi size again for Freon-114. These curves at least indicate the strong complexity of the situation, caused partly by the probable non-steady nature of the cavity, the important effects of turbulence, and the significant mass transfer between the cavity and main liquid stream. This complexity is further indicated by the proposed modelling Eq.(4- below showing the parameters which must be scaled to allow use of this predicting method. This relation shows the ratio between vapor and liquid volume.

$$\left(\frac{\mathcal{V}_v}{\mathcal{V}_l}\right)_{pred} = \left(\frac{\mathcal{V}_v}{\mathcal{V}_l}\right)_{ref} \left(\frac{\alpha_{ref}}{\alpha}\right)^m \left(\frac{V_0}{V_{0,ref}}\right)^n \left(\frac{D}{D_{ref}}\right)^{1-n} \left[\frac{\left(\frac{\Delta x}{D}\right)_{ref}}{\frac{\Delta x}{D}}\right]^p \text{---} \qquad (4\text{-}33)$$

$\mathcal{V}_v$ is volume of saturated liquid and

$\mathcal{V}_v$ volume of saturated vapor,

α is thermal diffusivity, V_0 is free stream velocity, D is diameter, and Δx is the axial length of the cavitated region. The exponents m, n, and p depend, at least in part, on the heat transfer process involved and must be determined by experiment. The derivation and use of Eq. (4-33) requires that (1) geometric similarity of cavitating flow is maintained for various liquids and flow conditions and (2) thermodynamic equilibrium conditions exist within the cavitated region. At present, these two requirements can only be assumed for untested liquids.

c) BuStd Studies

The BuStd work by Hord and colleagues (84-88,eg.) were at first intended to provide check-points in cryogenic liquids for the tests at NASA (81-83, eg.) in water and Freon-114, all in geometrically similar venturi flowpaths. The flow paths investigated, in addition to the NASA venturi, included a hydrofoil and three geometrically similar ogives. Thus cross-correlation of the developed cavity data for five different hydrodynamic bodies was possible to achieve eventual best-fit correlations. Test fluids were liquid hydrogen and nitrogen. A new theoretical model was developed and applied to data from these five stationary models, as well as the venturi and cavitating pump and axial inducer data from NASA. The techniques for predicting cavitation performance of pumping machinery are extended to include variations in flow coefficient, cavitation parameter (such as suction specific speed, or inlet cavitation number, K_c, eg.), and equipment geometry. Hopefully these new predictive formulations can be used as a pump design tool and for the eventual development of a universal method for correlating pumping machinery performance. Application of these predictive formulas requires prescribed cavitation test data, or an independent as yet unavailable method for estimating the cavitation performance of each pump. If such a method were available, such as a proven detailed numerical flow model for the relatively complex rotating geometries involved, it would then be possible to predict detailed cavitation performance of new machinery designs without testing. Unfortunately present state of the art does not as yet include this capability.

The proposed correlations are based upon the improved calculation of B-factors, assuming isentropic vaporization of the liquid. Convection heat transfer and two-phase mass flux were included in the analysis. The relevance to pumps and other rotating machinery of analysis and experimentation with stationary bodies was strengthened, i.e., the correlative expressions deviced for stationary bodies appear extendable to rotating equipment.

Equations (4-34) and 4-35) illustrate the proposed correlating parameters.

$$\frac{B}{B_{ref}} = \left(\frac{\alpha_{ref}}{\alpha}\right)^{E1}\left(\frac{V_o}{V_{o,ref}}\right)^{E2}\left(\frac{\ell}{\ell_{ref}}\right)^{E3}\left(\frac{\nu_{ref}}{\nu}\right)^{E4}\left(\frac{\sigma_{ref}}{\sigma}\right)^{E5}\left(\frac{D}{D_{ref}}\right)^{E6} \text{---- (4-34}$$

$$\frac{B}{B_{ref}} = \left(\frac{\alpha_{ref}}{\alpha}\right)^{E1}\left(\frac{MTWO}{MTWO_{ref}}\right)^{E2}\left(\frac{\ell}{\ell_{ref}}\right)^{E3}\left(\frac{\nu_{ref}}{\nu}\right)^{E4}\left(\frac{\sigma_{ref}}{\sigma}\right)^{E5}\left(\frac{D}{D_{ref}}\right)^{E6} \text{--- (4-35}$$

Equation (4-34) is an improved and extended version of the simplified expression of Gelder (81), discussed in the foregoing (Eq. 4-33). Equation (4-35) was derived as a part of the Hord, etal studies. The nomenclature is essentially the same as that of Eq. (4-33), previously explained, except for the new term MTWO (81,87). MTWO is the liquid phase velocity ratio, i.e., V_o/V_1 where V_o is bulk stream velocity of test liquid at inlet and V_1 is the characteristic liquid velocity component, normal to cavity liquid-vapor interface. Details for the calculation of MTWO are given in ref. 81.

From Hord NASA CR-2448 (pg. 84)

Table 4.4

Summary of correlative results for developed cavity data--venturi, hydrofoil, ogives, and combined venturi-hydrofoil-ogives (VHO).

Line No.	Hydrodynamic Body	Test Fluids	Correlative Equation	Source of Data	Exponents					Ref. Run No.	Standard † Deviation in B-Factor	Mean Percent Difference †† in B-Factor	$\overline{K}_{c,min}$
					E1	E2	E3	E4	E6				
1	Venturi	H_2	(4-2)**	This Study [20]	(0.10)	0.59	0.18	---	---	071C	0.2234	5.5	2.459
2	Hydrofoil	H_2 & N_2	(4-2)	This Study [21]	(-0.13)	0.59	0.27	---	---	255B	0.2565	9.9	1.833
3	Ogives	H_2 & N_2	(4-2)	This Study [22]	(-0.05)	0.43	0.25	---	0.59	338B	0.2126	11.1	0.531
4	VHO	H_2 & N_2	(4-2)	This Study	---	0.51	0.28	---	0.43	338B	0.2618	11.7	---
5	Venturi	H_2	(4-1)*	This Study [20]	-1.92	0.74	0.31	---	---	071C	0.3466	9.0	2.459
6	Hydrofoil	H_2 & N_2	(4-1)	This Study [21]	0.80	0.64	0.45	-1.00	---	255B	0.3717	12.7	1.833
7	Ogives	H_2 & N_2	(4-1)	This Study [22]	0.32	0.21	0.34	-0.84	0.60	338B	0.2620	14.3	0.531
8	VHO	H_2 & N_2	(4-1)	This Study	---	0.11	0.36	---	0.58	338B	0.4311	16.3	---
9	Venturi	H_2 & F-114	(4-1)	Reference [3]	1.0	0.8	0.3	---	-0.10	---	---	---	2.47

* $$\frac{B}{B_{ref}} = \left(\frac{\alpha_{ref}}{\alpha}\right)^{E1}\left(\frac{V_o}{V_{o,ref}}\right)^{E2}\left(\frac{\ell}{\ell_{ref}}\right)^{E3}\left(\frac{\nu_{ref}}{\nu}\right)^{E4}\left(\frac{\sigma_{ref}}{\sigma}\right)^{E5}\left(\frac{D}{D_{ref}}\right)^{E6}$$ ---eq (4-1).

** $$\frac{B}{B_{ref}} = \left(\frac{\alpha_{ref}}{\alpha}\right)^{E1}\left(\frac{MTWO}{MTWO_{ref}}\right)^{E2}\left(\frac{\ell}{\ell_{ref}}\right)^{E3}\left(\frac{\nu_{ref}}{\nu}\right)^{E4}\left(\frac{\sigma_{ref}}{\sigma}\right)^{E5}\left(\frac{D}{D_{ref}}\right)^{E6}$$ ---eq (4-2).

† Standard Deviation $\equiv \sqrt{\left[\sum(B-B_t)^2\right]/(NPTS-1)}$, where NPTS = number of data points (including "ref" data point), B_t = BFLASH and is computed from isentropic-flashing theory [23], and B is computed from eq (4-1) or eq (4-2).

†† Mean Percent Difference $\equiv \left[\sum\{|B-B_t|(100/B_t)\}\right]/(NPTS-1)$.

Table 4-4 (ref. 84) summarizes the results for the various hydrodynamic shapes and liquids tested, showing the best-fit empirical exponents for Eqs. (4-34) and (4-35), as well as the predicted standard deviations in predicted B-factors. The percent standard deviations so computed range from 5 to 16%, allowing a much more precise prediction of this parameter than would otherwise be possible, assuming that future data obtained on different machines and hydrodynamic shapes continue to fall within this range.

Pertinent values of cavitation B-Factor for liquid helium, nitrogen, flourine and oxygen, Freon-114, and water are tabulated in detail by Hord and Voth (88), thus allowing the relatively easy calculation of the necessary parameters for these liquids.

4) Penn State Studies, Holl, etal (89-92,94-96,eg.)

During roughly the same time period as the work at NASA-Lewis and BuStd-Boulder, a comprehensive series of relatively similar studies was underway at Pennsylvania State University by Holl and his colleagues(89-92,94-96,eg.) using a relatively small, high-speed tunnel over a range of temperatures, velocities, and size, using water and Freon-113 as test liquids. Test bodies were submerged ogives of various calibers.

The Penn State group recommend a predicting model based upon gas-vapor entrainment considerations rather than the B-factor methods discussed in the last section, and believe that a more realistic analytical approach to the prediction of the thermodynamic effect can be formulated in this way. The probability of success they believe is greater than that with the B-factor approach, since the model would be more closely based upon the actual physical phenomena observed.

The proposed "entrainment method" is a semi-empirical approach for correlating temperature depression data (91, eg.). Experimental values of temperature are compared with values predicted by the correlation equation. It is assumed that the vaporous cavity is continuously supplied with vapor from the cavity walls. The vaporization process requires energy in the form of heat which is transferred at the rate $\dot{q} = \lambda \dot{m}_v$, where λ is the latent heat of vaporization, and $\dot{m}_v = \rho_v V_v A_v$ where V_v is vapor velocity, and A_v cavity cross-sectional area. Then $\dot{m}_v = \rho_v D^2 V_\infty C_Q$, D is model diameter, and C_Q is a flow coefficient defined as $C_Q = \frac{Q_v}{D^2 V_\infty}$ where Q_v is volume flow rate of vapor into cavity. $\dot{q}$ is then evaluated using a film heat transfer coefficient, h, between cavity and main liquid stream. Combining all this, one obtains an expression for the cavity temperature depression,

$$\Delta T = (C_Q/h)(D^2/A_W)(V_\infty \lambda \rho_v) \quad \text{-----} \quad (4\text{-}36)$$

This relation can also be expressed in terms of dimensionless coefficients:

$$\Delta T = (C_Q/C_A)\ (Pe/Nu)\ (\rho_v/\rho_L)(\lambda/C_p) \quad \text{-----} \quad (4\text{-}37)$$

The equation can also be arranged so that the left-hand side corresponds to the Jacok number, J. Pe and Nu are Peclet and Nusselt numbers respectively, and C_p is specific heat of the liquid. The subscripts v and L refer to vapor and liquid. Equation (4-37) is similar to the relationship derived much earlier by Holl and Wisclicenus (92), but corresponds more closely to that proposed by Acosta and Parkin (93 It was then assumed that the volume flow rate of vapor required to sustain a vaporous cavity is equal to that required to maintain a ventilated cavity. The determination of C_Q was based upon experimental investigations at Penn State by Billet and Weir (94,95).

The flow coefficient is then expressed in the form:

$$C_Q = C_1 Re^a Fr^b (L/D)^c \qquad \text{--- (4-38)}$$

where C_1, a, b, and c are constants to be determined empirically, and Re and Fr are Reynolds and Froude numbers respectively. The area coefficient, C_A was determined from photographs by Billet, Holl, and Weir (96). The Nusselt number was determined by using measured values of cavity temperature, as a function of Re, Pr (Prandtl number), Fr, and L/D, again using empirically determined exponents for each parameter.

The entrainment theory described above can be related to the conventional B-factor approach according to the following relation:

$$B = C_Q/C_A \; Pe/Nu \qquad \text{--- (4-39)}$$

This relation indicates the truly complex nature of the B-factor, in that it depends upon four dimensionless coefficients as defined by the entrainment theory approach. This statement runs counter to Bonnin's earlier hypothesis (57-59, eg.) that two independent parameters would be sufficient to describe the thermodynamic effect.

A final relation for the calculation of ΔT follows (91)

$$\Delta T_{max} = C_4 \cdot \left(\frac{L}{D}\right)^i Re^j Fr^k Pr^l Pe \frac{\rho_V}{\rho_L} \frac{\lambda}{C_P} \qquad \text{---- (4-40)}$$

The constants for this equation for two model geometries are given in Table 4-5.

Table 4-5

Constants and exponents for entrainment theory correlations

Model	Quantity	Equation number	Constant (C_1, C_2, C_3, or C_4)	L/D exponent	Re exponent	Fr exponent	Pr exponent
Zero-caliber ogive	C_A	(12)	4.59	1.19	----------	----------	----------
	C_Q	(11)	0.424×10^{-2}	0.69	0.16	0.13	----------
	Nu	(13)	0.103×10^{-3}	−1.35	1.39	0.24	0.84
	ΔT_{max}	(17)	8.97	0.85	−1.23	−0.11	−0.84
Quarter-caliber ogive	C_A	(12)	2.06	1.18	----------	----------	----------
	C_Q	(11)	0.320×10^{-1}	0.74	0.46	0.26	----------
	Nu	(13)	0.546×10^{-2}	−0.74	1.00	0.34	0.49
	ΔT_{max}	(17)	0.284×10^{-2}	0.30	−0.54	−0.08	−0.49
Quarter-caliber ogive[a]	Nu	(13)	0.375×10^{-3}	−0.84	1.02	0.56	0.05
	ΔT	(17)	0.414×10^{-2}	0.40	−0.56	−0.30	−0.05

[a] Correlation using ΔT data from Hord (May 1973) as measured by the leading edge thermocouple and C_Q and C_A data from this study.

B. Boiling and Condensation vs. Cavitation

As discussed in the preceeding sections concerning "thermodynamic effects", there are many cases normally considered under the heading of "cavitation" which involve many elements of "boiling", or in the case of bubble collapse, more properly "condensation". Historically, cavitation bubble dynamics analyses (1,4,eg.) concern themselves only with cases where heat transfer, or "thermodynamic" effects can be neglected, and mechanical effects as inertia, viscosity, and surface tension predominate. On the other hand, boiling or condensation bubble dynamics analyses neglected inertial and viscous effects, and concerned themselves primarily with heat transfer and surface tension restraints to bubble growth or collapse (97-99, eg.). As indicated previously, there are many cases where both thermodynamic and mechanical effects are important. Physically, then, these are intermediate between classical cavitation and boiling models.

Bubble dynamics in highly sub-cooled boiling is then indistinguishable from cavitation cases where thermodynamic effects are important. In practice, sub-cooled boiling is distinguished from cavitation primarily by the way in which the bubbles are created. For any form of boiling, the predominent mechanism for bubble generation is heat transfer, whereas for cavitation, it is pressure reduction due to fluid dynamic effects, or to acoustic radiation in "ultrasonic" cavitation. Bubble generation in sub-cooled boiling ordinarily occurs adjacent to a heated wall, under conditions where the bulk liquid temperature is below the saturation temperature for the existing pressure. Once generate the bubbles are ejected from the wall by mechanisms beyond the scope of this discussion, but covered in detail in the boiling

heat transfer literature. Reference 97 provides a good summary. Once reaching the bulk stream beyond the thermal boundary layer, they are "cooled", so that their collapse is motivated by the fact that they are now in a region of relatively sub-cooled liquid. At this point, they are essentially indistinguishable from collapsing cavitation bubbles.

Damage, however, seldom results from boiling situations for several reasons. The bubbles are not adjacent to the wall when collapse starts, the driving suppression pressure differential is not large, and the liquid conditionsare usually such that "thermodynamic effects" could be expected to severely restrict damaging capability as discussed in the previous section on cavitation thermodynamic effects. In addition boiling applications do not usually involve large enough bulk velocities to make cavitation damage a likely contingency.

Even though cavitation damage is not normally a problem even in highly sub-cooled boiling applications, its possibility obviously cannot be absolutely excluded from consideration. However, aside from the damage possibility, there is also the noise associated with collapsing sub-cooled boiling bubbles. Thus the reliable acoustic detection of boiling in such applications as liquid-cooled nuclear reactor cores becomes difficult, if not impossible, unless the possibility of cavitation in the system can be absolutely eliminated. In the present state-of-the art such an absolute exclusion of the possibility of cavitation is very difficult.

C. Miscellaneous Engineering Effects

1. Degree and Intensity of Cavitation and Damage

"Degree" and "intensity" of cavitation are taken to

describe first the extent of the cavitating region, i.e., the "cavitation condition", and secondly, the intensity of bubble collapse in that region, which is governed by the suppression pressure at the point of bubble collapse. From a slightly different viewpoint, the degree of cavitation is primarily a function of cavitation number "sigma", σ_i). As a first approximation, constant sigma implies a fixed degree of cavitation, assuming geometrical similarity is otherwise maintained. However, as discussed in detail in another chapter, very substantial cavitation "scale effects" are observed to exist in most cases for reasons not yet entirely understood, so that constant degree of cavitation in most practical cases can be maintained for changes in overall velocity, suppression pressure, or size,only if precise empirical information is available for the particular case. Nevertheless, assuming classical scaling laws to apply, constant sigma implies constant degree of cavitation, which then implies fixed conditions for individual bubble dynamics growth and collapse. Thus the effects of asymmetries, bubble collapse volume ratios, etc., should be modelled in such a case to a first approximation.

For any degree of cavitation for a given geometry, various cavitation intensities are possible, depending upon absolute values of stream velocity or suppression pressure. The "intensity" reflects the actual collapse velocities, etc., which presumably scale as the root of suppression as in any fluid dynamic situation. Thus the probability and rate of damage increases in general for increased "intensities", at fixed degree of cavitation. As a practical example, cavitating condensate pumps generally do not represent a

damaging situation, whereas cavitating boiler feed pumps, in which mean velocities and NPSH are much higher, do represent an important cavitation damaging situation. Again, as with degree of cavitation, there are large and important damage "scale effects", not at present entirely understood, but discussed in detail elsewhere in this book.

2. Thermodynamic Effects

The general thermodynamic effect in providing a maximum damage temperature for all liquids so far tested, with a damage fall-off at either lower or higher temperature, was discussed in a previous section. This damage fall-off exists for lower as well as for higher temperature, but it is much more substantial at the high-temperature end, so that cavitation damage is apparently not an important problem in many cases for high temperature liquids. The reason for the low temperature fall-off in damage rate is not well understood, but that at high temperature is presumably primarily the result of the classical thermodynamic effect. Of course, these results are as yet primarily from "vibratory" damage tests (74-78, eg.), so that their application to flowing systems is not as well documented. Nevertheless, there is no reason to believe that the trends are not approximately correct, and they are in fact consistent with some existing industrial experience (1,54-56,eg). Thesetrends are illustrated for water (Fig. 39), and from sodium tests here and elsewhere (100, 79 , eg.) by Figs. 46 and 47.

An example of pertinent industrial experience is the fact that cavitation damage has not been a problem for the coolant circulating pumps for water-cooled nuclear reactor systems such as PWR, BWR, or CANDU. This is presumably because the operating temperature is very far above the probable maximum damage temperature for water (Fig. 39), which is very unlikely to be above $\sim$130°C even at these very elevated pressures. Unfortunately, this is probably not the case for the sodium-cooled fast-breeder reactor (LMFBR), since the maximum damage temperature appears (Fig. 46) to lie in the range 200-400°C. However, insufficient field experience is yet available to allow definite conclusions in this regard.

3. Corrosion and Mechanical Damage Effects

It has long been realized that corrosion and mechanical effects are often inextricably mixed in many apparent cavitation damage cases. A very important example is that of cavitation of marine propellors and other ship's components. In fact, "cathodic protection" has long been used to suppress the corrosion component of the overall erosion (101, eg.). More recently it has been found that at least a portion of the beneficial effect of cathodic protection may be due to generation of electrolytic non-condensable gases along the material wall which thus "cushions" the bubble collapse (102, eg.). This mechanism is similar to some extent to that of the "thermodynamic effect", where vapor cushioning is involved.

There is certainly a substantial experimentally demonstrable difference between the corrosion contributions to the overall erosion in corrosive liquids such as sea-water between different

materials, depending upon their corrodability, i.e., the additive corrosion effect is much greater for carbon steel than for austenitic stainless steels. This has been shown in recent tests here (103, eg.) and elsewhere (104,105,eg.). Presumably one of the major reasons for the unreliability of "accelerated" laboratory cavitation damage tests such as eg., the vibratory test, to field systems, is the fact that only the mechanical component is normally accelerated. Thus the comparison obtained between a hardened carbon steel and a stainless steel, e.g., in a vibratory test, where they may appear to be about equal, is not substantiated in most field tests, especially with sea water, but also in some fresh water applications, where the stainless steel is normally far superior.

This problem was addressed by Plesset[105,106] who utilized a "pulsed" vibratory test, where short pulses of cavitation were interspersed between much longer periods of "dead-time". It was found that the ratio between cavitation and dead-time period durations affected drastically the relative damage resistence of various materials such as carbon steels and stainless steels,when the tests were in salt water, but there was no effect for distilled water or an inert liquid such as toluene.

It is also generally recognized that the total damage resulting from combined cavitation and corrosive attack can be many times that which would result from the total of the two effects acting separately. This is presumably due to the interplay between these two forms of attack, i.e., cavitation provides a roughening and weakening of the surface resulting in increased mechanical cavitation attack, while mechanical cavitation removes the oxide or other film which would normally protect the material surface from rapid corrosive attack.

Figures 46 and 47 for vibratory facility damage data in sodium illustrate the interplay between mechanical and corrosive effects for that liquid on type 304 stainless steel (Fig. 46), and various other relatively incorrodible materials as well (Fig. 47). Figure 46 illustrates that for temperatures up to 500°C, damage rate continues to fall as the temperature is raised. However, Fig. 47 shows that for a further temperature increase to 550°C, damage rate again rises. Presumably this high temperature damage increase results both from reduced mechanical material properties at that temperature, and increased corrosion. Figure 48 plots the product of volume loss rate and ultimate resilience of the material, taking into account its decrease with increasing temperature, against test temperature. Ultimate resilience (discussed in a different section) is taken as the best present parameter to represent failure energy per unit volume of the test material. Figure 48 thus essentially removes the effect of decreasing material properties at high temperature. Since the damage rate at the maximum temperature (550°C) is still greater than that at 500°C even in these terms, presumably the remaining effect is simply that of increased corrosivity at high temperature.

4. Effects of Asymmetrical Collapse

The relatively recent studies indicating the importance of asymmetrical bubble collapse, already discussed, have shown the probable substantial importance of liquid "microjet" impact, as well as pressure pulses from bubble rebound, in cavitation damage. This heightened understanding is particularly important in showing the close relationship between liquid droplet impact damage (where internal cavitation, discussed elsewhere, may also occur) and cavitation damage. This has historically been assumed to be the

case, primarily because of the close similarity between the different forms of damage, so that straight-forward impact tests were often used to evaluate the cavitation damage of materials (107, eg.).

Another important practical effect of the recently increased understanding of the asymmetrical collapse mode as opposed to the classical Rayleigh spherical collapse model (4) is the effect of material surface rigidity upon the collapse model. As discussed in previous sections, a rigid surface "attracts" the bubble centroid during collapse and results in microjet generation toward the wall. Thus the possible damaging effect of bubbles not initially adjacent to the wall is increased. In addition, the complexity of the process is increased considerably, since both velocity and direction of the microjet are involved, as opposed to the Rayleigh model where spherical shock waves impinging upon the wall alone were supposed to be responsible for the damage, so that only initial bubble size and position were involved. Thus an additional "sorting mechanism" is created by the microjet model. This helps to explain the experimental observation that only one out of a very large number of bubbles, $\sim 10^4$ - $\sim 10^9$, (1,2,108,109, eg.) observed to collapse near damaged surface by high-speed photography, actually produces a detectable crater, even in relatively soft materials.

A further important effect of the asymmetrical collapse model and its dependence upon surface rigidity is the fact that a sufficiently flexible surface (or a free surface) will reverse the collapse model direction and result in the "repulsion" of the bubble centroid from the surface and the generation of the microject away from the

surface (35-38, eg.). Experiments here with spark-generated bubbles collapsing near a thin rubber diaphragm sealing a small air pocket behind it, in a static water beaker, indicated precisely such jet reversal and migration of the bubble centroid during collapse away from the diaphragm (36,37). Such a thin rubber diaphragm arrangement could of could be considered either as an extremely flexible solid boundary, or alternatively as a quasi-free surface. Hence it does not necessarily represent a practical construction for a flexible boundary. However, experiments by Gilmore and Brunton at Cambridge University with soft rubber (35) showed relatively similar results.

These relatively scanty experiments, and the confirming analyses, do indicate the possibility of designing a practical and sufficiently flexible surface to prevent or greatly reduce microjet impact, as well as shock waves originating from rebound upon a material wall containing a cavitating liquid. Thus such a surface could be extremely resistant to cavitation damage, and could represent a practical engineering solution for some cases. There is considerable past experimental data (38,110, eg.) confirming the good cavitation erosion resistance of certain rubber and elastomeric coatings in both vibratory and rotating disc facilities. This is probably best explained in terms of the bubble-repulsion mechanism. In fact, our vibratory facility tests (38) showed that some such elastomerics exhibited cavitation damage resistance superior to stainless steels in the same test facility. However, this may not be the case in some field applications where elastomeric coatings are proposed, since the bond between coating and base metal may fail due to high temperatures induced in the elastomeric material by mechanical strains

under cavitation attack (110). This thermal problem is augmented by their relatively poor thermal conductivity.

The droplet impact resistance (38) of these same materials, however, was relatively very much worse, compared to the metals, than was their cavitation resistance. This is explicable by the fact that the existence of the impact, as opposed to the damaging cavitation bubble collapse, is in no way deterred by the flexibility of the surface. However, the resultant pressures upon the surface are somewhat reduced according to numerical studies here (111,112). This problem is discussed in detail in the chapter under Impact.

In summary, it thus appears that while the best cavitation damage resistance is usually provided by very hard materials, it is also true that in some cases very soft materials are also much more resistant than materials of intermediate hardness such as many metallic alloys. Of possible structural metallic alloys many aluminums, brasses, and bronzes, cast iron, and others are much more vulnerable to cavitation damage than materials such as 300-series stainless steels, eg. The best resistance for metals is provided by certain very hard alloys, and also by materials such as Stellite-6. These questions are discussed in much greater detail in the chapter concerning cavitation damage.

BIBLIOGRAPHY - 1

1. R.T. Knapp, J.W. Daily, F.G.Hammitt, Cavitation, McGraw-Hill

2. R.T. Knapp, "Recent Investigations of Cavitation and Cavitation Damage", Trans. ASME, 77, 1045-1054, 1955.

3. W. H. Besant, "Hydrostatics and Hydrodynamics", art. 158, Cambridge University Press, London, 1859.

4. Lord Rayleigh, (J. W. Strutt), "On the Pressure Developed in a Liquid During the Collapse of a Spherical Cavity", Phil. Mag., 34, 94-98, Aug., 1917.

5. J. Nieto and W. Smith, "An Exact Solution of the Rayleigh - Besant Equation" Univ. of Michigan Int. Rep. 18, ORA Project 03424, Oct., 1962.

6. R. T. Knapp and A. Hollander, "Laboratory Investigations of the Mechanism of Cavitation", Trans. ASME, 70, 419-435, 1948.

7. H. Poritsky, "The Collapse or Growth of a Spherical Bubble or Cavity in a Viscous Fluid", Proc. First U.S. Natl. Congr. Appl. Mech. (ASME), pp. 813-821, 1952.

8. S. Goldstein, "Modern Developments in Fluid Dynamics, Oxford Univ. Press, London

9. R.D. Ivany, "Collapse of a Cavitation Bubble in Viscous Compressible Liquid - Numerical and Experimental Analysis", Ph.D. thesis, The Univ.

10. R. H. Cole, Underwater Explosions , Princeton Univ. Press, 1948.

11. J. G. Kirkwood and H.A. Bethe, "The Pressure Wave Produced by an Underwater Explosion, I", OSRD No. 588, 1942.

12. F. R. Gilmore, "The Growth or Collapse of a Spherical Bubble in a Viscous Compressible Liquid", 1952 Heat Transfer and Fluid Mech. Inst., Stanford Univ. Press, pp. 53-64.

13. R. D. Ivany and F.G. Hammitt, "Cavitation Bubble Collapse in Viscous Compressible Liquids - Numerical Analysis," Trans. ASME, 87, Ser. D, J. Basic Engr. , 977-985, 1965.

14. P.G. Tait, "Report on Some of the Physic Properties of Fresh Water and Sea Water", Phys. Chem. 2, 1888, p. 71.

15. H. G. Flynn, "Collapse of a Transient Cavity in a Compressible Liquid", Tech. Mem. No. 38, Acous. Res. Lab., Harvard Univ., Cambridge, Mass., 1957.

16. R. H. Mellen, "An Experimental Study of the Collapse of a Spherical Cavity in Water", USL Res. Rpt. No. 279, U.S. Navy Underwater Sound Lab., Ft. Trumbull, New London, Conn., 1956.

17. R. H. Mellen, "Spherical Pressure Waves of Finite Amplitude from Collapsing Cavities", USL Res. Rpt. No. 279, U.S. Navy Underwater Sound Lab., Ft. Trumbull, New London, Conn., 1956.

18. A. J. R. Schneider, "Some Compressibility Effects in Cavitation Bubble Dynamics", PhD Thesis, Calif. Inst. Tech., 1949.

19. R.S. Brand, "The Collapse of a Spherical Cavity in a Compressible Liquid", PhD Thesis, Brown Univ., 1960.

20. R.S. Brand, "The Shock Wave Produce by Collapse of a Spherical Cavity", Tech. Rpt. No. 1, Mech. Eng. Dept., Univ. of Conn., Storrs Conn., 1962.

21. R. Hickling and M.S. Plesset, "Collapse and Rebound of a Spherical Bubble in Water", Physics of Fluids, 7, 7-14, 1964.

22. R. Hickling, "Effects of Thermal Conduction in Sonoluminescence", J. Acoust. Soc. Am., 35, 967-974, 1963.

23. T. M. Mitchell and F.G. Hammitt, "On the Effects of Geat Transfer Upon Collapsing Bubbles", Nucl. Sci. and Engr., 53, 3, March 1974, 263-276.

24. M.S. Plesset and T. P. Mitchell, "On the Stability of the Spherical Shape of a Vapor Cavity in a Liquid", Quarterly Appl. Math., 13, 1956, p. 419-430.

25. J. E. Welch, F. H. Harlow, J. P. Shannon, and B. J. Daly, A Computing Technique for Solving Viscous, Incompressible, Transient Fluid-Flow Problems Involving Free Surfaces", Los Alamos Sci. Lab., LA-3425, 1966.

26. F. H. Harlow, "The Particle - in - Cell (PIC) Computing Method for Fluid Dynamics", Methods in Computational Physics, 3, 1964, 319-343.

27. F. H. Harlow and J. E. Welch, "Numerical Calculation of Time-Dependent Viscous Incompressible Flow of Fluid with Free Surface", Phys. Fluids, 8, 1965, 2182-2189.

28. F. H. Harlow and A. A. Amsden, "Numerical Calculation of Almost Incompressible Flow," J. of Comp. Phys., 3, 1968, 80-93.

29 F. H. Harlow, "Numerical Methods for Fluid Dynamics, an Annotated Bibliography", Los Alamos Sci. Lab., LA-4281, 1969.

30. R. B. Chapman, "Nonspherical Vapor Bubble Collapse", Ph.D. Thesis, Cal, Inst. Tech., 1970.

31. M. S. Plesset and R. B. Chapman, "Collapse of an Initially Spherical Vapor Cavity in Neighborhood of a Solid Boundary", J. Fluid Mech., 2, 47, May, 1971, p. 283.

32. T. B. Benjamin and A. T. Ellis, "The Collapse of Cavitation Bubbles and the Pressures Thereby Produced Against Solid Boundaries", Phil. Trans. Royal Soc. (London), A, 260, 221-240, 1966.

33. L. Chincholle, "Bubbles and the Rocket Effect", J. Applied Physics, 41, 11, Oct., 1970, p. 4532-4538.

34. L. Chincholle, "L'Effet Fusée et L'Erosion Mecanique de Cavitation", Bull. Tech. Suisse Romande, 94 année, No. 19, Sept., 1968, p. 269-279.

35. D. C. Gibson, "Cavitation Adjacent to Plane Boundaries", Proc. Conf. Inst. Eng., Australia, April, 1969, p. 210-214.

36. E. E. Timm, and F. G. Hammitt, "Bubble Collapse Adjacent to a Rigid Wall Flexible Wall and a Second Bubble", 1971 ASME Cavitation Forum, p. 18-20.

37. E. E. Timm, "An Experimental Photographic Study of Vapor Bubble Collapse and Liquid Jet Impingement", Ph.D. Thesis, Univ. of Mich., Ann Arbor, Mich., 1970, Chem. Engr. Dept.; also available as ORA Proj. Rept. 01357-39-T, Univ. of Mich.

38. F. G. Hammitt, "Cavitation and Droplet Impingement Damage of Aircraft Rain Erosion Materials", Proc. 3rd International Rain Erosion Congress, Farnborough, England, Aug. 1970; edit. A.A. Fyall, Royal Aircraft Establishment, p. 907-932.

39. T. M. Mitchell, F. G. Hammitt, "Asymmetric Cavitation Bubble Collapse" Trans. ASME, J. Fluids Engr., 95, 1, March 1973, p. 29-37.

40. T. M. Mitchell, R. Cheesewright, and F. G. Hammitt, "Numerical Studies of Asymmetric Bubble Collapse", 1968 Cavitation Forum, ASME, May 1968, p. 4-5.

41. C. L. Kling, "A High Speed Photographic Study of Cavitation Bubble Collapse", Ph.D. Thesis, Dept. of Nuclear Engr., Univ. of Mich, Ann Arbor, Mich., 1970, also available ORA Report No. UMICH 03371-2-T, March 1970.

42. C. L. Kling, and F. G. Hammitt, "A Photographic Study of Spark Induced Cavitation Bubble Collapse", Trans. ASME, J. Basic Engr., 94, D, 4, Dec. 1972, p. 825-833.

43. R. D. Ivany, F. G. Hammitt, and T. M. Mitchell, "Cavitation Bubble Collapse Observations in a Venturi", Trans. ASME, 88, D, J. Basic Engr., 1966, p. 649-657.

44. J. H. Brunton, "Cavitation Damage", Proc. 3rd International Congress on Rain Erosion, Meersburg, Germany, Aug. 1970, see also "Cavitation Erosion", Proc. IUTAM Congress, Leningrad, 1971.

45. M. J. Robinson, and F. G. Hammitt, "Detailed Damage Characteristics in a Cavitating Venturi", Trans. ASME, J. Basic Engr., 89, D, 1, March 1967, p. 161-173.

46. M. S. Plesset, "Shock Waves from Cavitation Collapse," Phil. Trans. Royal Soc. (London), A, 260, 241-244, 1966.

47. H.-C. Yeh, and W.-J. Yang, "Dynamics of Bubbles Moving in Liquids with Pressure Gradient", J. Appl. Phys., 39, 1968, 3156-3165.

48. T. M. Mitchell, "Numerical Studies of Asymmetric and Thermodyamic Effects on Cavitation Bubble Collapse", Ph. D. Thesis, Dept. of Nuclear Engr, Univ. of Mich., Ann Arbor, Mich., 1970, also available, ORA Rept. No. UMICH 03371-5-T, Dec. 1970.

49. D. C. Gibson, "The Collapse of Vapour Cavities", Ph.D. Thesis, Cambridge University, 1967.

50. D. C. Gibson, "The Kinetic and Thermal Expansion of Vapor Bubbles", Trans. ASME, J. Basic Engr., 94, March 1972, 89-96.

50-a. G. Chahine, "Interaction Between a Collapsing Bubble and a Free Stream", Trans. ASME, J. Fluids Engr., 1977.

51. W. Lauterborn and H. Bolle, "Experimental Investigations of Cavitation-Bubble Collapse in the Neighbourhood of a Solid Boundary", J. Fluid Mech., 72, 2, 1975, p. 391-399.

52. H. Bolle, and W. Lauterborn, "Nichtsymmetrischer Kollaps Lasererzeugter Kavitationsblasen", Drittes Physikalisches Institut der Universitat Gottingen, DAGA, 1975, p. 645-648.

53. S. P. Kozyrev, "On Cumulative Collapse of Cavitation Cavities", Trans. ASME, J. Basic Engr., 90, D, 1, March 1968, p. 116-124.

54. H. A. Stahl, and A .J. Stepanoff, "Thermodynamic Aspects of Cavitation in Centrifugal Pumps", Trans. ASME, J. Basic Engr., 78, Nov. 1956, 1956, p. 1691-1693.

55. A. J. Stepanoff, "Cavitation in Centrifugal Pumps with Liquids Other than Water," Trans. ASME, 83, Ser. A., Jr. Engr. for Power 79-90, 1961.

56. A. J. Stepanoff, " Cavitation Properties of Liquids," Trans. ASME 86, Ser. A, Jr. Engr. for Power, 195-200, 1964; see also Stepanoff, A.J., and Kawaguchi, K., Proc. 1962 IAHR Symp. on Cavitation and Hydraulic Machinery, Sendai, Japan, F. Numachi (ed), pp. 71-85, 196

57. J. R. Bonnin, "Incipient Cavitation in Liquids Other Than Cold Water", 1971 Cavitation Forum, ASME, p. 14-16.

58. J. R. Bonnin, ASME Paper No. 72-WA/FE-31, 1972.

59. J. R. Bonnin, "Influence de la Temperature sur le Début de Cavitation dans l'Eau", Soc. Hyd. de France, XII Journées de l'Hyraulique, Paris, 1972, Question 1, Rapport 1, p. 1-7.

60. L. W. Florscheutz and B. T. Chao, "On the Mechanics of Vapor Bubble Collapse -- A Theoretical and Experimental Investigation", Trans. ASME J. Heat Transfer, C, 87, 1965, p. 209-220.

61. D. D. Wittke, and B. T. Chao, "Collapse of Vapor Bubbles with Translatory Motion", Trans. ASME, J. Heat Transfer, 89, 1967, 17-24.

62. R. Hickling, "I. Acoustic Radiation and Reflection from Spheres; II. Some Effects of Thermal Conduction and Compressibility in the Collapse of a Spherical Bubble in a Liquid", Ph.D. Thesis, Div. of Engr., Inst. of Tech., 1962, Pasadena, Cal.

63. R. Hickling, "Some Physical Effects of Cavity Collapse in Liquids", Trans ASME, J. Basic Engr., D, 1966, p. 229-235, 88 .

64. M. S. Plesset and S. A. Zwick, "On the Dynamics of Small Vapor Bubbles in Liquids", J. Math. and Phys., 33, 4, Jan. 1955, p. 308-330.

65. M. S. Plesset and D. Y. Hsieh, "Theory of Gas Bubble Dynamics in Oscillating Pressure Fields", Physics of Fluids, 3, 1960, p. 882-892.

66. P. D. Jarman, "Sonoluminescence: A Discussion", J. Acoust. Soc. of America, 11, 11, nov. 1960, p. 1459-1462.

67. P. D. Jarman and K. J. Taylor, "Light Emission from Cavitating Water", Brit. J. Appl. Phys., 15, 1964, p. 321-322.

68. V. V. Gavranek, D. N. Bol'shutkin and V. I. Zel'dovich, "The Thermal and Mechanical Action of a Cavitation Zone on the Surface of a Metal", Fizika metallov i metallovedeniye, 10, 2, 1960, p. 262-268.

69. T. M. Mitchell, and F. G. Hammitt, " On the Effects of Heat Transfer Upon Collapsing Bubbles", Nucl. Sci. and Engr., 53, 3, March 1974, p. 263-276.

70. T. G. Theofanous, L. Biasi, H. Isbin and H. Fauske, "Nonequilibrium Bubble Collapse - A Theoretical Study", AIChE Preprint 1, Presented at 11th National Heat Transfer Conf., Minneapolis, August, 1969.

71. T. G. Theofanous, L. Biasi, H. S. Isbin, and H. K. Fauske, "A Theoretical Study on Bubble Growth in Constant and Time Dependent Pressure Fields", Chem. Eng. Sci., 24, 1969, p. 885-897.

72. W. J. Bornhorst, and G. N. Hatsopoulos, "Bubble-Growth Calculation Without Neglect of Interfacial Discontinuities", Trans. ASME, J. Appl. Mech., 34, E, 1967, p. 847-853.

73. W. J. Bornhorst, and G. N. Hatspoulos, " Analysis of a Liquid Vapor Phase Change by the Methods of Irreversible Thermodynamics", Trans. ASME, J. Appl. Mech., 34, E, 1967, p. 840-846.

74. R. Devine and M. S. Plesset, "Temperature Effects in Cavitation Damage", Rept. 85-27, Div. Engr. and Appl. Sci., Calif. Inst. Tech., 1964.

75. R. Garcia, "Comprehensive Cavitation Damage Data for Water and Various Liquid Metals Including Correlations with Material and Fluid Properties", Dept. of Nuclear Engr., Ph. D. Thesis, Univ. of Michigan, Ann Arbor, Mich., 1966; also available as ORA Rept. No. UMICH 05031-6-T, August, 1966.

76. R. Garcia and F. G. Hammitt, "Cavitation Damage and Correlations with Material and Fluid Properties", Trans. ASME, J. Basic Engr., 89, Dec. 1967, p. 755-763.

77. F. G. Hammitt and N. R. Bhatt, "Cavitation Damage at Elevated Temperature and Pressure", ASME 1972 Polyphase Flow and Cavitation Forum, p. 11-13.

78. F. G. Hammitt, and D. O. Rogers, "Effects of Pressure and Temperature Variation in Vibratory Cavitation Damage Test", J. Mech. Engr. Sci., 12, 6, 1970, p. 432-439.

79. F. G. Hammitt and N. R. Bhatt, "Sodium Cavitation Damage Tests in Vibratory Facility - Temperature and Pressure Effects", ASME 1975 Cavitation and Polyphase Flow Forum, p. 22-23.

80. R. T. Knapp, "Recent Investigations of Cavitation and Cavitation Damage," Trans. ASME, 77, p. 1045-1054, 1955.

81. T. F. Gelder, R. S. Ruggeri, and R. D. Moore, "Cavitation Similarity Considerations Based on Measured Pressure and Temperature Depressions in Cavitated Regions of Freon-114", NASA TN D-3509, 1966.

82. R. S. Ruggeri and R. D. Moore, "Method for Prediction of Pump Cavitation Performance for Various Liquids, Liquid Temperatures, and Rotative Speeds", NASA TN D-5292, 1969.

83. R. S. Ruggeri, "Experimental Studies on Thermodynamic Effects of Developed Cavitation", Proc. Int. Symp. on the Fluid Mech. and Design of Turbomachinery, Penn. State Univ., Aug. 30- Sept. 3, 1970, NASA - SP 304.

84. J. Hord, "Cavitation in Liquid Cryogens - IV. Combined Correlations for Venturi , Hydrofoil, Ogives, and Pumps", NASA CR-2448, 1974.

85. J. Hord, L. M. Anderson, and W. J. Hall, "Cavitation in Liquid Cryogens, Volume I: Venturi," NASA Rept. CR-2054, May 1972.

86. J. Hord, "Cavitation in Liquid Cryogens, Volume II: Hydrofoil", NASA Rept. CR-2156, Jan. 1973.

87. J. Hord, "Cavitation in Liquid Cryogens, Volume III: Ogives", NASA Rept. CR-2242, May 1973.

88. J. Hord and R. O. Voth, "Tabulated Values of Cavitation B-Factor for Helium, H_2, N_2, F_2, O_2, Refrigerant 114, and H_2O", Nat. Bur. Stand., Tech. Note 397, Feb. 1971.

89. J. W. Holl and A. L. Kornhauser, "Thermodynamic Effects on Desinent Cavitation on Hemispherical Nosed Bodies in Water at Temperatures From 80 Deg F to 260 Deg F", Trans. ASME, J. Basic Engr., 92, March 1970, p. 44-58.

90. A. L. Kornhauser, "Thermodynamic Effects on Desinent Cavitation in Water", MS Thesis, Dept. of Aerospace Engr., Penn. State Univ., June 1967.

91. J. W. Holl, M. L. Billet and D. S. Weir, "Thermodynamic Effects on Developed Cavitation", Trans. ASME, J. Fluids Engr., 97, Dec. 1975, p. 507-514.

92. J. W. Holl, and G. F. Wislicenus, "Scale Effects on Cavitation", Trans. ASME J. Basic Engr, 83, D, 1961, p. 385-398.

93. A. J. Acosta and B. R. Parkin, Discussion of Ref. 92.

94. M. L. Billet and D. S. Weir, "The Effect of Gas Diffusion and Vaporization on the Entrainment Coefficient for a Ventilated Cavity", Appl. Research Lab. TM 74-15, Jan. 24, 1974, Penn State Univ.

95. M. L. Billet and D. S. Weir, "The Effect of Gas Diffusion on the Flow Coefficient for a Ventilated Cavity", Proc. Symp. on Cavity Flows, Joint Conf. of Fluids Engr. and Lubrication Div., ASME, Minneapolis, Minn., May 5-7, 1975.

96. M. L. Billet, J. W. Holl and D. S. Weir, "Geometric Description of Developed Cavities on Zero and Quarter Caliber Ogive Bodies", Appl. Research Lab. TM 74-136, May 6, 1974, Penn State Univ.

97. L. S. Tong, Boiling Heat Transfer and Two-Phase Flow, John Wiley and Sons, Inc., 1965.

98. L. E. Scriven, "On the Dynamics of Phase Growth", Chem. Engr. Sci, 10, 1959, p. 1-13.

99. M. S. Plesset and J. A. Zwick, "The Growth of Vapor Bubbles in Superheated Liquids", J. Appl. Phys., 25, 1954, p. 493-500.

100. F. G. Hammitt, etal., "Predictive Capability for Cavitation Damage from Bubble Collapse Pulse Count Spectra", Proc. I. Mech. E. Conf. "Scaling for Performance Prediction in Rotodynamic Machines", 6-8 Sept., 1977, Univ. of Stirling, U.K., also available: ORA Rept. UMICH 014456-3-I, Nov. 1976.

101. G. Petracchi, "Investigations of Cavitation Corrosion", Metallurgia Italiana, 41, 1, p. 1-6, 1949, see English Summary in Engr. Digest, 10, 9, p. 314, 1949.

102. M. S. Plesset, "On Cathodic Protection in Cavitation Damage", Trans. ASME J. Basic Engr., 82, 4, Dec. 1960, p. 808-820.

103. F. G. Hammitt, "Progress Rept. No. 3 - Period: 1 September - 1 December, 1976", ORA Rept. No. UMICH 014456-3-PR, Nov. 1976, Univ. Michigan.

104. A. Thiruvengadam, "Intensity of Cavitation Damage Encountered in Field Installations", Cavitation in Fluid Machinery, Trans. ASME, p. 32-46, 1965, New York.

105. M. S. Plesset, "Pulsing Technique for Studying Cavitation Erosion of Metals", Corrosion, 18, 5, 1962, p. 181-188.

106. M. S. Plesset, "The Pulsation Method for Generating Cavitation Damage", ASME Paper No. 62-WA-315, 1962, Trans. ASME, J. Basic Engr., 85, 3, Sept. 1963, p. 360-364.

107. J. Ackeret and P. DeHaller, "Study of Corrosion through the Impact of Water", Schweiz. Bauztg., 98, 309, 1931.

108. M. J. Robinson, "On the Detailed Flow Structure and the Corresponding Damage to Test Specimens in a Cavitating Venturi", Ph.D. Thesis, Dept. of Nuclear Engr., Univ. of Michigan, Ann Arbor, Mich., 1965, also available: ORA Rept. No. UMICH 03424-16-T, Aug. 1965.

109. M. J. Robinson, and F. G. Hammitt, "Detailed Damage Characteristics in a Cavitating Venturi", Trans. ASME, J. Basic Engr., 89, D, 1, March 1967.

110. J. Z. Lichtman and D. H. Kallas, "Erosion Resistance of Coatings - Methods for Evaluating Erosion (Cavitation)Damage", Materials Protection, 6, 4, p. 40-45, April 1967.

LIST OF TABLES

LIST OF FIGURES

FIGURES (cont.)

TABLE 4-1 Values of the Dimensionless Time $t' = t/R_0\sqrt{\rho/p_\infty}$ from Eq. [4-5]. (Error less than 10^{-6} for $0 < \beta < 0.96$)

β	$t\frac{\sqrt{p_\infty/\rho}}{R_0}$	β	$t\frac{\sqrt{p_\infty/\rho}}{R_0}$	β	$t\frac{\sqrt{p_\infty/\rho}}{R_0}$
0.99	0.016145	0.64	0.733436	0.29	0.892245
0.98	0.079522	0.63	0.741436	0.28	0.894153
0.97	0.130400	0.62	0.749154	0.27	0.895956
0.96	0.174063	0.61	0.756599	0.26	0.897658
0.95	0.212764	0.60	0.763782	0.25	0.899262
0.94	0.247733	0.59	0.770712	0.24	0.900769
0.93	0.279736	0.58	0.777398	0.23	0.902182
0.92	0.309297	0.57	0.783847	0.22	0.903505
0.91	0.336793	0.56	0.790068	0.21	0.904738
0.90	0.362507	0.55	0.796068	0.20	0.905885
0.89	0.386662	0.54	0.801854	0.19	0.906947
0.88	0.409433	0.53	0.807433	0.18	0.907928
0.87	0.430965	0.52	0.812810	0.17	0.908829
0.86	0.451377	0.51	0.817993	0.16	0.909654
0.85	0.470770	0.50	0.822988	0.15	0.910404
0.84	0.489229	0.49	0.827798	0.14	0.911083
0.83	0.506830	0.48	0.832431	0.13	0.911692
0.82	0.523635	0.47	0.836890	0.12	0.912234
0.81	0.539701	0.46	0.841181	0.11	0.912713
0.80	0.555078	0.45	0.845308	0.10	0.913130
0.79	0.569810	0.44	0.849277	0.09	0.913489
0.78	0.583937	0.43	0.853090	0.08	0.913793
0.77	0.597495	0.42	0.856752	0.07	0.914045
0.76	0.610515	0.41	0.860268	0.06	0.914248
0.75	0.623027	0.40	0.863640	0.05	0.914406
0.74	0.635059	0.39	0.866872	0.04	0.914523
0.73	0.646633	0.38	0.869969	0.03	0.914604
0.72	0.657773	0.37	0.872933	0.02	0.914652
0.71	0.668498	0.36	0.875768	0.01	0.914675
0.70	0.678830	0.35	0.878477	0.00	0.91468
0.69	0.688784	0.34	0.881062		
0.68	0.698377	0.33	0.883528		
0.67	0.707625	0.32	0.885876		
0.66	0.716542	0.31	0.888110		
0.65	0.725142	0.30	0.890232		

4-2

TABLE 4-2 Properties of Various Liquids

MATERIAL	WATER		MERCURY		LEAD-BISMUTH†	
PROPERTY	70°F	300°F	70°F	500°F	500°F	1500°F
Density, slugs/ft³	1.939	1.779	26.27	25.17	20.13	18.69
Specific weight, γ(lb/ft³)	62.43	57.3	845.9	810.3	648.0	601.8
Surface tension, σ(lb/ft) × 10³	0.5015	0.322	3.187	2.875	2.735	2.528
Bulk modulus, (psi) × 10⁻⁴	0.31	0.248	4.11	3.94	3.16	2.92
Specific heat, Btu/(lbm-°F)	1.00	1.03	0.033	0.032	0.035	0.035
Thermal diffusivity, (ft²/sec) × 10⁴	0.147	0.186	4.694	7.03	12.69	14.5
Heat of vaporization, Btu/lbm	1054	910	127.7	126.5	113.3	113.3
Vapor pressure, psia	0.36	67.62	2.5×10^{-6}	1.93	<0.001	<0.001
Prandtl number (dimensionless)	6.8	1.18	0.026	0.0091	0.014	0.009
Kinematic viscosity, ν(ft²/sec) × 10⁵	10.8	2.17	1.174	0.75	1.78	1.306

† Eutectic mixture (44.5 weight per cent Pb).

SODIUM		POTASSIUM		LITHIUM		ETHANAL	GLYCERIN
500°F	1500°F	500°F	1500°F	500°F	1500°F	68°F	68°F
1.724	1.474	1.518	1.249	0.97	0.891	1.53	2.45
55.50	47.45	48.88	40.20	31.21	28.35	49.3	78.8
1.202	0.83	0.545	0.425	2.625	2.122	0.153	
0.765	....	....	....	0.160	0.140	....	0.630
0.3155	0.3030	0.1864	0.1891	1.03	0.991	0.581 (77°F)	0.57
71.4	63.6	73.1	62.8	19.44	21.42		
1970	....	932.0	812.4	2600.0	2600.0		
~10⁻⁴	7.737	0.001	24.66	0.001	0.1 1	0.85	2 × 10
0.0065	0.0038	0.0047	0.0032	0.05	0.022	....	12.5
4.6	2.34	3.46	2.15	10.8	6.17	16.4	12,700

rates of strain $\partial\epsilon_1/\partial t$, $\partial\epsilon_2/\partial t$, $\partial\epsilon_3/\partial t$ by

$$p_1 = p - 2\mu\frac{\partial\epsilon_1}{\partial t} + \frac{2}{3}\mu\frac{\partial e}{\partial t}$$

$$p_2 = p - 2\mu\frac{\partial\epsilon_2}{\partial t} + \frac{2}{3}\mu\frac{\partial e}{\partial t}$$

$$p_3 = p - 2\mu\frac{\partial\epsilon_3}{\partial t} + \frac{2}{3}\mu\frac{\partial e}{\partial t}$$

where $p = \frac{1}{3}(p_1 + p_2 + p_3)$ = mean pressure, and $e = \epsilon_1 + \epsilon_2 + \epsilon_3$ = volume dilation. In the bubble problem the radial direction is a principal axis, and

$$\frac{\partial\epsilon_1}{\partial t} = \frac{\partial u}{\partial r} = -2\frac{dR/dt}{R}$$

At the cavity wall the pressure p in the liquid becomes P, and if sur tension is absent the resultant principal pressure p_1 must equal the pres P_i exerted on the cavity wall by any interior gas or vapor.† Then

$$P = P_i - 4\mu\frac{dR/dt}{R} - \tfrac{3}{3}\mu\frac{\partial e}{\partial t}$$

With surface tension we have

$$P = P_i - \frac{2\sigma}{R} - 4\mu\frac{dR/dt}{R} - \tfrac{3}{3}\mu\frac{\partial e}{\partial t}$$

† In case of contents without viscosity, P_i will equal the pressure given by the equation for the contents. If viscosity and shear exist inside the cavity, P_i can differ from the p given by the equation of state.

TABLE A-3 Computed Collapse Pressures of Gases in Compressible Liquid

	EXTERNAL PRESSURE	GAS CONSTANT	INITIAL BUBBLE PRESSURE	INITIAL BUBBLE RADIUS	BUBBLE RADIUS AT COLLAPSE	MAX. PRESSURE AT COLLAPSE INSTANT	ATTENUATED PRESSURE† AT $(r/R_0) = 2$
	p_∞ (ATM)	$\frac{c_p}{c_v}$	P_0 (ATM)	R_0 (IN.)	$\left(\frac{R}{R_0}\right)_{min}$	p_{max} (ATM)	(ATM)
Trilling (49)	1.5	1.4	2×10^{-3}	0.394	0.064	2,200	
Hickling and Plesset (16)	1.0	1.4	10^{-3}	.....	0.017	25,000	200
Hickling and Plesset (16)	1.0	1.4	10^{-4}	.....	0.006	250,000	1000
Ivany (19)	1.0	1.3	10^{-3}	0.05	0.0098	67,700	350
Ivany (19)	1.0	1.3	10^{-4}	0.05	0.0031	582,000	800

† Approximate for attenuation proportional to $1/r$.

difference between the damage potential of large and small bubbles. The number and average diameter of the cavities on this interface were determined by direct measurements from the high-speed motion-picture record of the same experiment. The photographs showed that they were closely packed, completely covering the surface of the fixed cavity. Their average diameter was about 0.025 in. and their mean velocity slightly higher than the free-stream velocity. On the basis of these measurements, approximately 1.8×10^6 cavities per second would be swept into the stagnation zone per inch of circumference of the test specimen. This is a tremendous number in comparison with the observed pitting rate of 60 pits per second per inch of circumference. It implies that only one in 30,000 traveling cavities produced a damaging blow on this soft metal. The question may be asked: What happened to the other 29,999? Similarly, enormous ratios have also been observed in venturi tests (17,54,55) and vibratory-horn tests (40,50).

Figure 8-7 is a schematic of the after end of a fixed cavity with a portion of the reentrant flow. The stagnation line is indicated, and pressure contours show the increase of pressure as the stagnation point is approached. A traveling cavity (bubble) is seen at the point where the pressure commences to rise above vapor pressure. Spherical pressure contours are shown, radiating from the point of complete collapse, if it is assumed for a first approximation that spherically symmetric collapse exists. For this example of flow along the stagnation line toward the body,† the distance of the collapse point from the surface will be a function of the initial size of the cavity since the larger the cavity, the longer the time of collapse, and hence the greater the time available for the cavity to be carried toward the surface

† Johnson and Hsieh (31) showed that, because of the variable pressure gradients around a curved body, only bubbles originating from nuclei within a critical size range will be able both to "nucleate" and to approach closely to the body.

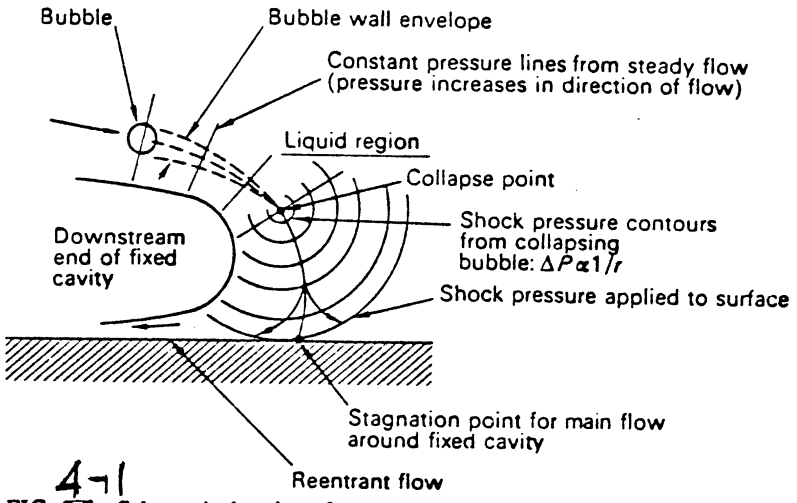

FIG. 8-7 Schematic drawing of reentrant flow and collapsing traveling bubbles.

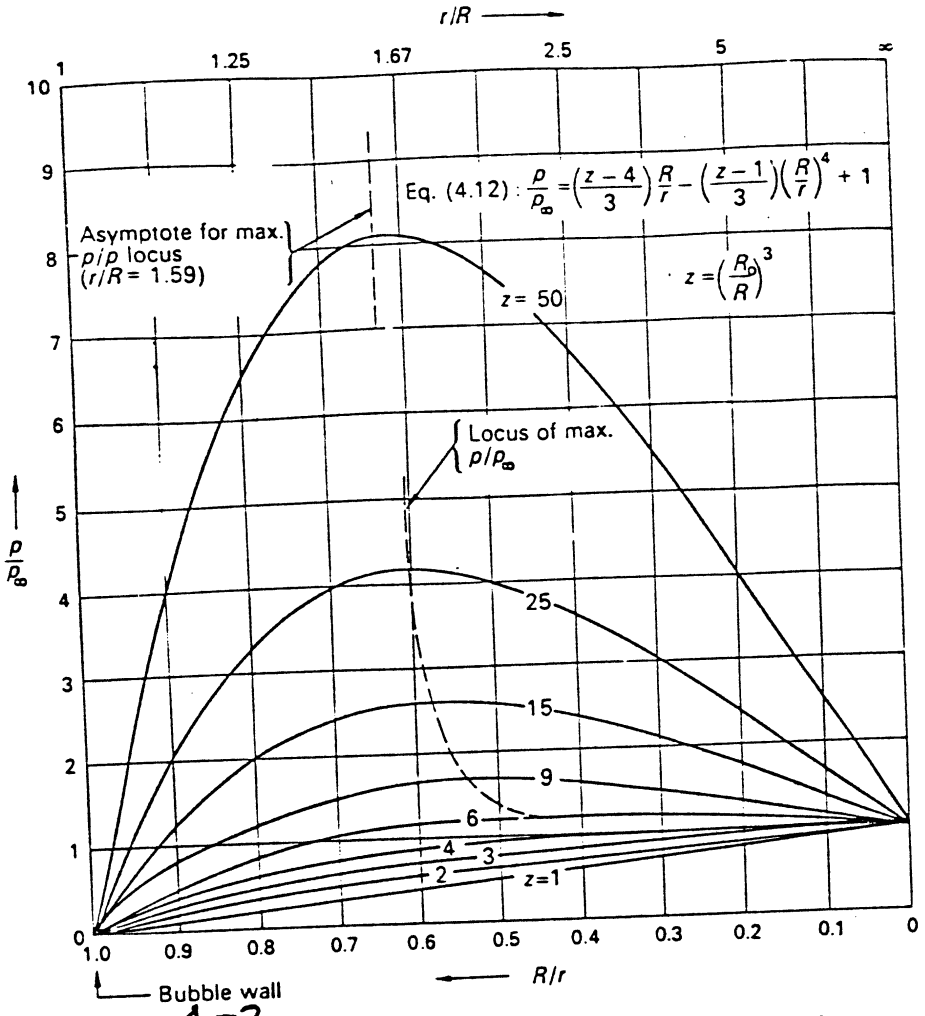

FIG. 4-3 Rayleigh analysis: pressure profile near a collapsing bubble.

As the cavity approaches complete collapse, z becomes great, and Eqs. [4-14] and [4-15] may be approximated by

$$r_m = 4^{\frac{1}{3}}R = 1.587R \qquad [4\text{-}16]$$

and

$$\frac{p_{max}}{p_\infty} = \frac{z}{4^{\frac{1}{3}}} = \frac{R_0^3}{4^{\frac{1}{3}}R^3} \qquad [4\text{-}17]$$

Equations [4-16] and [4-17] taken together show that, as the cavity becomes very small, the pressure in the liquid near the boundary becomes very great in spite of the fact that the pressure at the boundary is always zero. Although Rayleigh did not mention it, this would suggest the possibility that in compressing the liquid some energy can be stored which would add an additional term to Eq. [4-4]. This would invalidate the assumption of

incompressibility. Rayleigh himself abandoned this assumption in considering what happens if the cavity collapses on an absolutely rigid sphere of radius R, which, he noted, was previously examined by S. S. Cook. In this treatment, later published by Cook (36), the supposition of incompressibility is abandoned only at the instant that the cavity wall comes in contact with the rigid sphere. From that instant on it is assumed, as is common in water-hammer calculations, that the kinetic energy of each particle of fluid is changed to elastic energy of deformation of the same particle as determined by the bulk modulus of elasticity of the fluid. On this basis it is found that

$$\frac{(P')^2}{2E} = \tfrac{1}{2}\rho U^2 = \frac{p_\infty}{3}\left(\frac{R_0^3}{R^3} - 1\right) = \frac{p_\infty}{3}(z - 1) \qquad [4\text{-}18]$$

where P' is the instantaneous pressure on the surface of the rigid sphere and E is the bulk modulus of elasticity. Both must be expressed in the same units.

It is instructive to compare the collapse of the cavity described in Section 4-2 with the predicted collapse as based on this simple theory. Figure 4-4

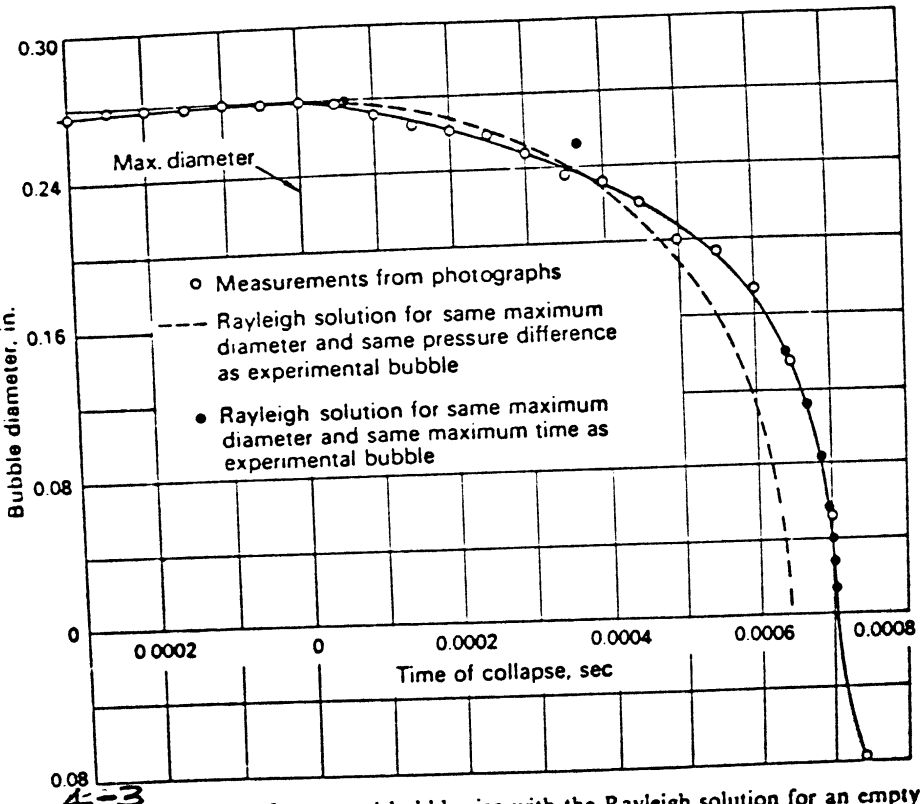

FIG. 4-3 Comparison of measured bubble size with the Rayleigh solution for an empty cavity in an incompressible liquid with a constant pressure field. [Knapp and Hollander (25).]

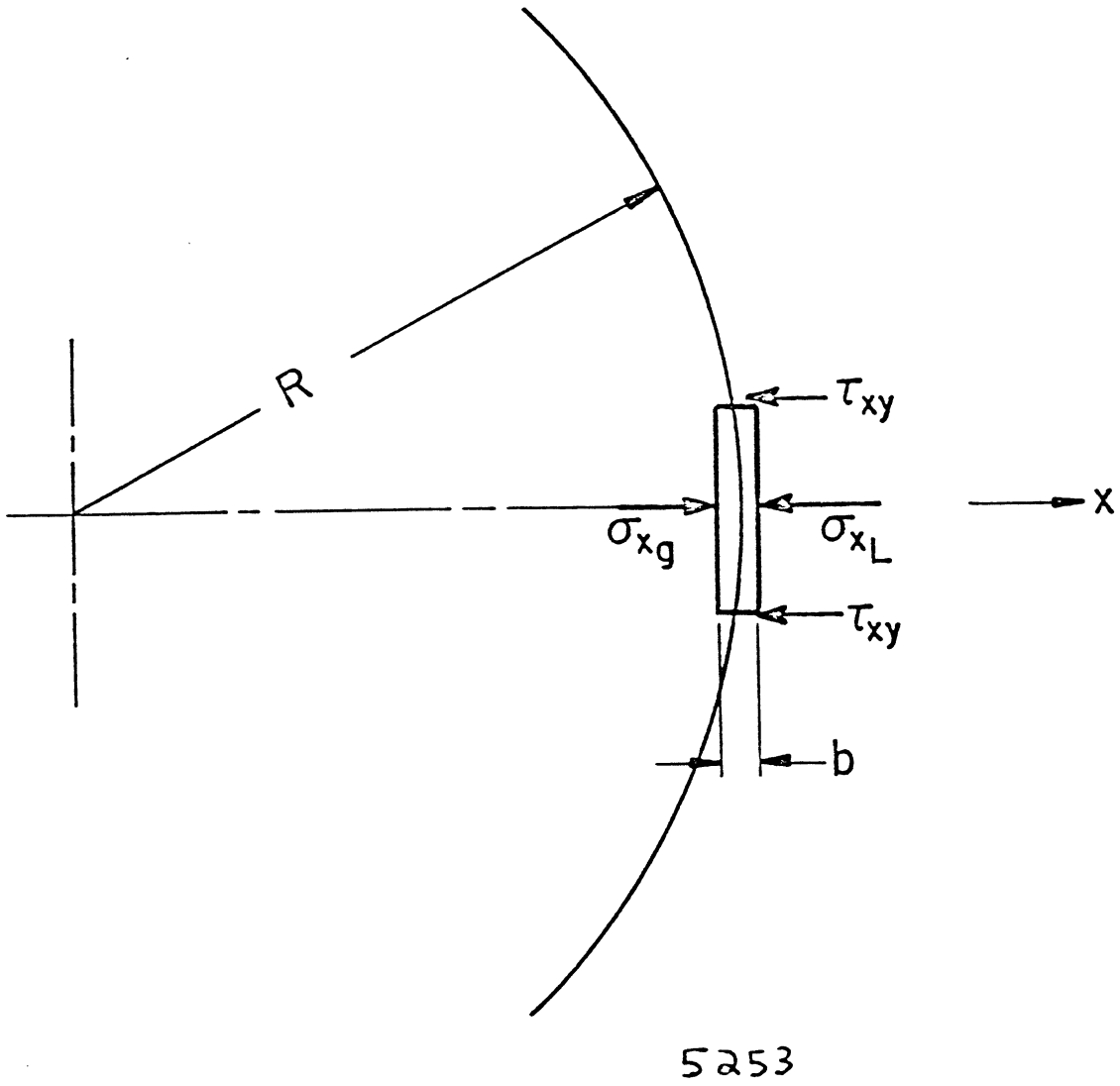

Fig. A-4. Pill Box Balance for Bubble Wall.

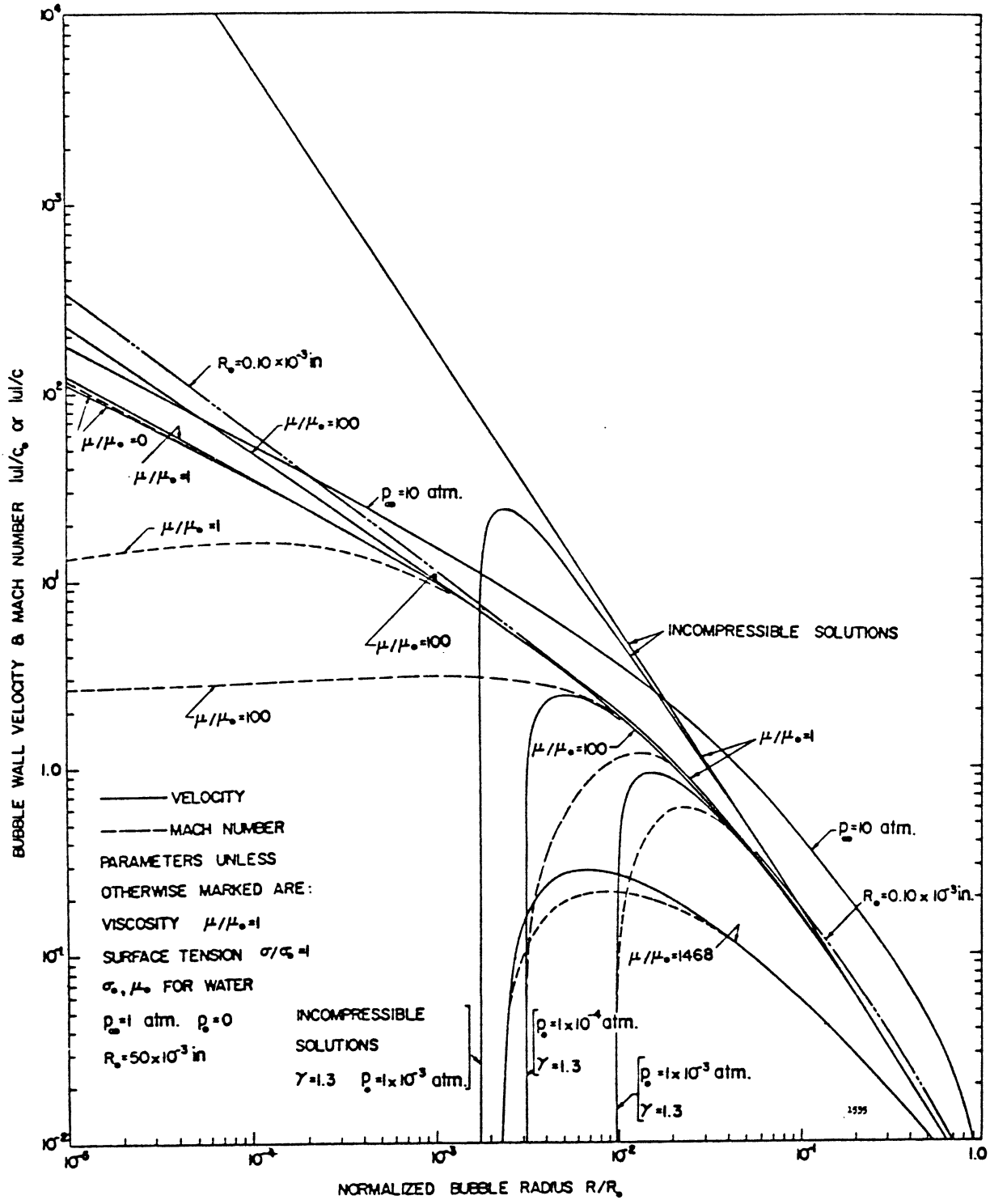

Figure A-5 Bubble Wall Velocity and Mach Number vs Normalized Bubble Radius for Reference Bubble Parameters Except Where Noted Otherwise on Individual Curves.

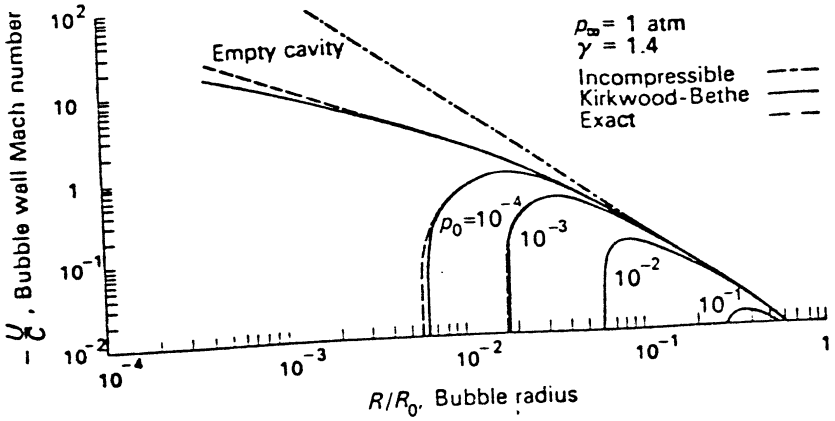

(*a*) Gas constant $\gamma = 1.4$; ambient pressure $p_\infty = 1$ atm.

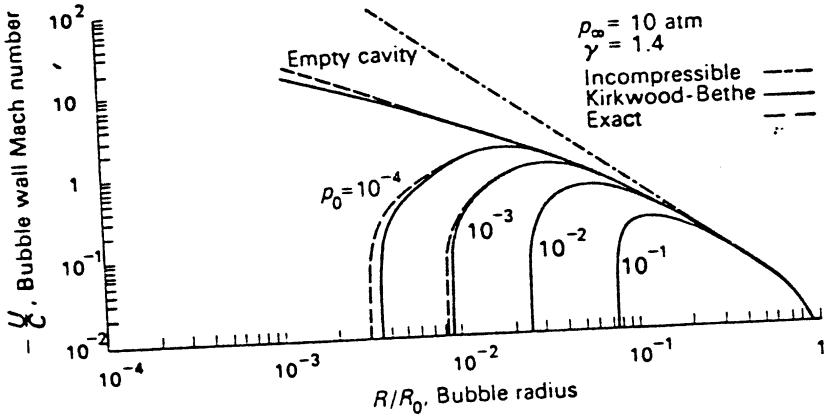

(*b*) Gas constant $\gamma = 1.4$; ambient pressure $p_\infty = 10$ atm.

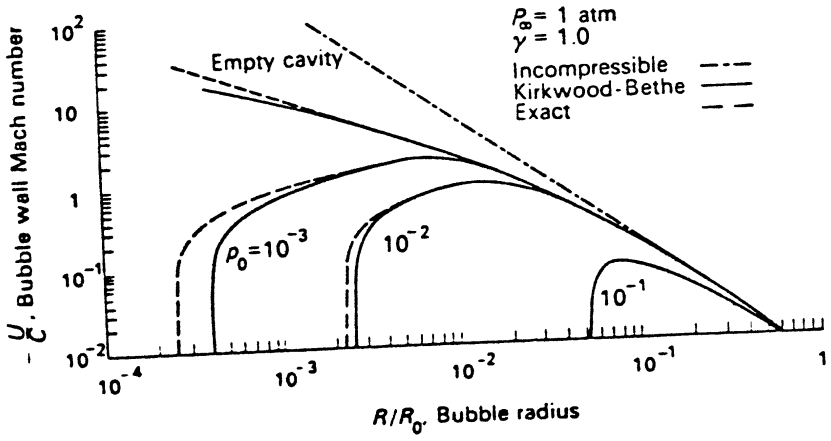

(*c*) Gas constant $\gamma = 1.0$; ambient pressure $p_\infty = 1$ atm.

FIG. ~~4-12~~ 4.6 Bubble-wall velocity versus bubble radius for decreasing gas content. Compressible liquid without viscosity or surface tension; gas content determined by initial pressure P_0. [Hickling and Plesset (16).]

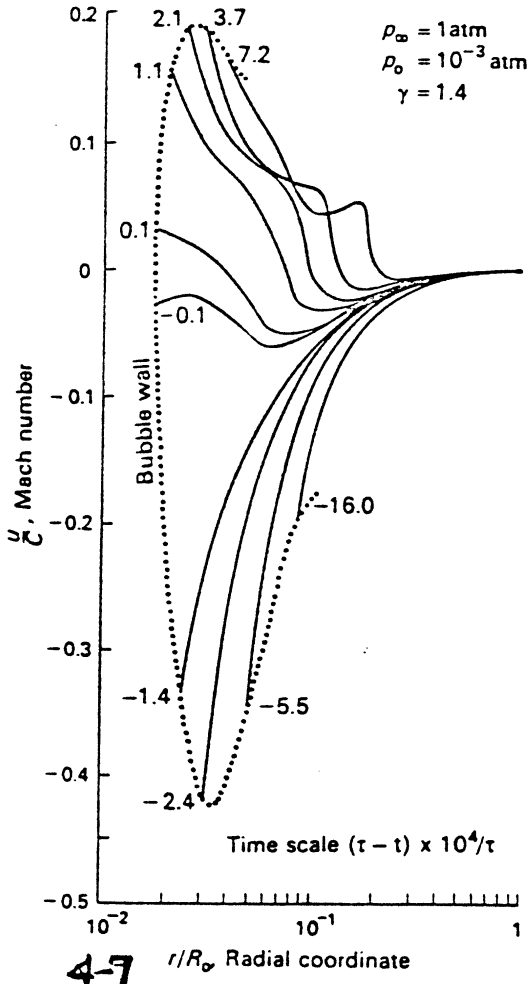

4-7

FIG. ~~4-13~~ Curves of instantaneous velocity in the liquid versus distance from the bubble wall during collapse and rebound. Compressible liquid without viscosity or surface tension. Gas constant $\gamma = 1.4$; ambient pressure $p_\infty = 1$ atm; initial pressure $P_0 = 10^{-3}$ atm. [Hickling and Plesset (16).]

short distance from a rigid surface to cause mechanical damage to some materials. For very strong materials, however, the maximum computed collapse pressures do not appear sufficient to cause the observed damage even if the collapse center is as close as $2R_0$ to the adjacent wall.

Here it should be noted that the initial pressure P_0 in the preceding computations can be considered to include the gas partial pressure and the vapor pressure. Then any vapor is assumed to compress like a permanent gas. The low values of $P_0 = 10^{-3}$ and 10^{-4} atm correspond to very low

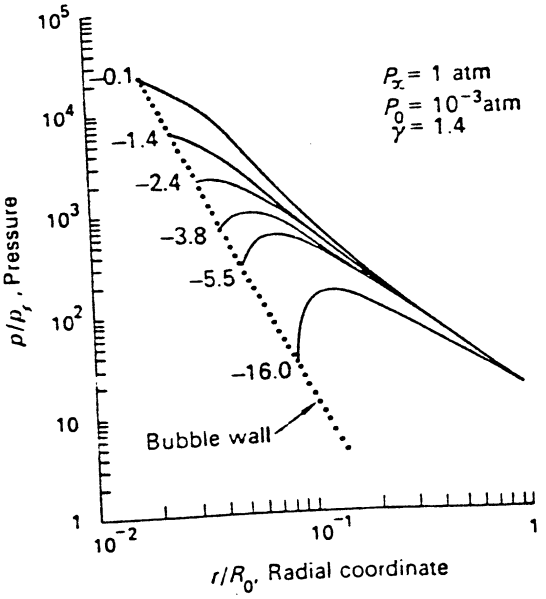

(*a*) Bubble collapse.

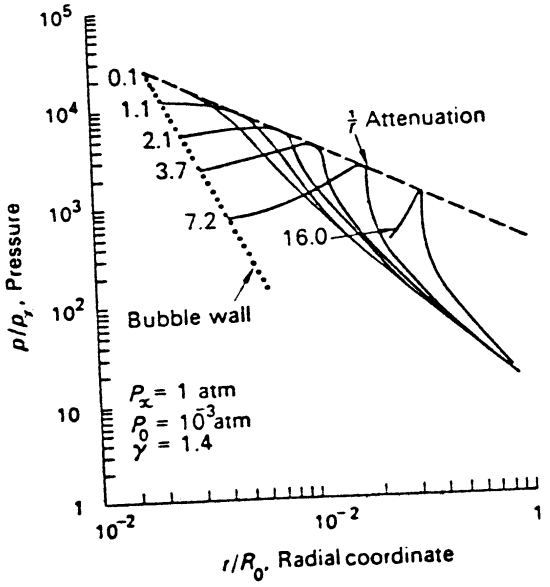

(*b*) Bubble rebound.

FIG. 4.14 Curves of instantaneous pressure in the liquid versus distance from the bubble wall. Compressible liquid without viscosity or surface tension. Gas constant $\gamma = 1.4$; ambient pressure $p_\infty = 1$ atm; initial pressure $P_0 = 10^{-3}$ atm. [Hickling and Plesset (16).]

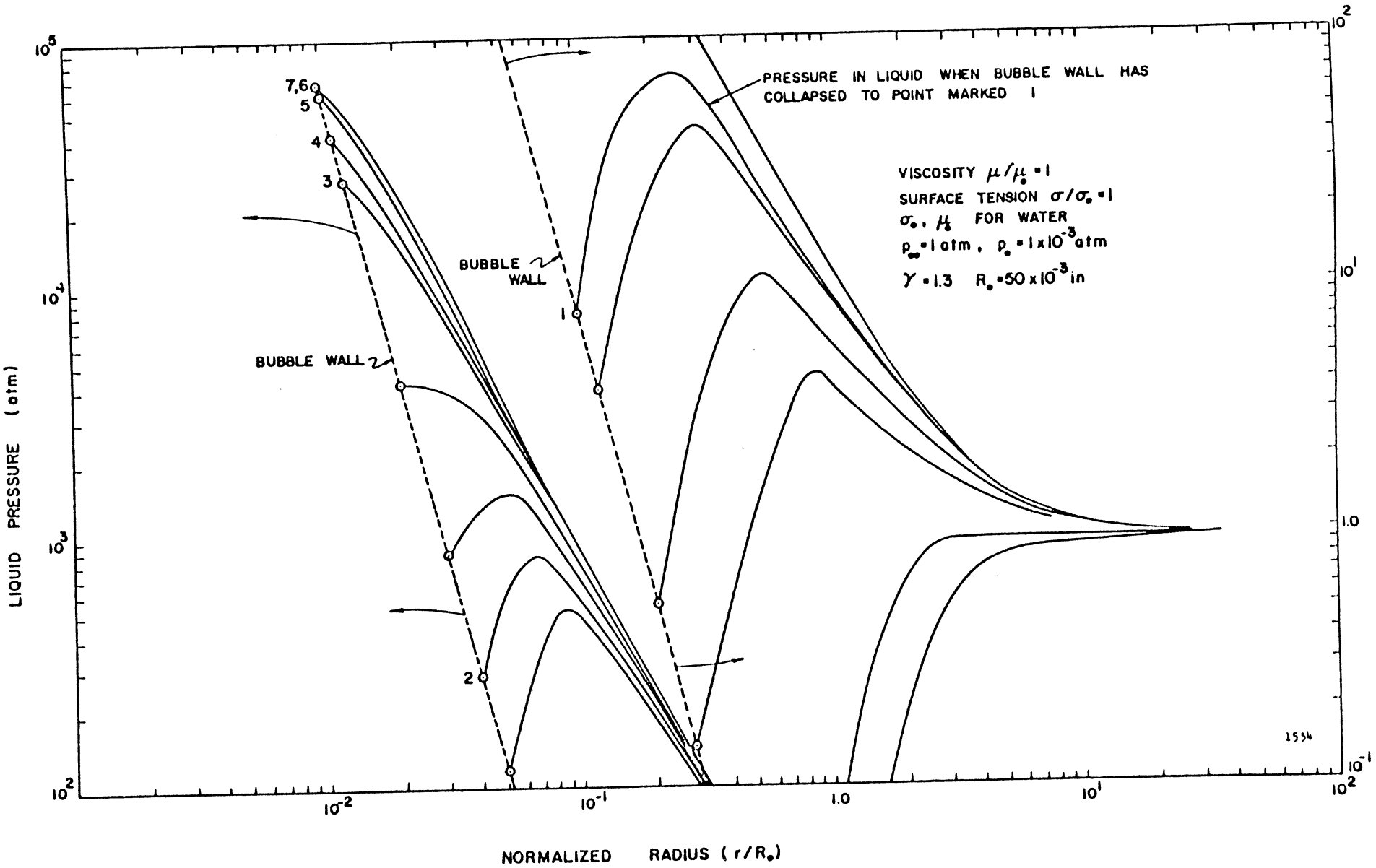

Fig. A-9 Liquid pressure vs. normalized radius for bubble containing gas. (Ivany)

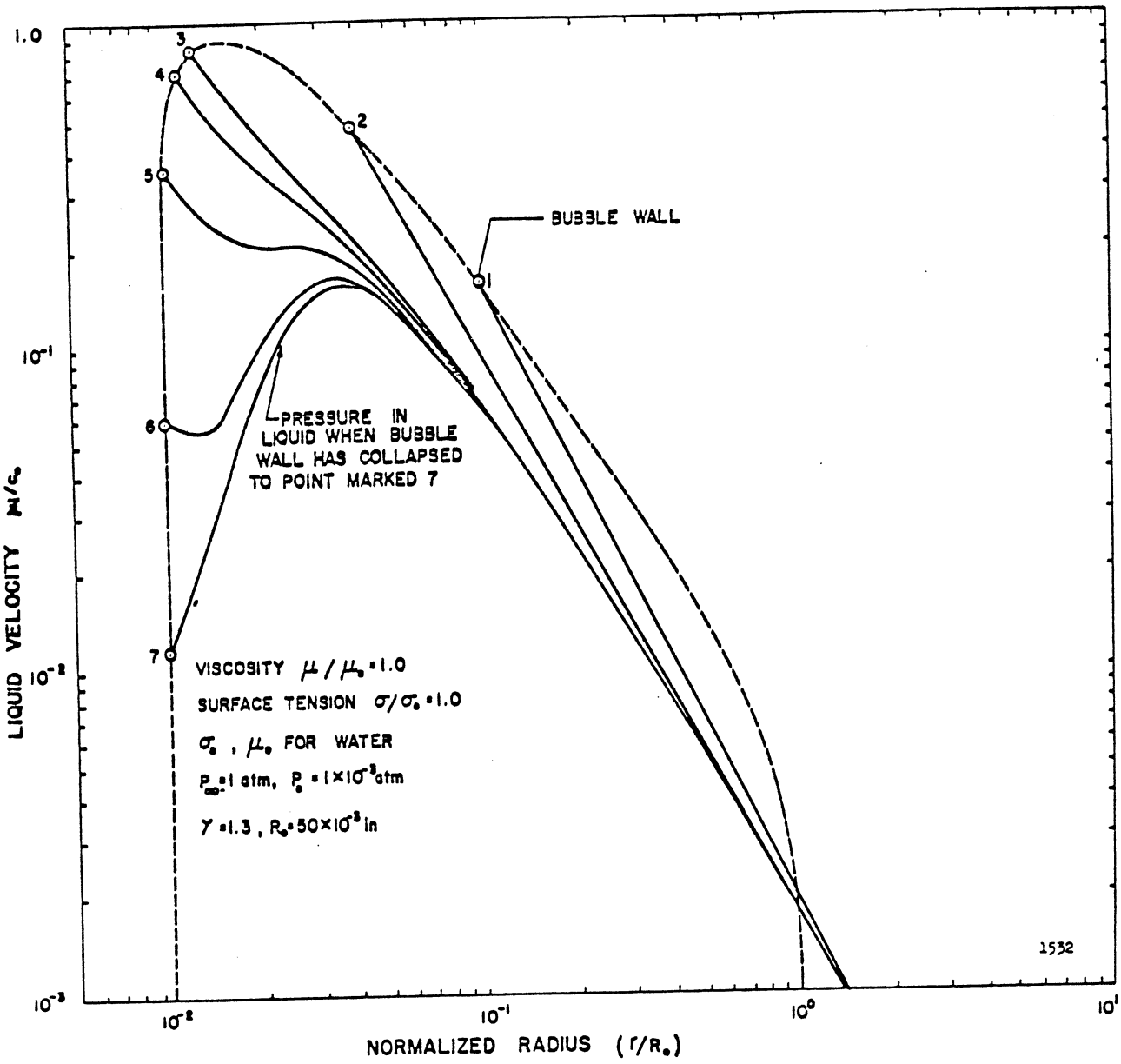

Fig. A-10. Liquid Velocity vs Normalized Radius for Bubble Containing Gas.

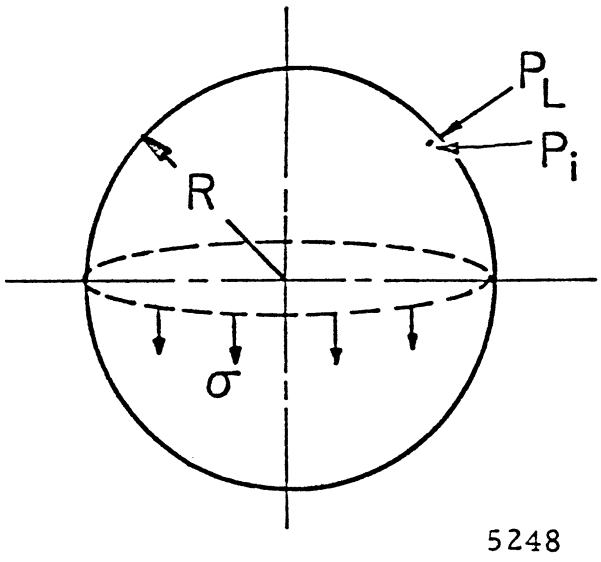

Fig. A - 11. Schematic of Surface Tension Term Derivation.

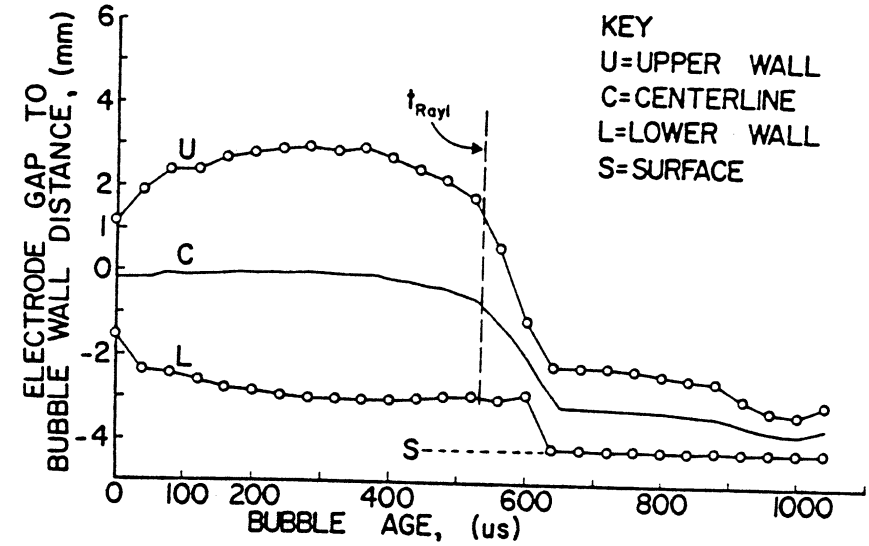

Figure 4. Apparent Wall Position Alor the Axis of Symmetry as a Fun tion of Time for a Bubble Colla sing next to a Brass Plate

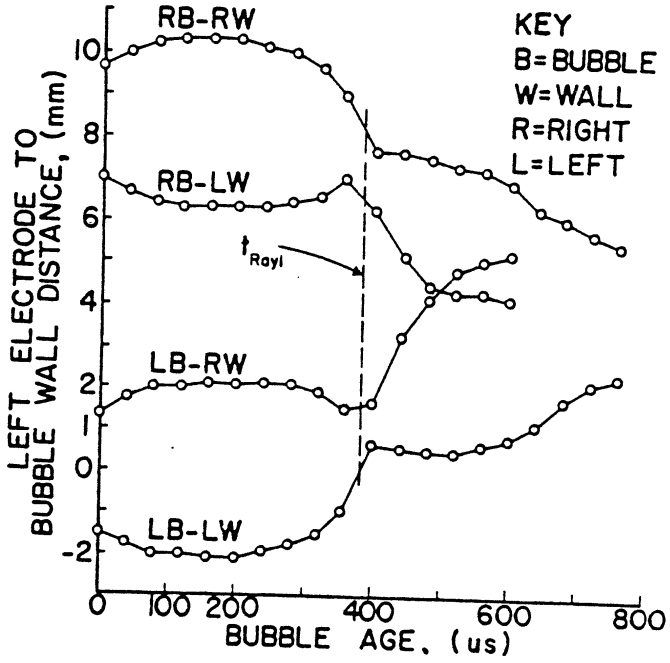

Figure 5. Apparent Wall Position Alon the Axis of Symmetry as a Fun tion of Time for a Bubble Colla sing Adjacent to Another Bubbl

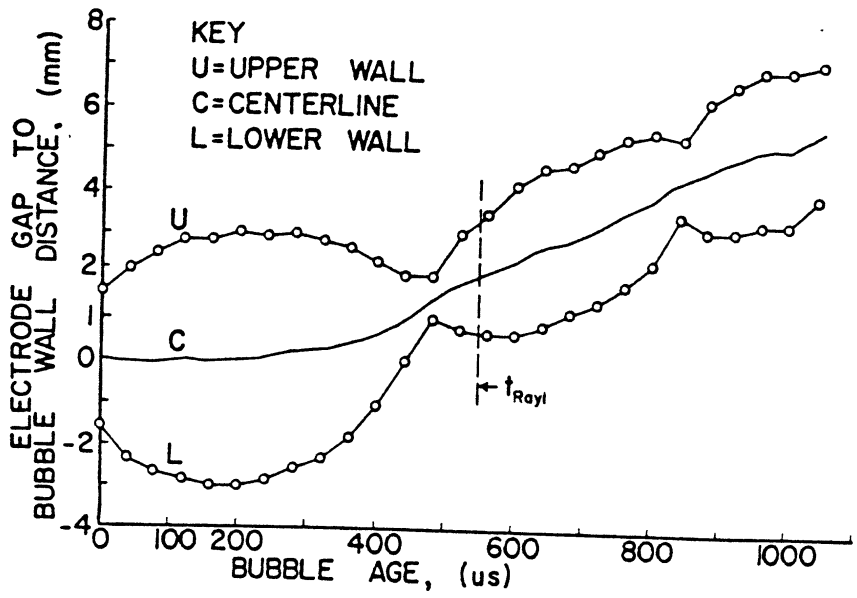

Figure 6. Apparent Wall Position Alon the Axis of Symmetry as a Func- tion of Time for a Bubble Collap- sing Adjacent to a Rubber Mem- brane.

3265

Fig. 12

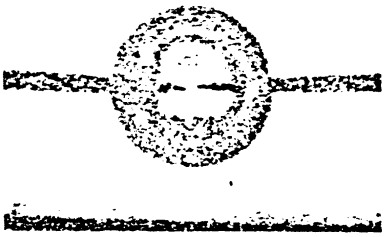

t = 200 μs

t = 440 μs

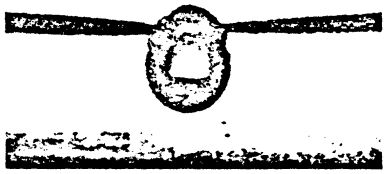

t = 560 μs

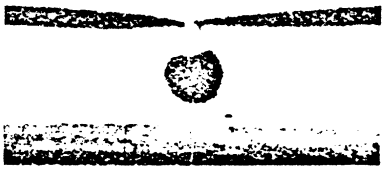

t = 600 μs

t = 640 μs

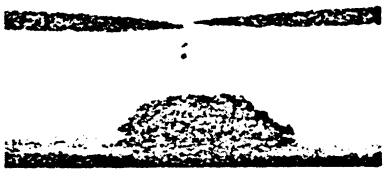

t = 840 μs

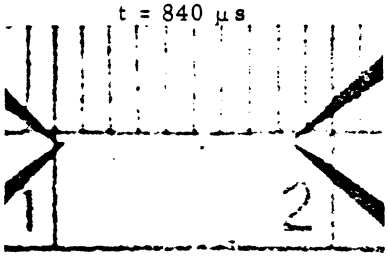

Scale

Figure 1. Bubble Collapse Adjacent to a Brass Plate

t = 200 μs

t = 360 μs

t = 400 μs

t = 480 μs

t = 560 μs

t = 720 μs

t = 800 μs

Figure 2. Bubble Collapse Adjacent to Another Bubble

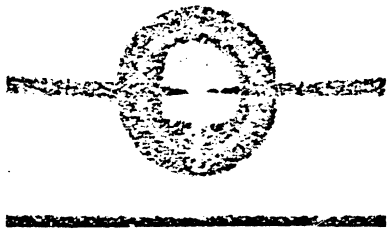

t = 200 μs

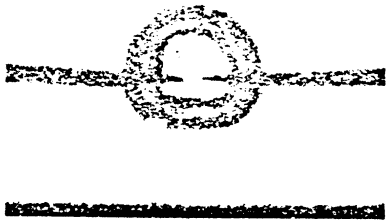

t = 360 μs

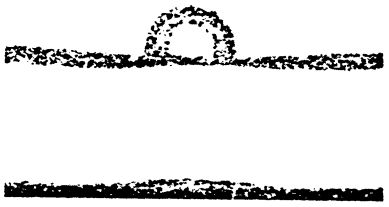

t = 440 μs

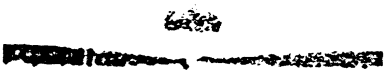

t = 480 μs

t = 600 μs

t = 800 μs

t = 1040 μs

Figure 3. Bubble Collapse Adjacent to a Rubber Membrane

Fig. 13

3264

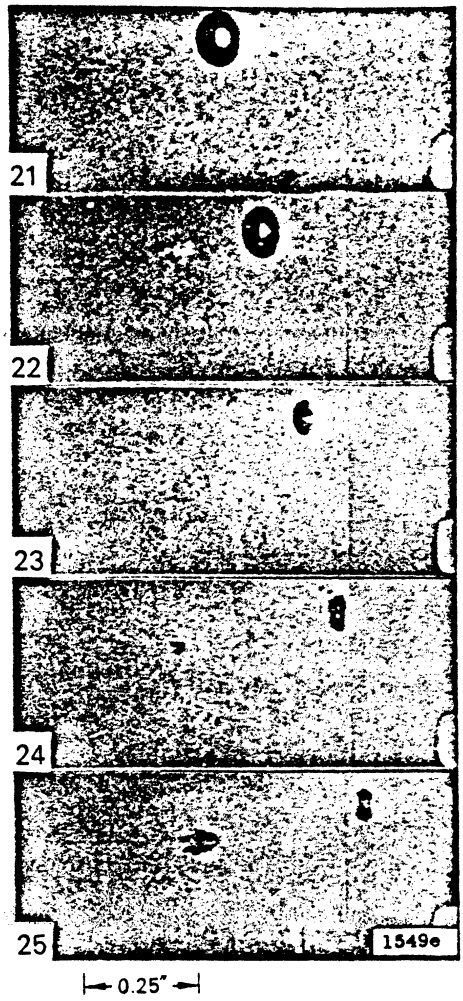

FIG. 8-13 Nonsymmetric collapse of a bubble in a pressure gradient. High-speed photographs of collapse in a two-dimensional venturi with a ½-in. throat in water at 74.6 ft/sec. Air content 2.35 percent by volume, 132 microsec between frames, 1-microsec exposure, flow left to right. [Ivany and Hammitt (27).]

be suitable. The existence of either of these two mechanisms does not rule out the other on the basis of the present state of our knowledge.

8-12 ACCELERATION OF DAMAGE RATE BY "WAVE-GUIDE" EFFECT

Since the evidence is fairly clear that in most instances the intensity of the hydrodynamic attack does not vary with time until surface roughening becomes sufficient to influence the flow pattern, variations in the rate of

Fig. 14

formation of the microjets described in Section 4-9. This was first suggested, to our knowledge, by Kornfeld and Suvarov (36). That it might apply in such cases has been more recently reemphasized and strengthened by Ellis and his coworkers (1,38). Photographs of collapsing bubbles in static fluids show distortion on collapse. These effects are exaggerated with pressure gradients or near boundary surfaces. Moreover, the distortion sometimes seems to form a liquid microjet of very high velocity moving through the interior of the cavity in the instant before complete closure. It is postulated that such jets will cause damage if the collapse is close enough to a boundary. Later confirmatory photographs in a static fluid with an arrangement very similar to that of Naudé and Ellis (38) were obtained by Shutler and Mesler (57); similar photographs for venturis or water tunnels were published by Fabula (5), Harrison (19), Ellis (3b), Ivany, Hammitt, and Mitchell (27),

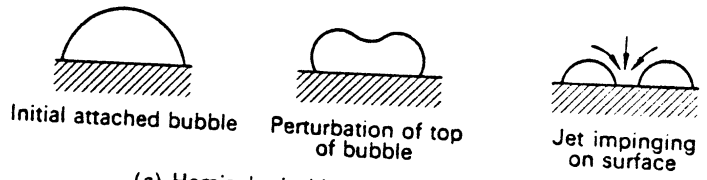

(*a*) Hemispherical bubble attached to wall

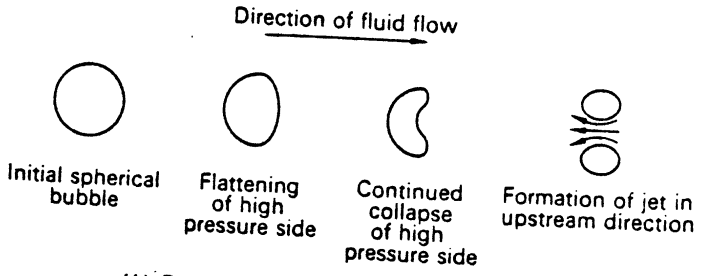

(*b*) Bubble moving into pressure gradient (such as venturi diffuser flow)

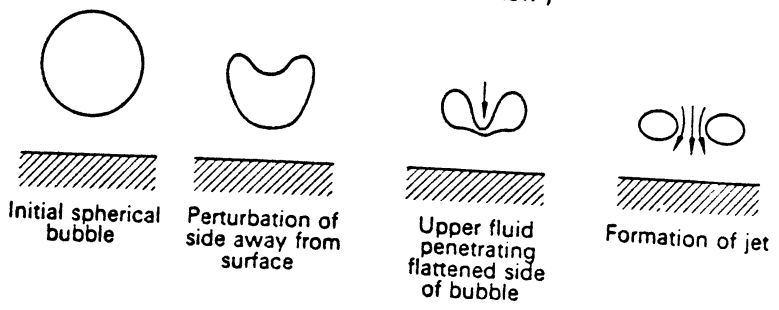

(*c*) Bubble collapsing near wall

FIG. 8-11 Jet-collapse models.

Fig. 15

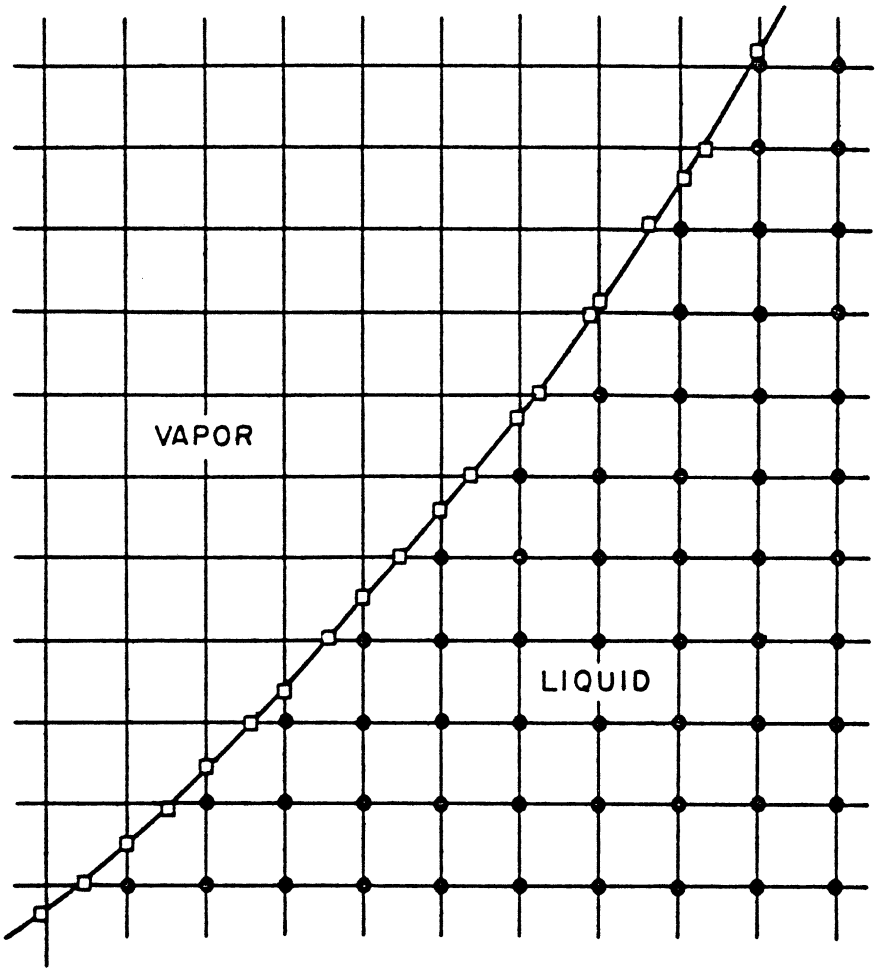

Fig. 1 Representation of the Bubble
by Free Boundary Points

Fig. 16

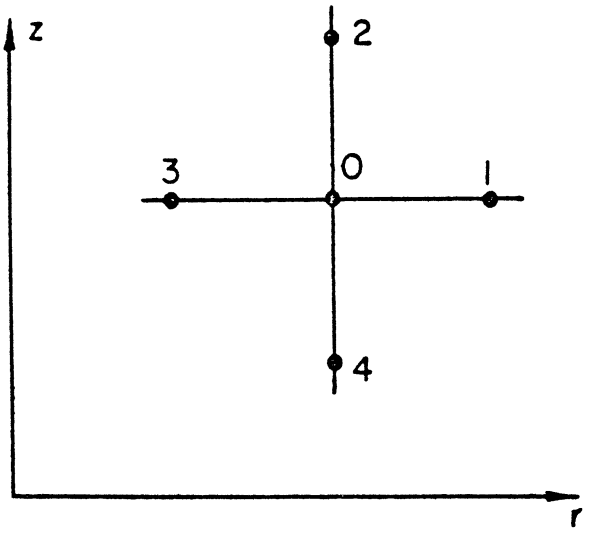

Fig. 2 Numbering System for Stars

Fig. 17

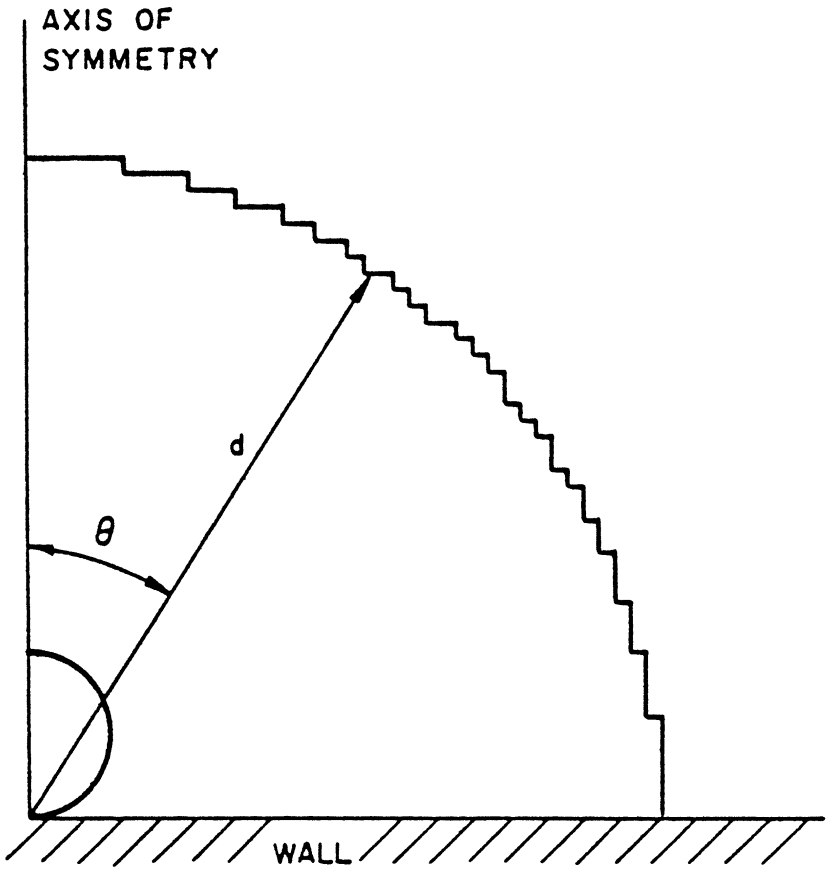

Fig. 3 Net Used to Apply the Condition at Infinity

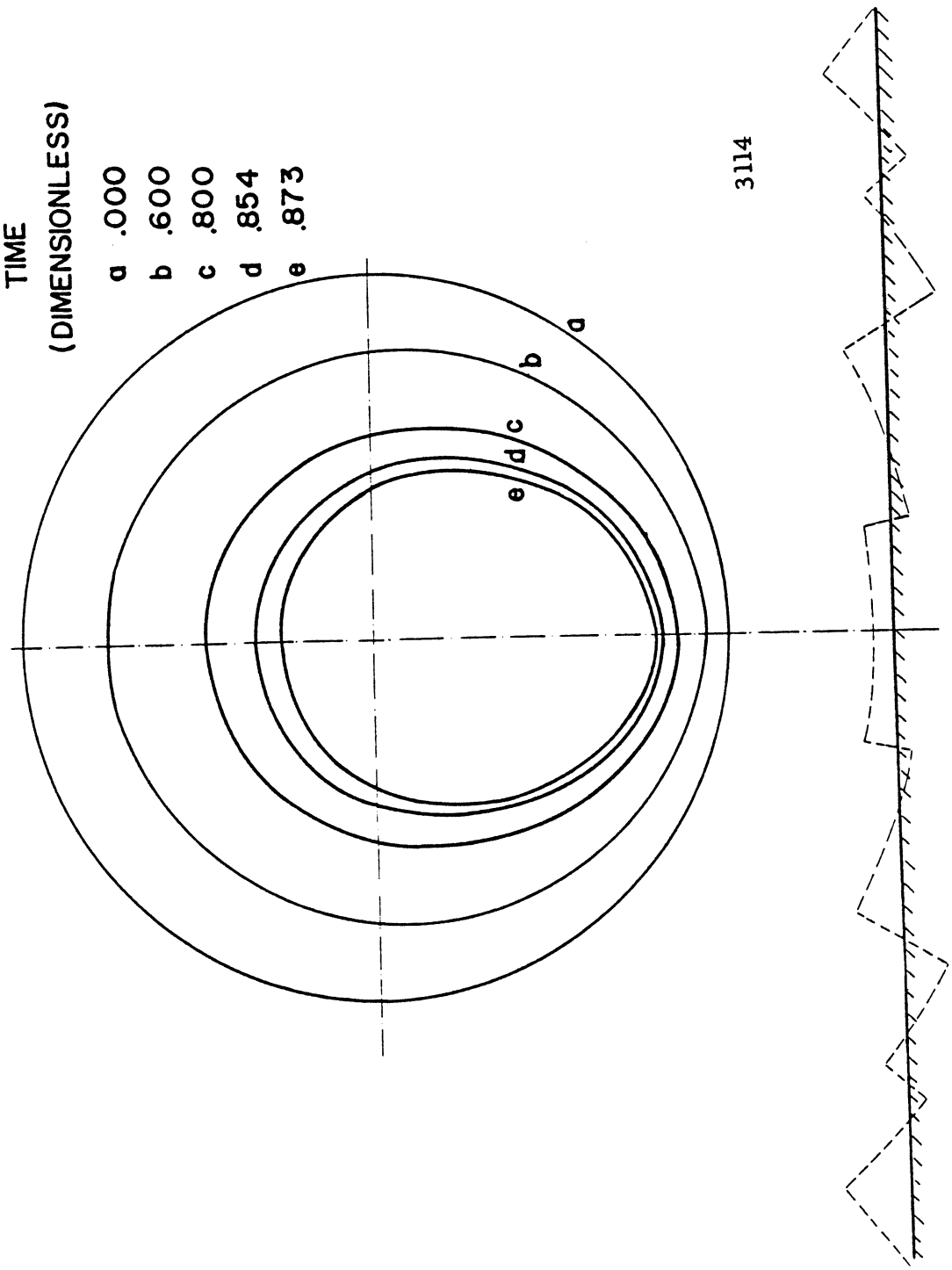

Figure 24. Bubble Surface Profiles for Initially Spherical Bubble with Center 1.5 R_o from Rigid Wall

Fig. 18

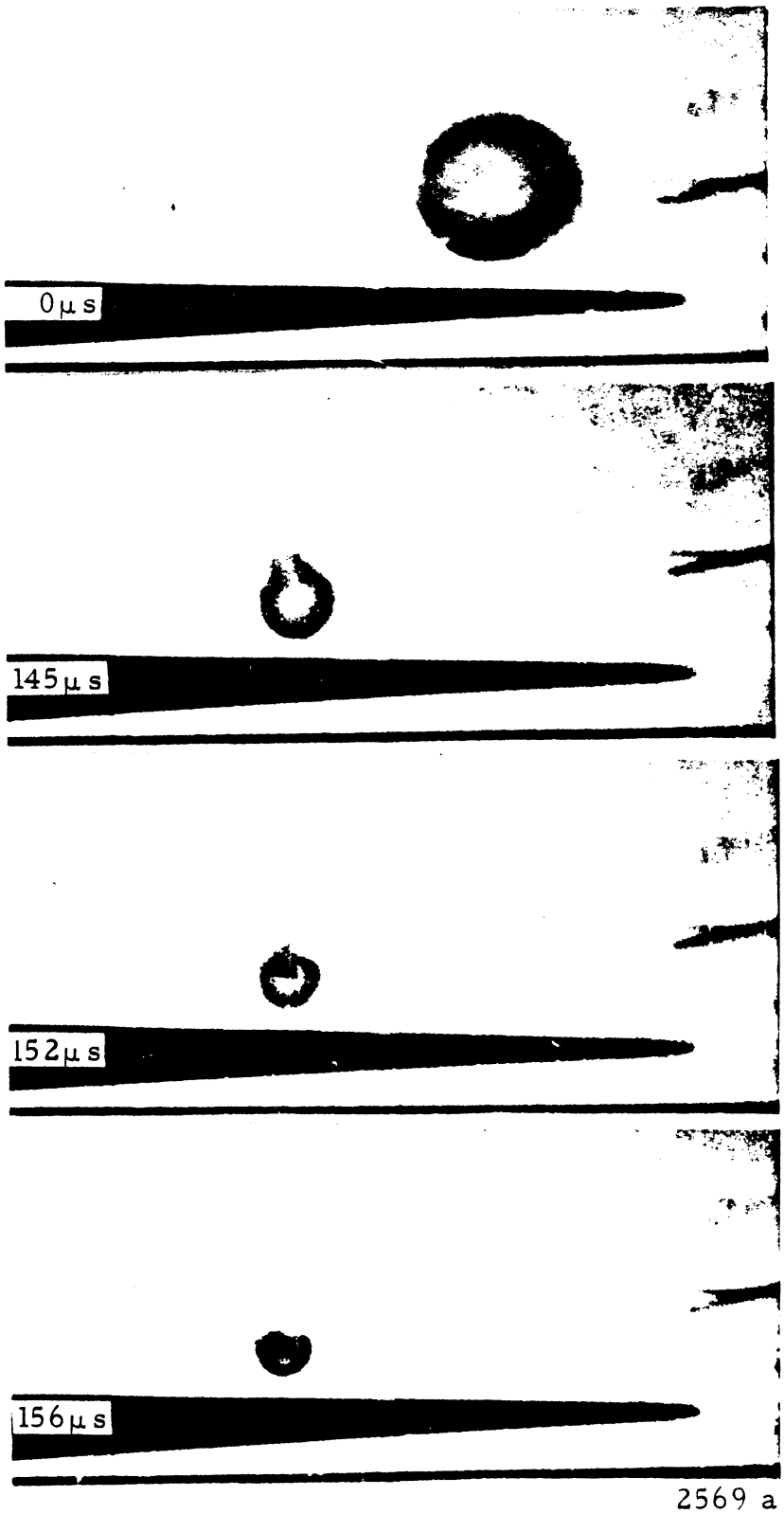

Kling High-Speed Pictures

Fig. 19

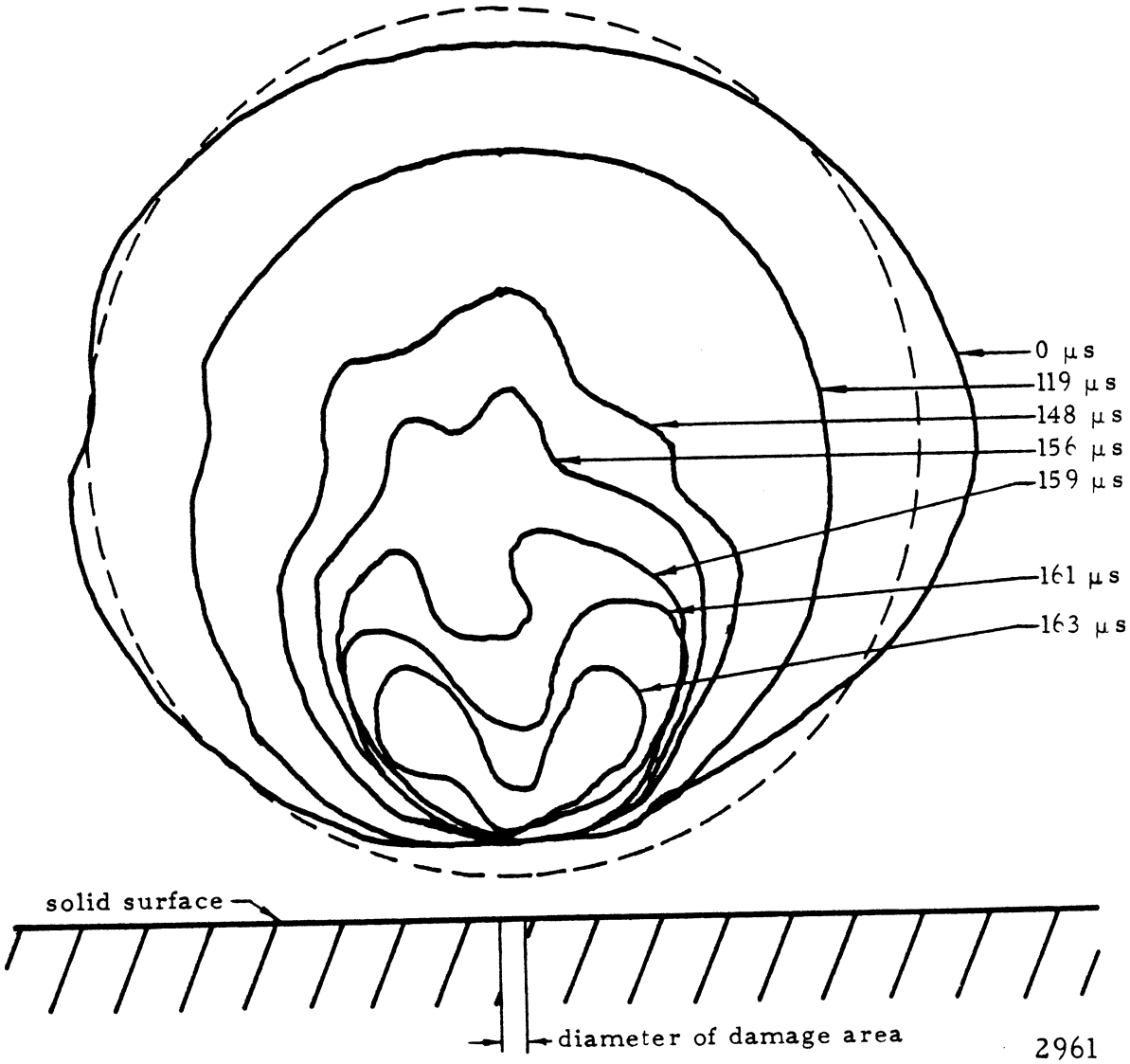

Figure 5.37 Outlines of the Spark Induced Cavitation Bubble 5.30 at Various Stages of Collapse Showing the Mode of Deformation

Kling thesis

Fig. 20

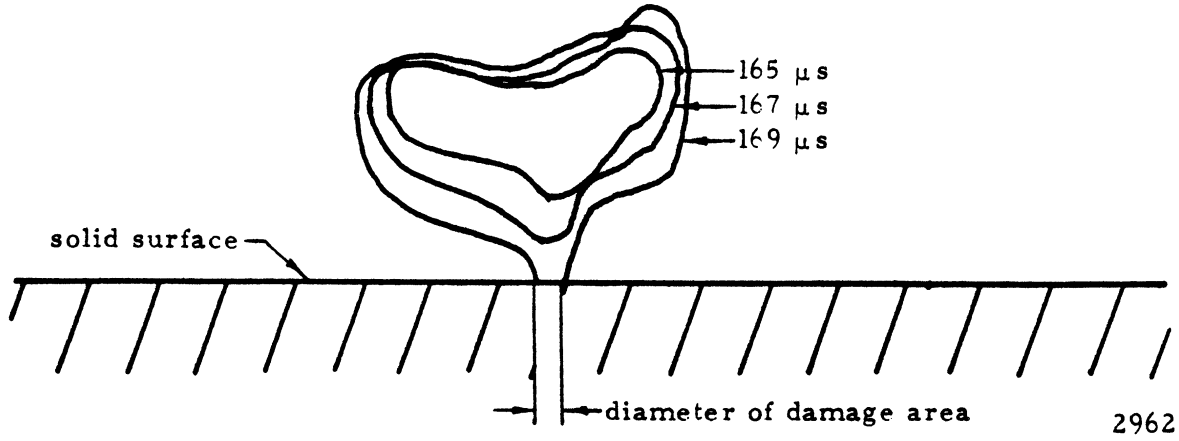

Figure 5.38 Outlines of the Spark Induced Cavitation Bubble 5.30 at Various Stages of Rebound Showing the Bubble Impinging on the Nearby Solid Surface

Kling thesis

Fig. 21

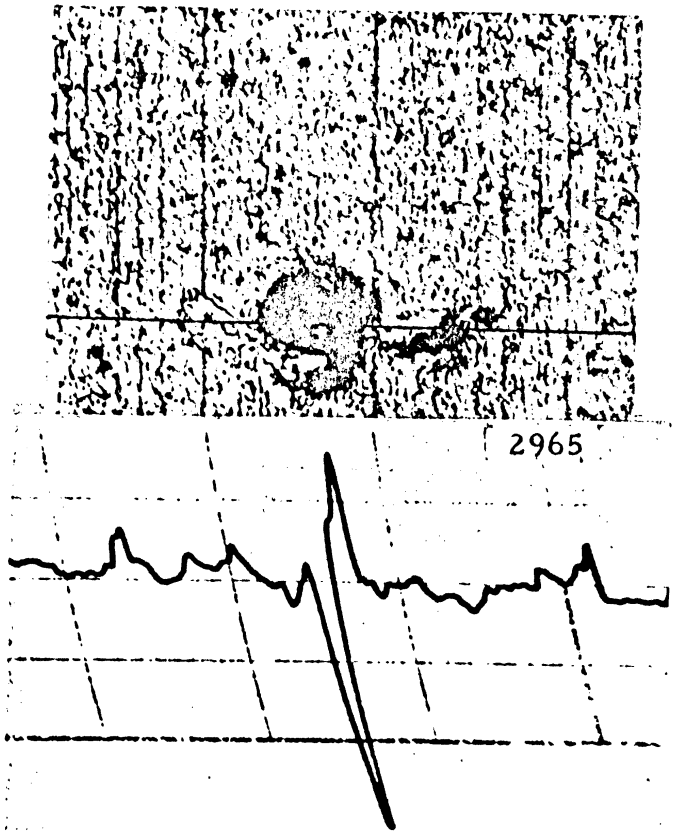

Figure 5.42 Photomicrograph and Accompanying Proficorder Trace of Damage Produced on the 0.5 mm Thick Aluminum Sheet by the Collapse with an Initial Normalized Wall Distance b_o, of 1.15. Scale Divisions 66.0 μ Horizontal, 0.635 μ Verticle

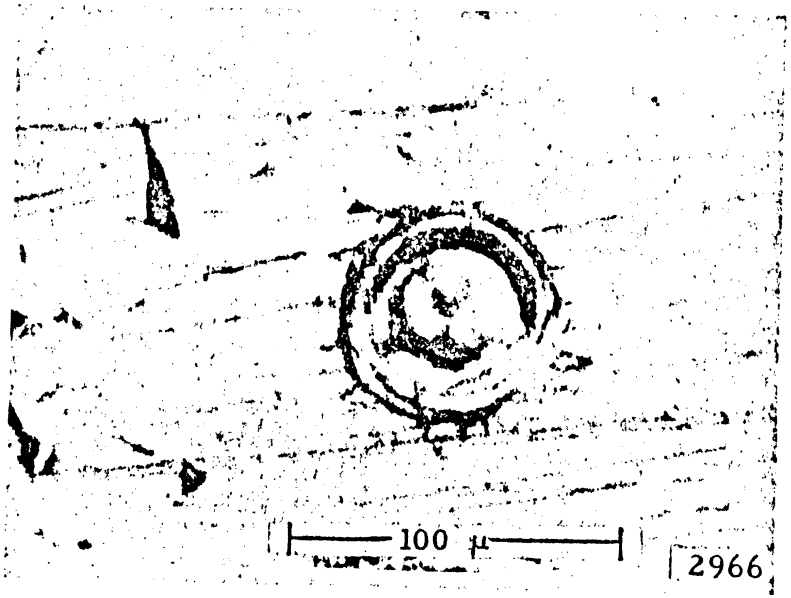

Figure 5.43 Photomicrograph of Damage Produced on the 0.5 mm Thick Aluminum Sheet by the Initiating Spark of a Spark Induced Cavitation Bubble with an Initial Normalized Wall Distance, b_o, of 1.15

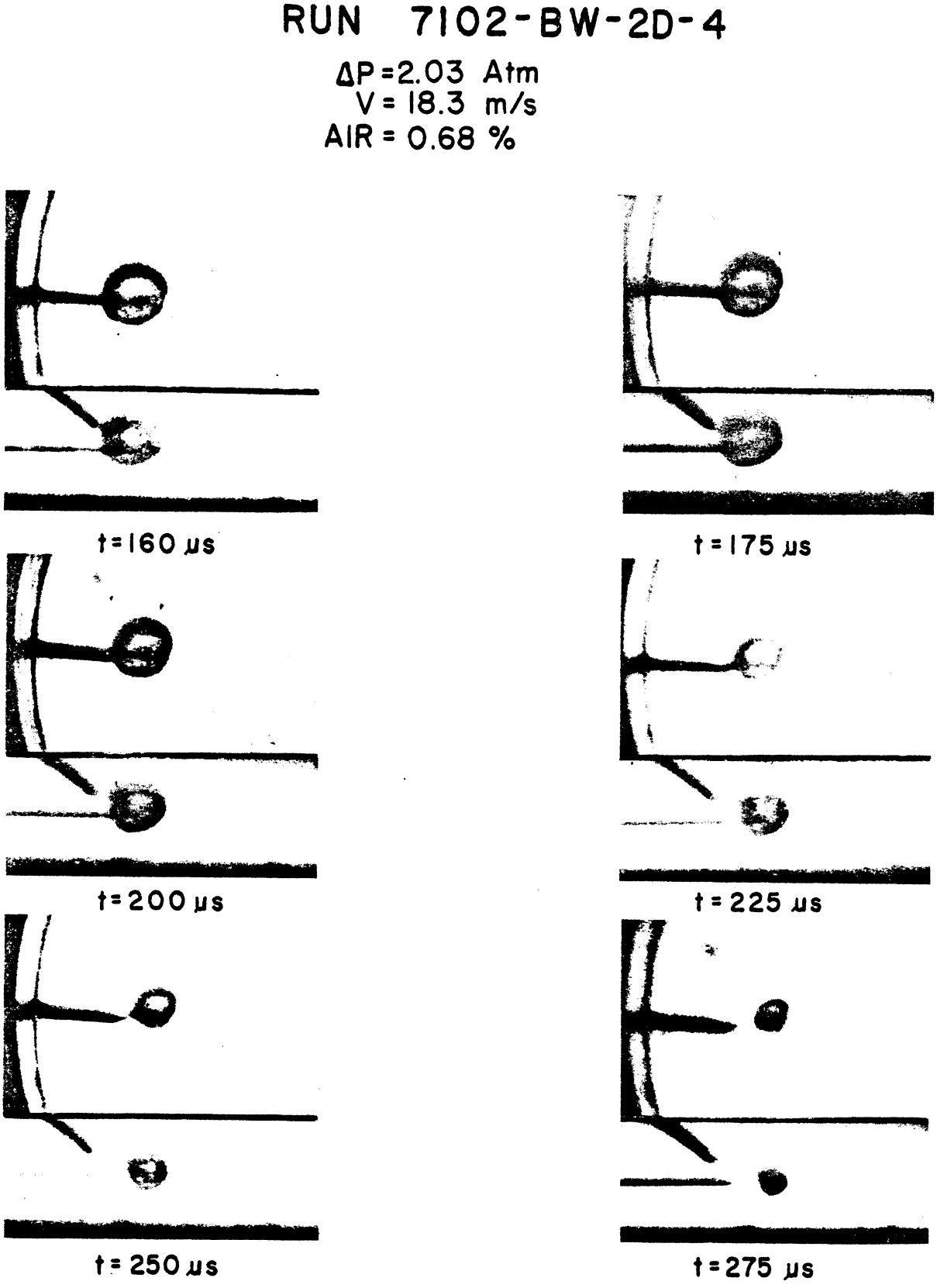

Figure 4.19 Prints, Run 7102-BW-2D-4, p. 1

4249

Timm thesis

Fig. 23 a

7102-- 4

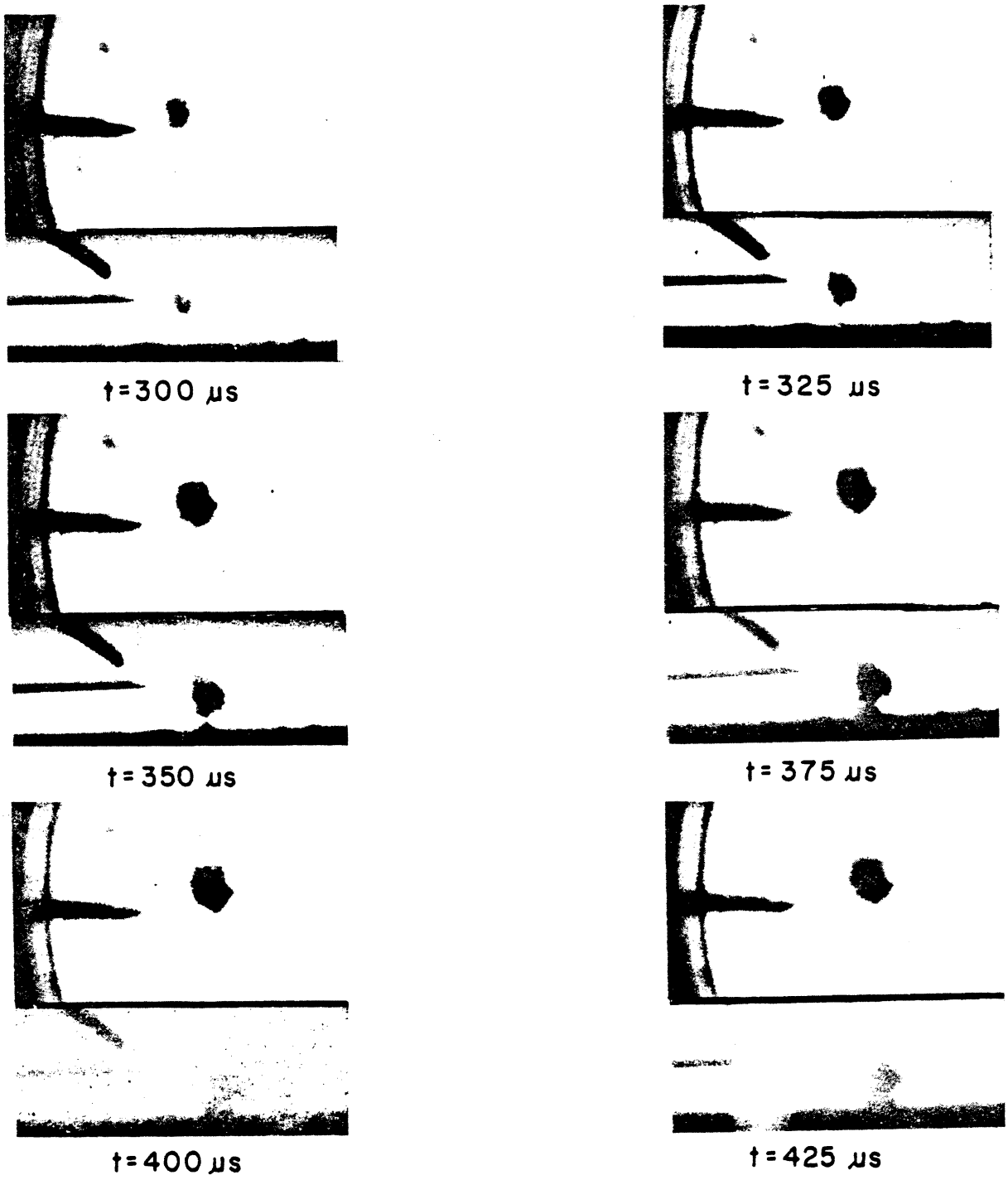

Figure 4.19 Prints, Run 7102-BW-2D-4, p. 2

4250

Timm Thesis
Fig. 23b

7102--4

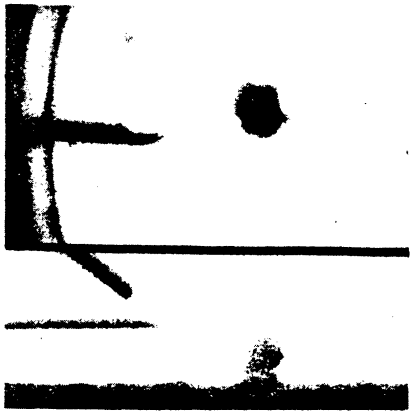

t=450 μs

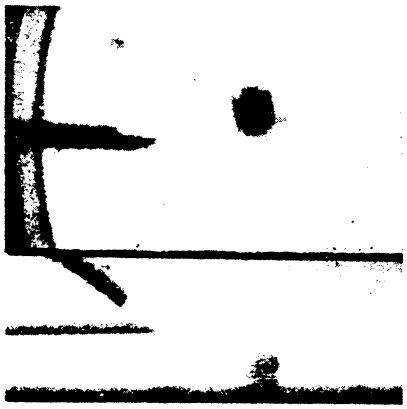

t=475 μs

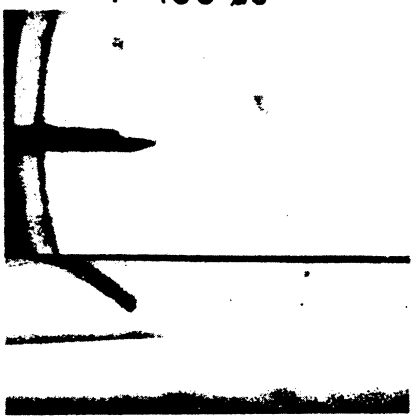

t=500 μs

Figure 4.19 Prints, Run 7102-BW-2D-4, p. 3

4251

Timm Thesis

Fig. 23c

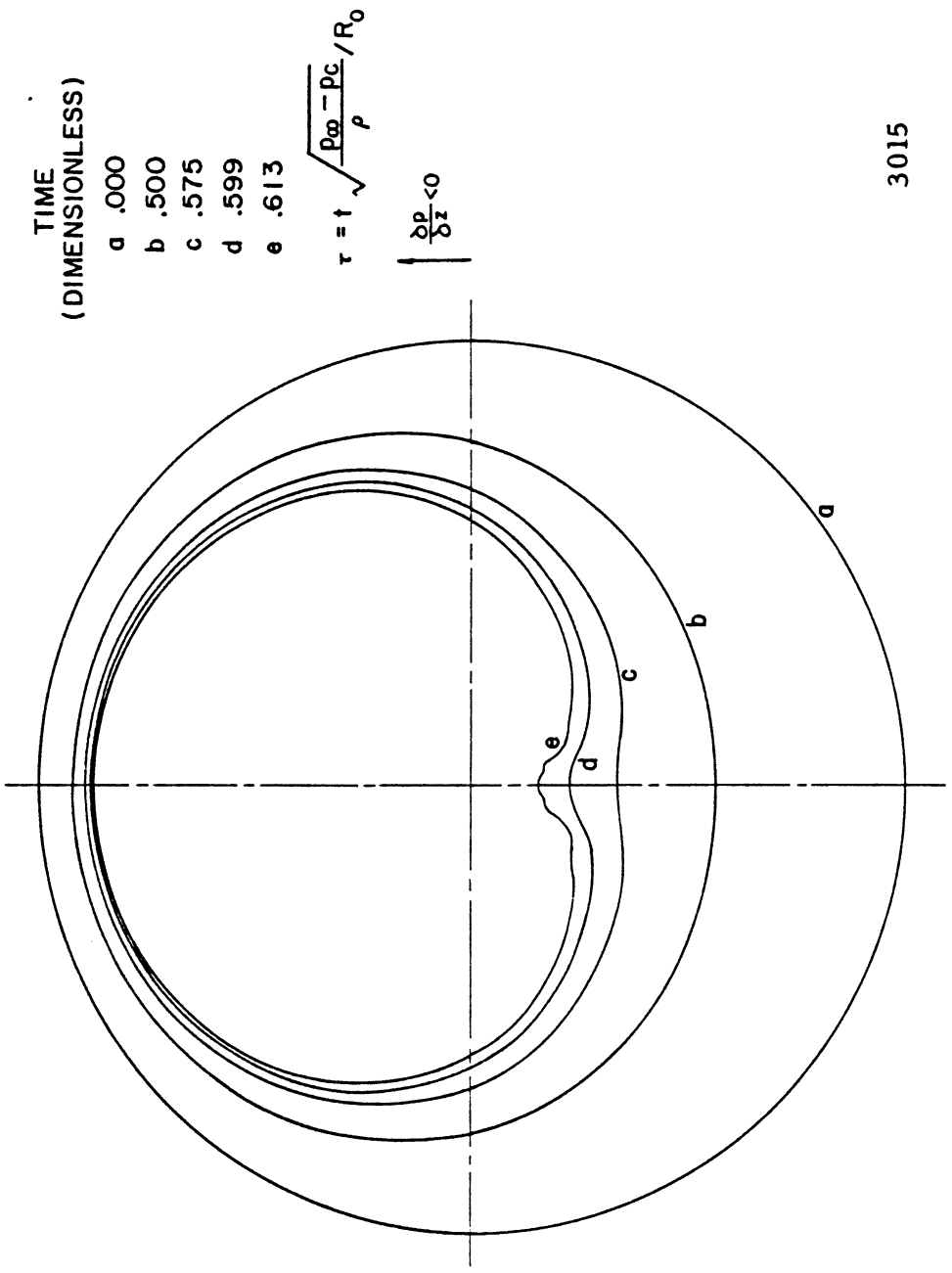

Figure 16. Bubble Surface Profiles for Initially Spherical Bubble in Linear Pressure Gradient, $\sigma = 0.57$

Mitchell thesis

Fig. 24

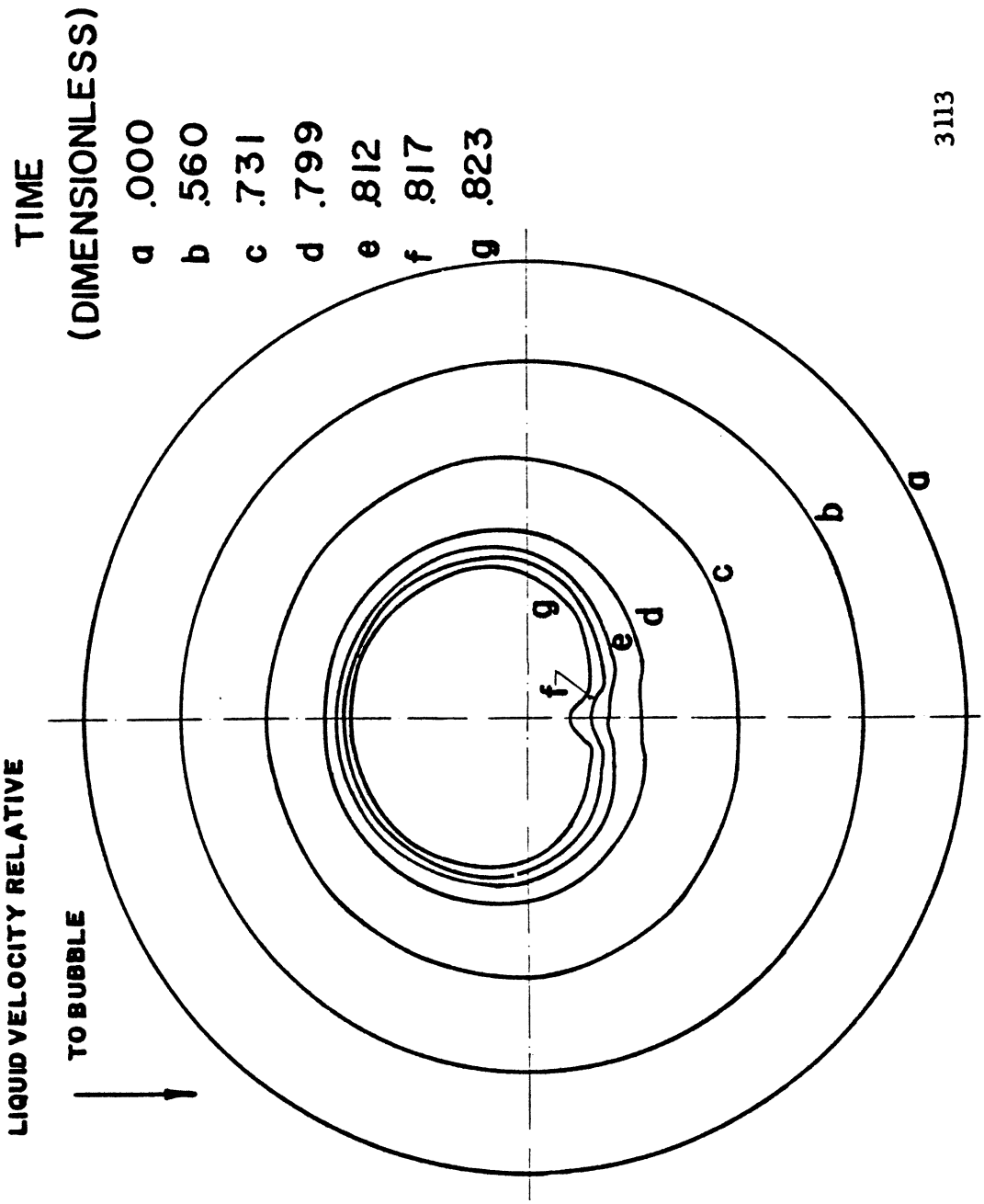

Figure 22. Bubble Surface Profiles for Initially Spherical Bubble Moving Relative to Surrounding Liquid, $V_\infty = 0.1515$

Mitchell thesis

Fig 25

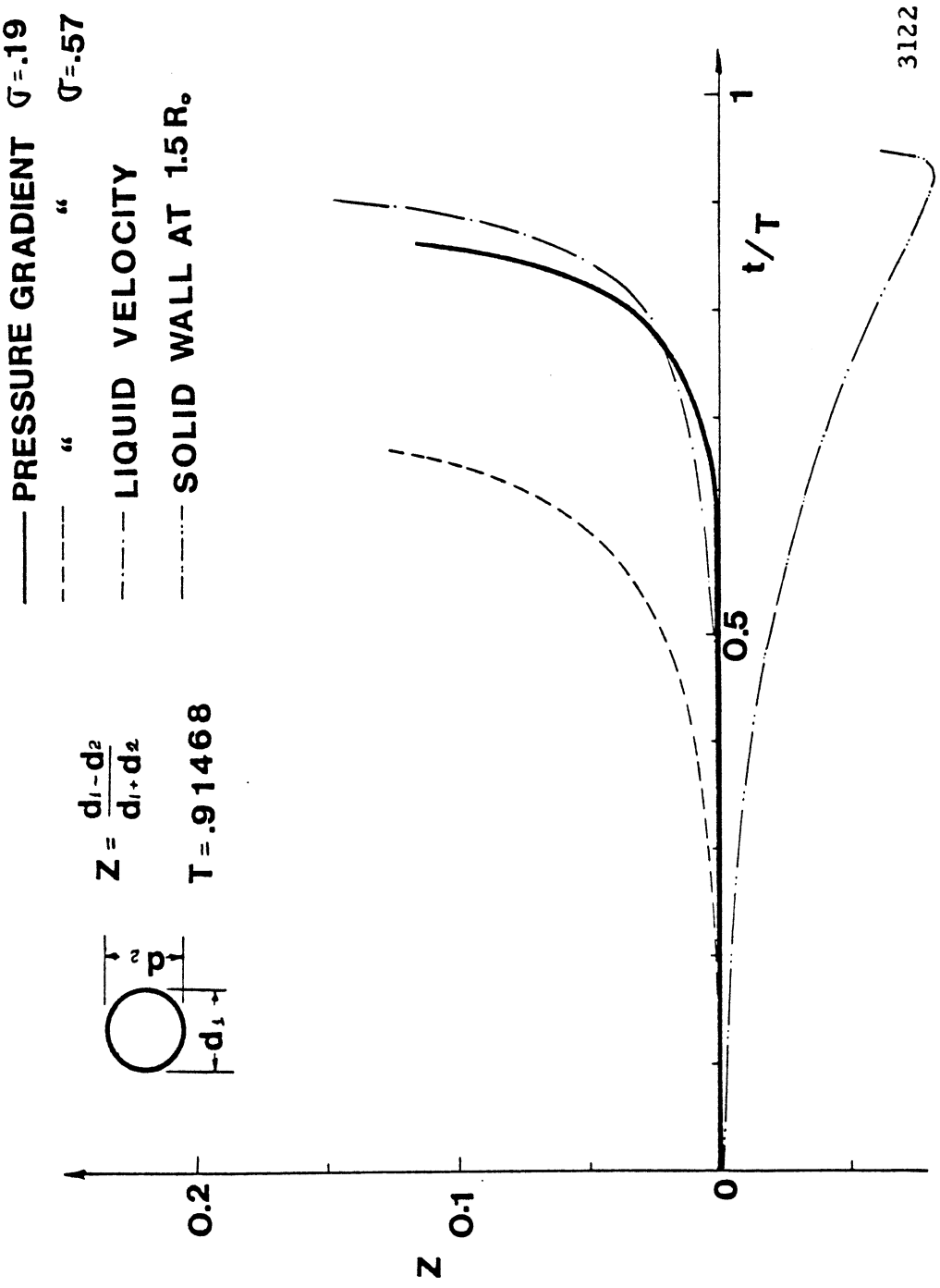

Figure 29. Comparison of Distortions of Initially Spherical Bubbles Collapsing under the Various Asymmetric Conditions

Mitchell thesis

Fig. 26

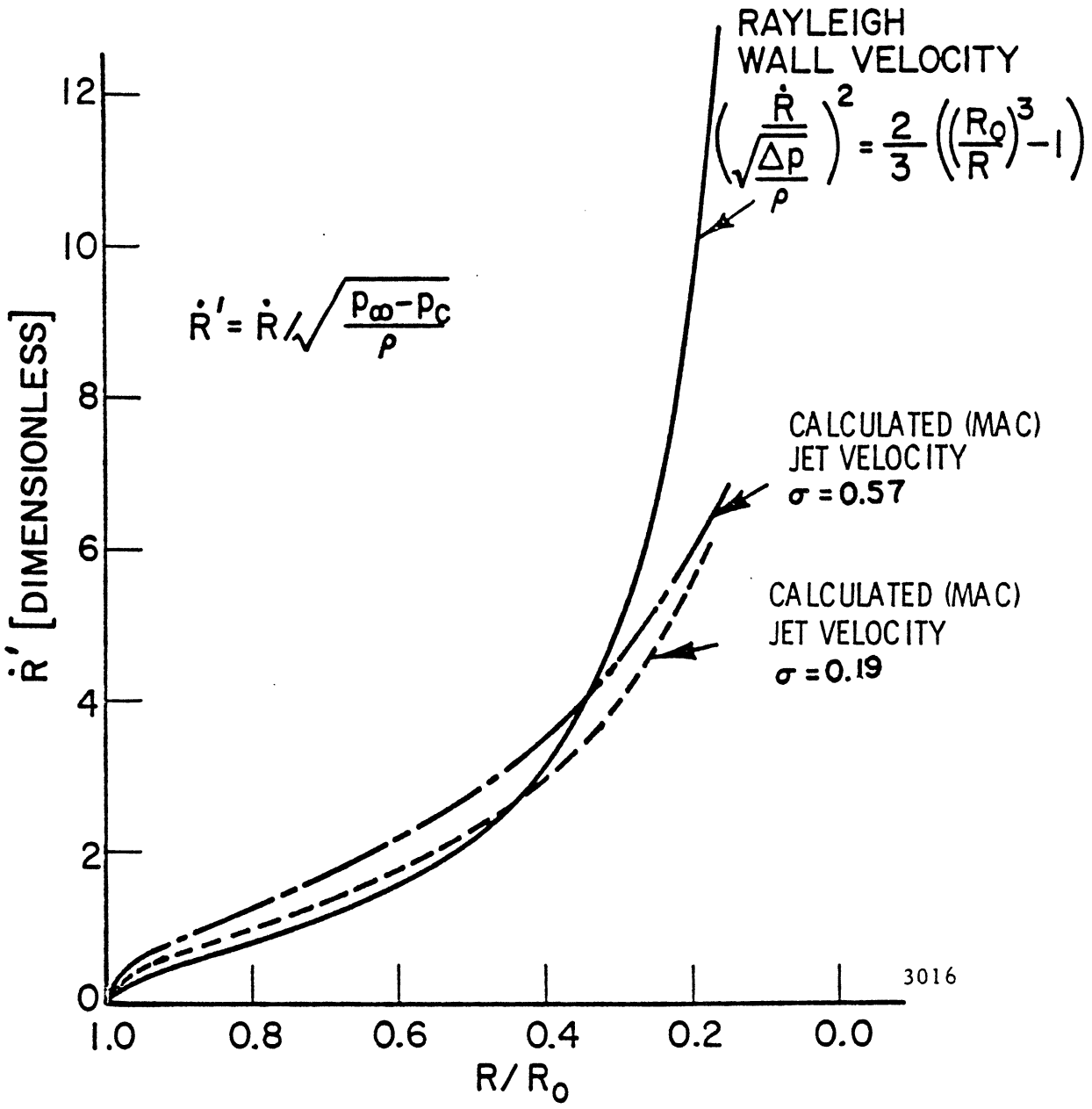

Figure 21. Jet Velocity as Function of Radial Position for Bubbles Collapsing in Linear Pressure Gradients

Mitchell thesis

Fig. 27

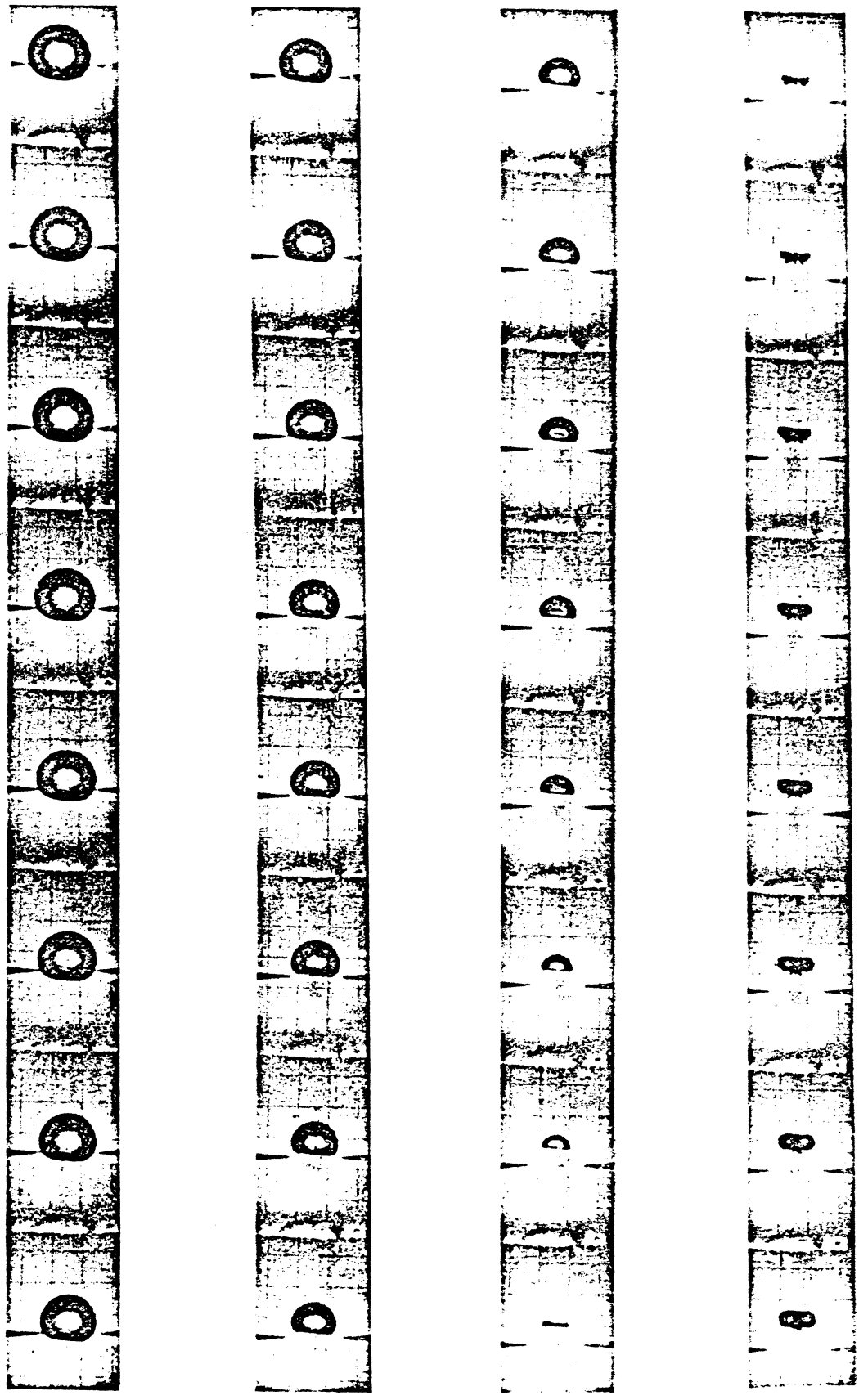

3146

Figure 18. High-Speed (2500 frames/sec) Photographs of Initially Spherical Bubble Collapsing and Rebounding in Linear Pressure Gradient, σ = 0.186 (from Ref. 50)

Mitchell thesis
Fig. 28

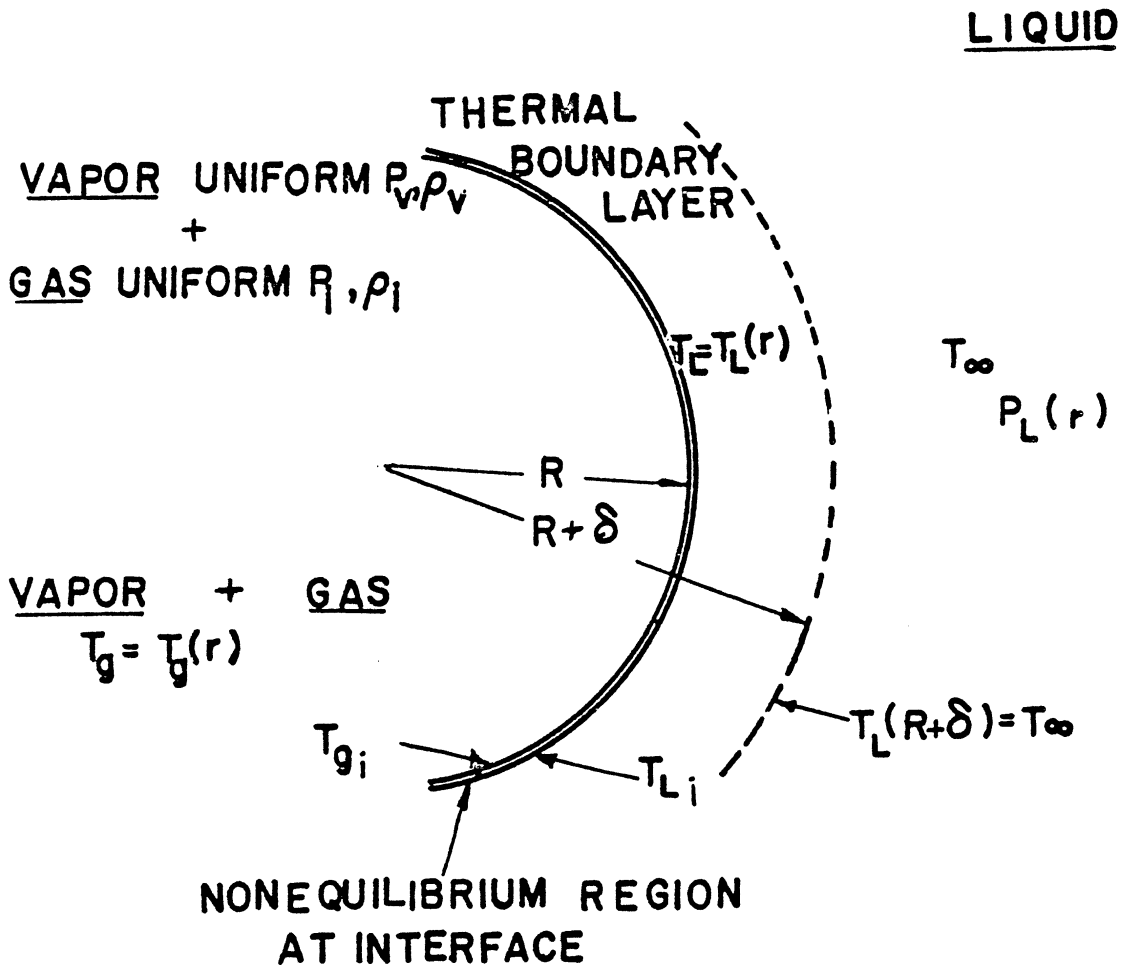

Figure 31(a). Location of Variables for Thermodynamic Effects Study

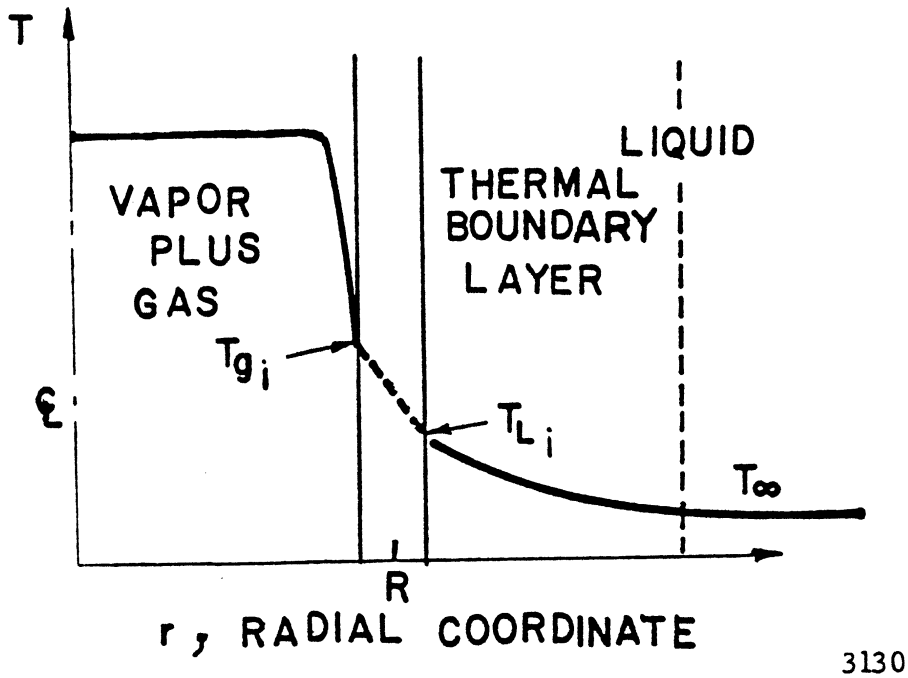

Figure 31(b). Sample Temperature Profile During Collapse

Mitchell Thesis Fig. 29

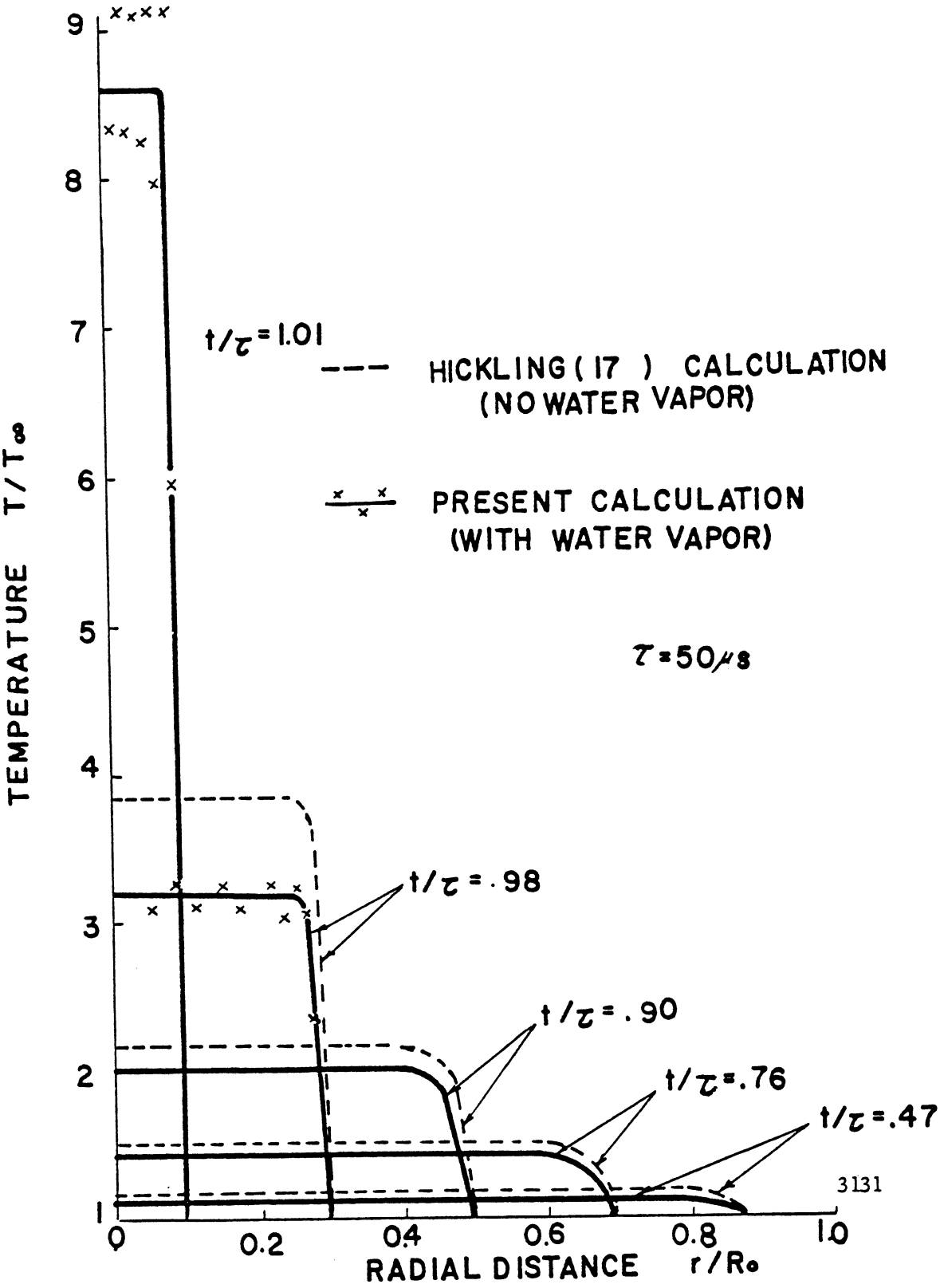

Figure 32. Internal Temperature Distributions at Different Radii for Bubbles Containing Nitrogen Gas with and without Water Vapor; $\alpha = 0.1$, $p_{i_o} = 0.075$ atm., $p_{v_o} = 0.0277$ atm., $\Delta p = 2.925$ atm., $R_o = 0.1$ cm., $T_o = 528^\circ$R.

Mitchell thesis

Fig. 30

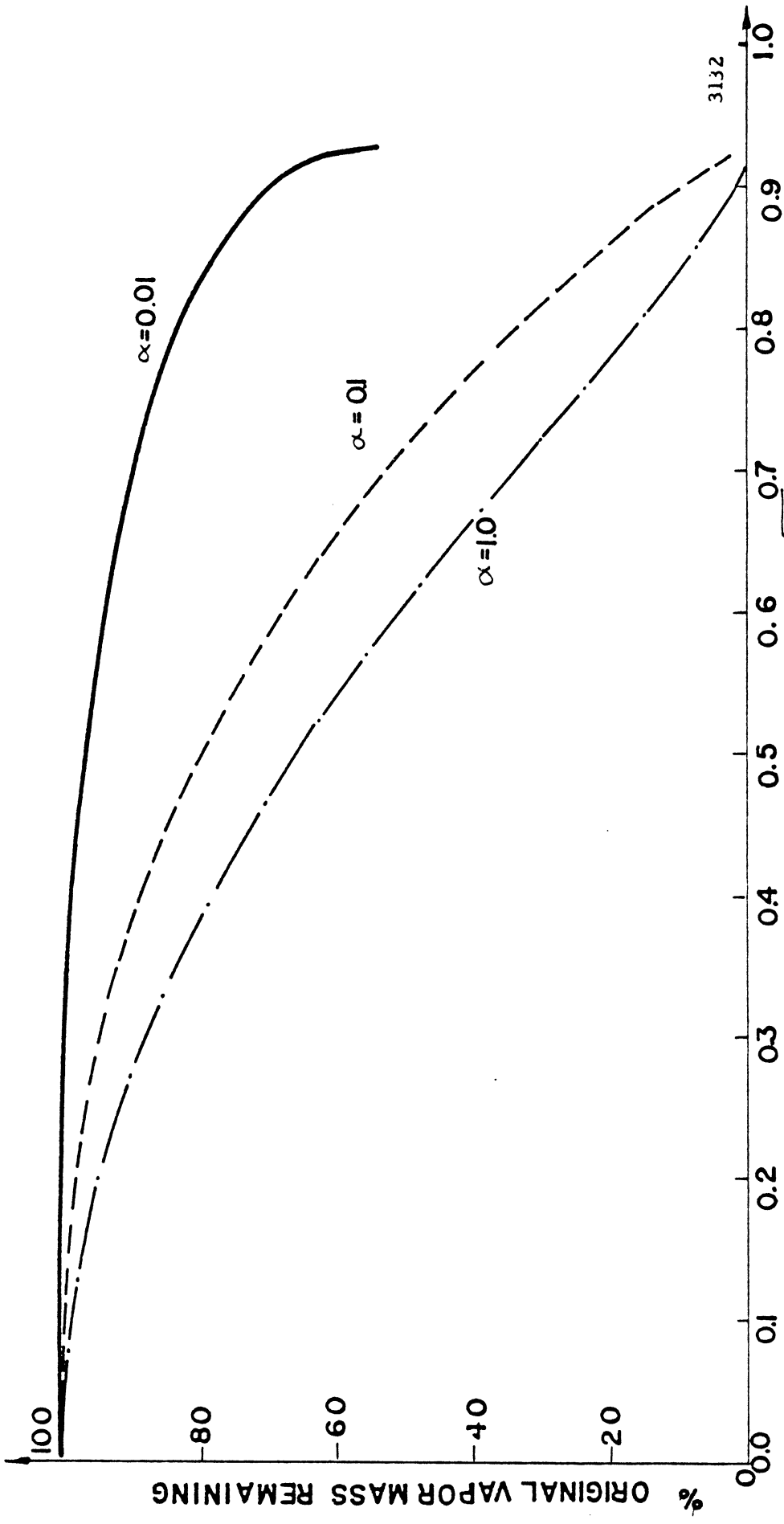

Figure 33. Effect of Evaporation Coefficient α on Quantity of Vapor Condensed During Bubble Collapse; "Standard" Bubble: $R_o = 50 \times 10^{-3}$ in., $T_o = 537^oR$, $Pi_o = 10^{-3}$ atm., $p_{v_o} = .0277$ atm., $p_\infty = 1$ atm.

Mitchell thesis Fig. 31

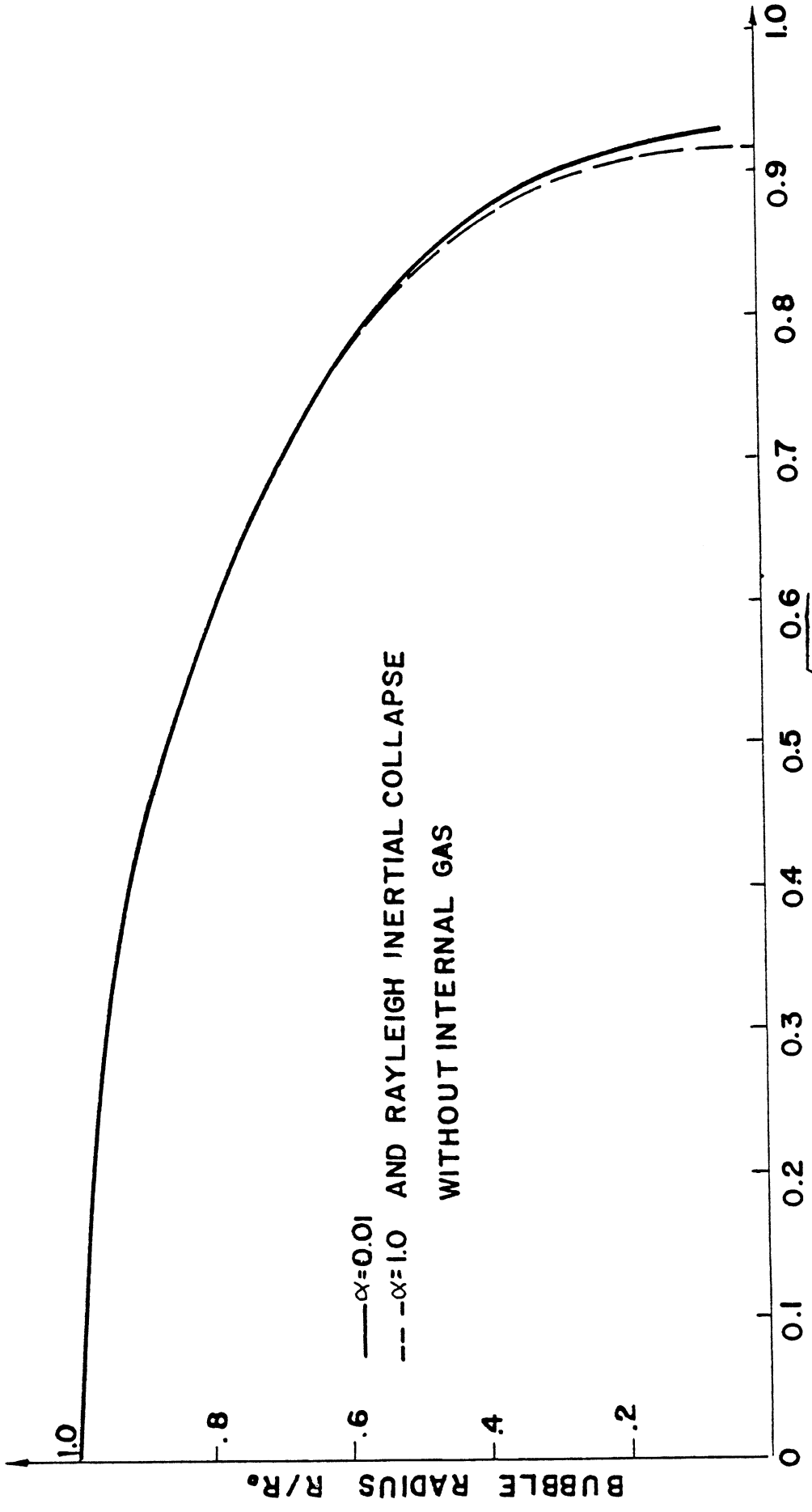

3133

Figure 34. Effect of Evaporation Coefficient α on Bubble Radius Change with Time for "Standard" Bubble (see Fig. 33)

Mitchell thesis Fig. 32

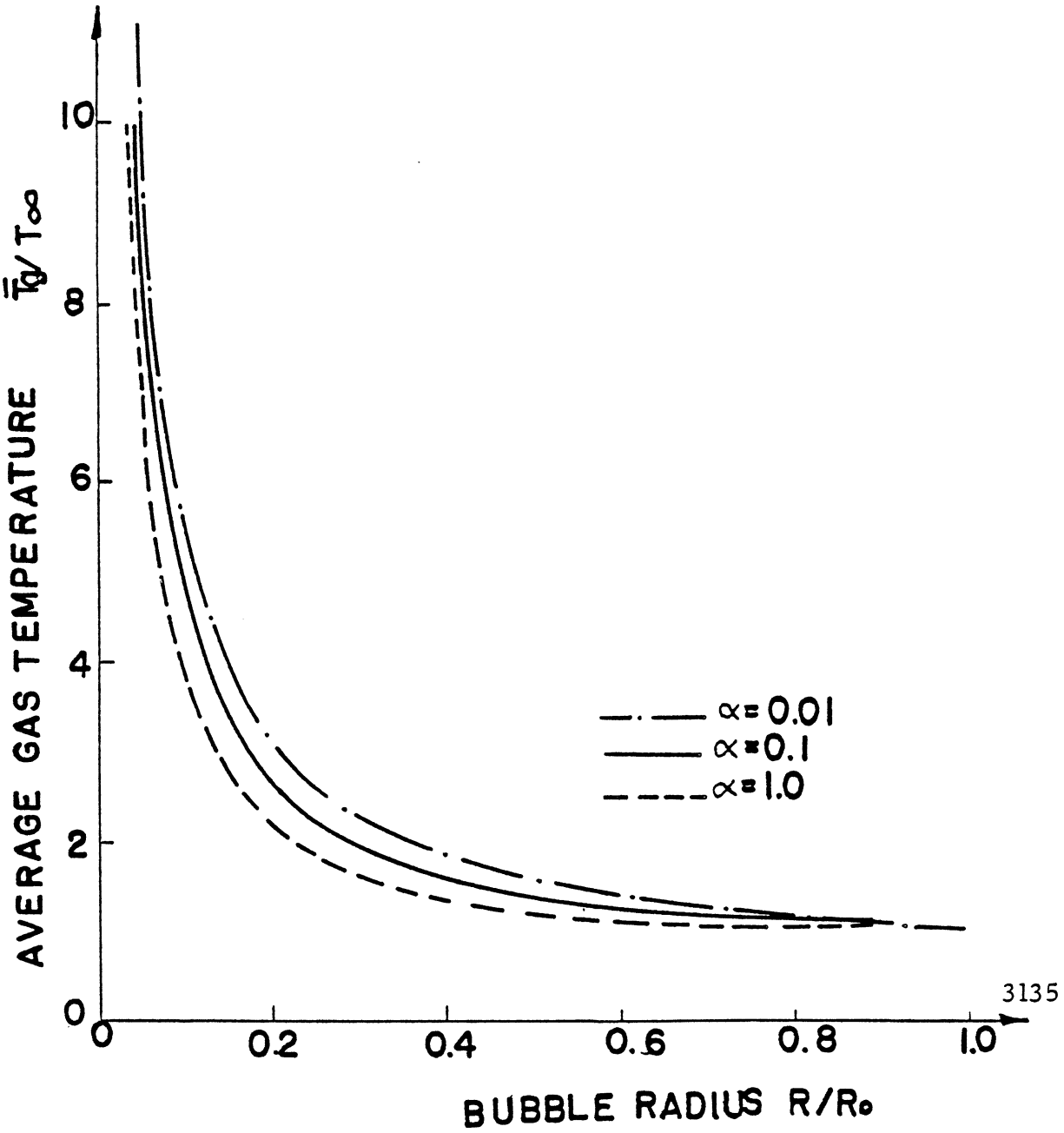

Figure 36. Effect of Evaporation Coefficient α on Average Internal Temperature Change with Radius for "Standard" Bubble (see Fig. 33)

Mitchell thesis

Fig. 33

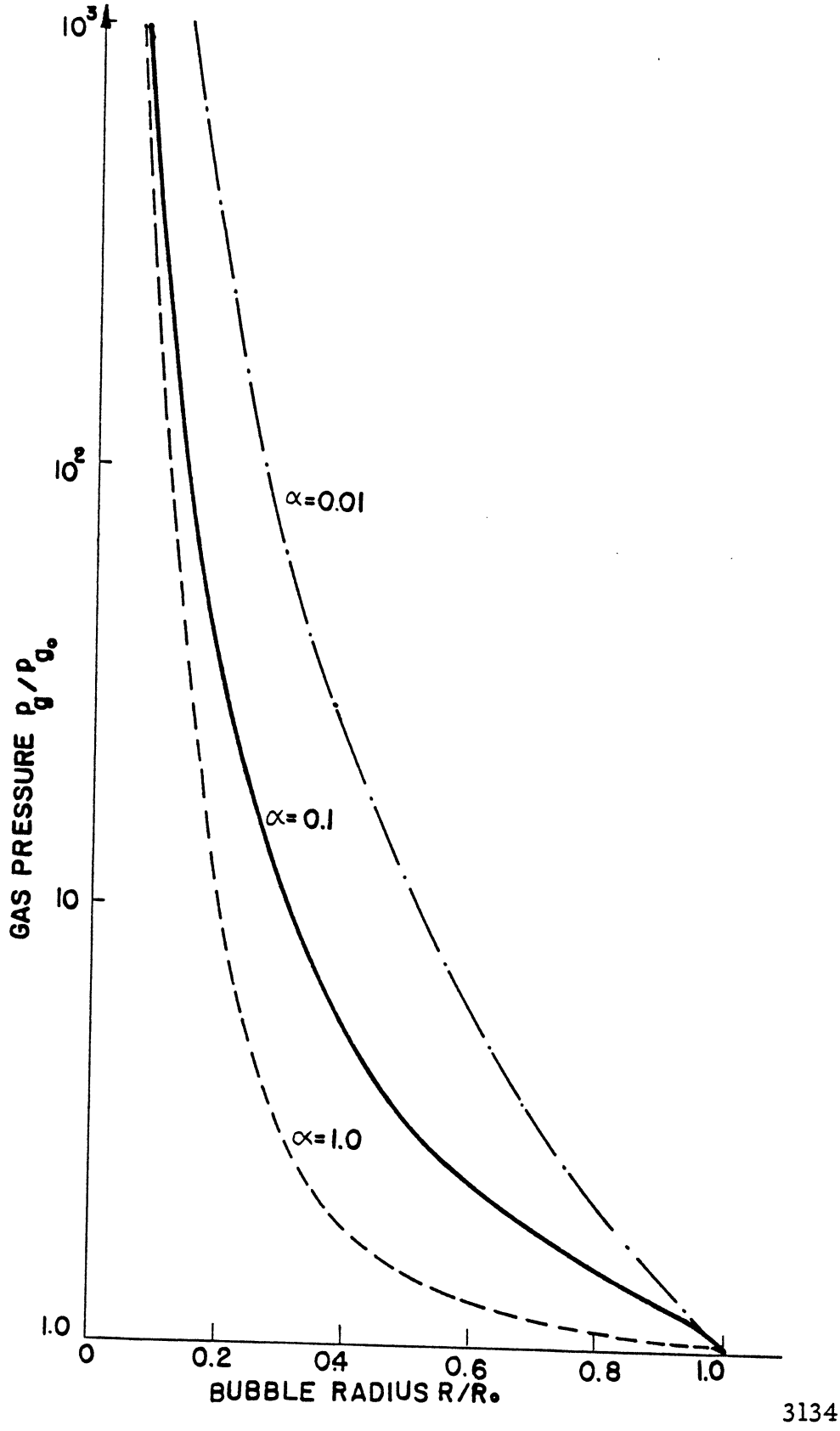

Figure 35. Effect of Evaporation Coefficient α on Internal (Gas + Vapor) Pressure Change with Radius for "Standard" Bubble (see Fig. 33)

Mitchell thesis

Fig. 34

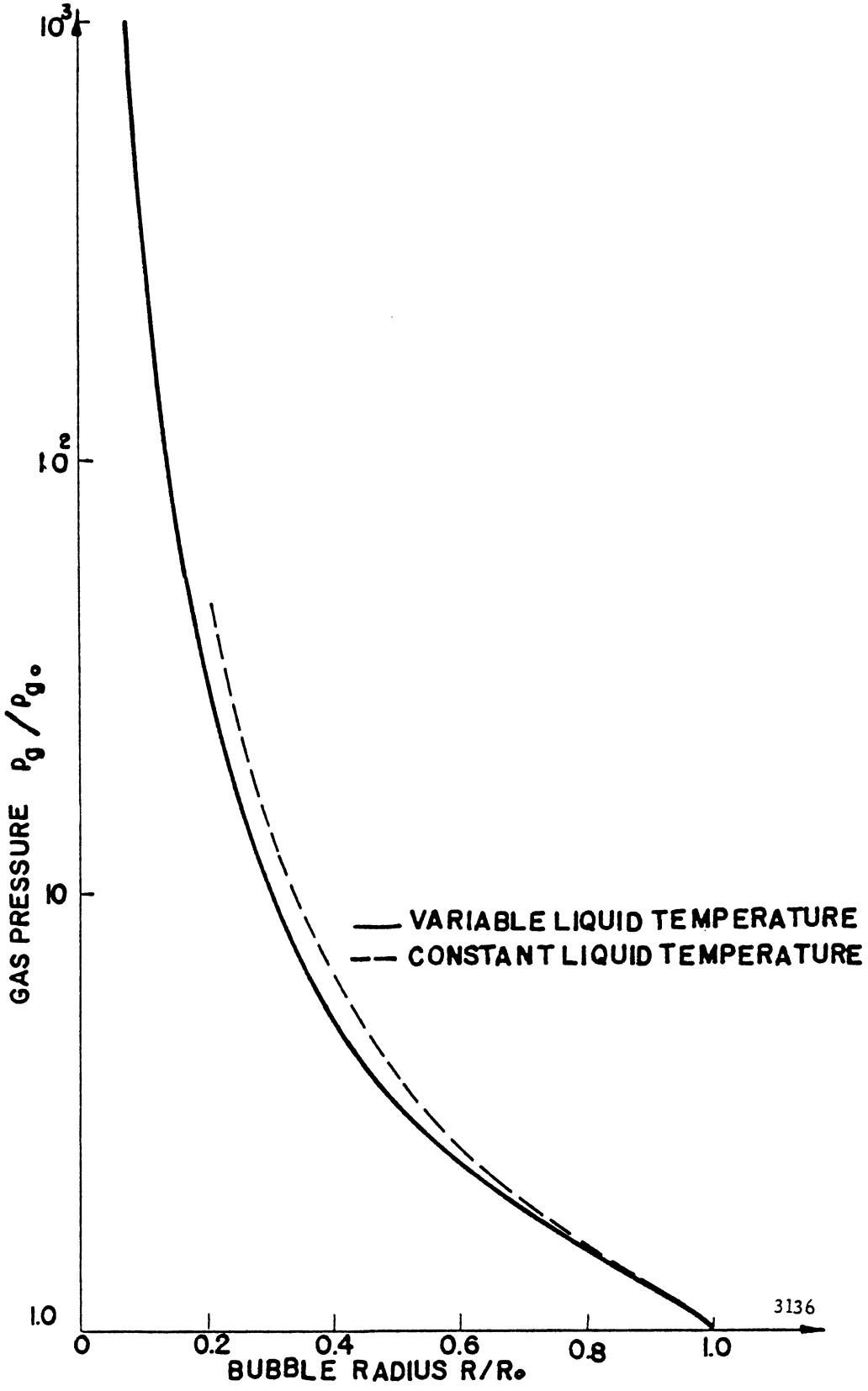

Figure 37. Effect of Assumption of Constant Temperature in Liquid on Internal (Gas + Vapor) Pressure Change with Radius for "Standard" Bubble (see Fig. 33) $\alpha = 0.1$

Mitchell thesis
Fig. 35

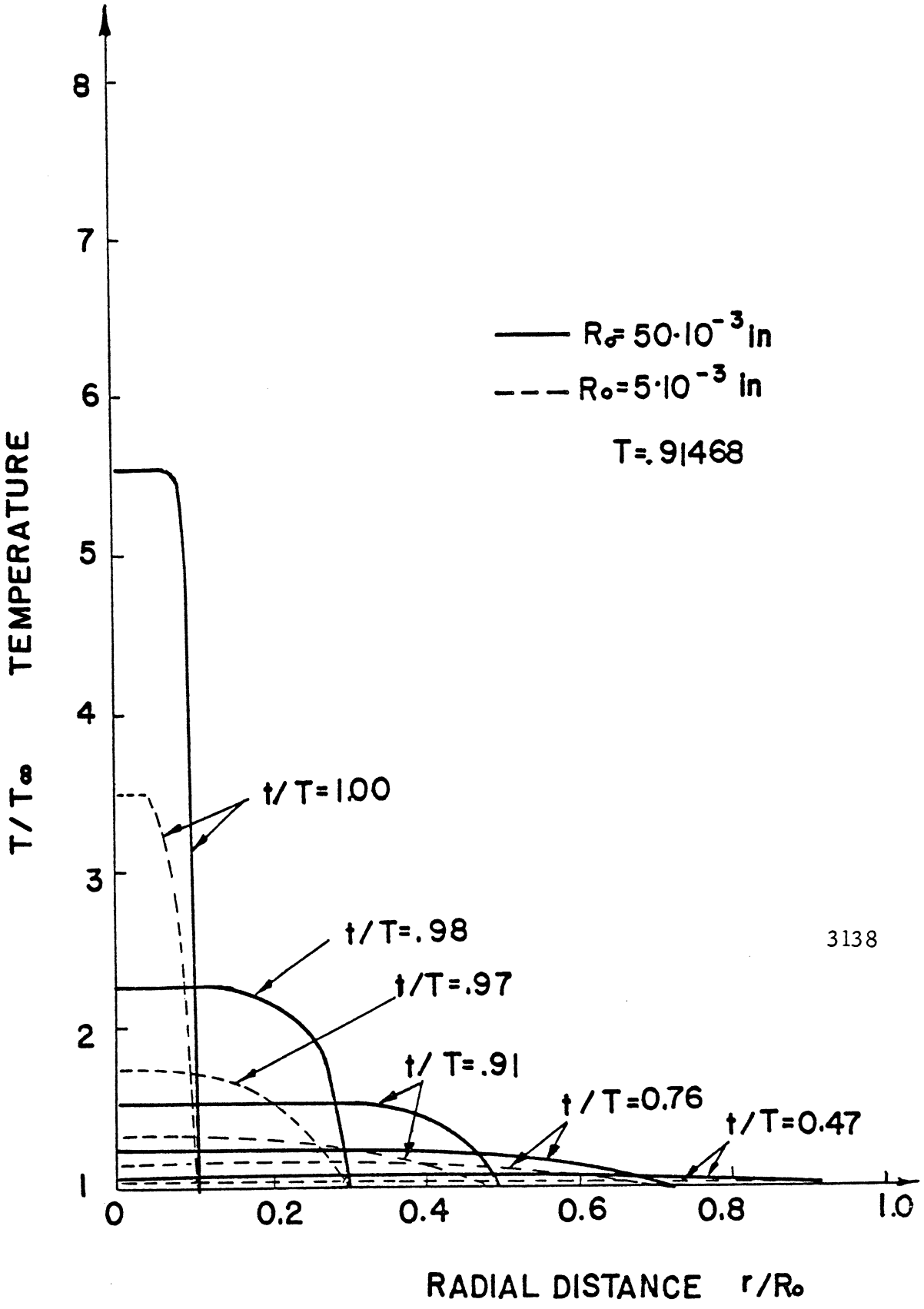

Figure 39. Internal Temperature Distributions at Different Stages of Collapse for "Standard" Bubbles (see Fig. 33) with Different Initial Radii, α = 0.1

Mitchell thesis
Fig. 36

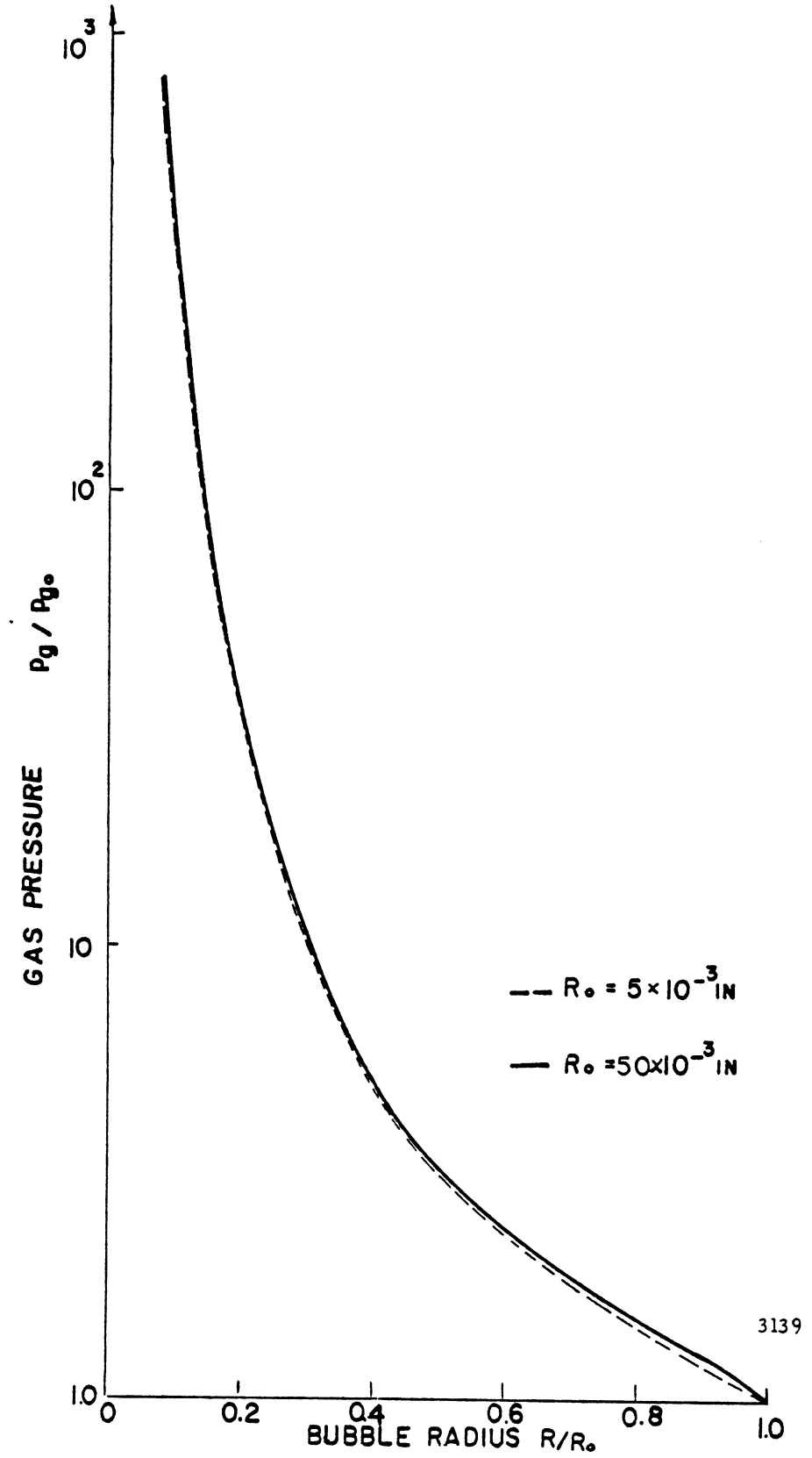

Figure 40. Effect of Initial Bubble Radius on the Internal (Gas + Vapor) Pressure History During Collapse of Otherwise "Standard" Bubbles (see Fig. 33), $\alpha = 0.1$

Mitchell Thesis

Fig. 37

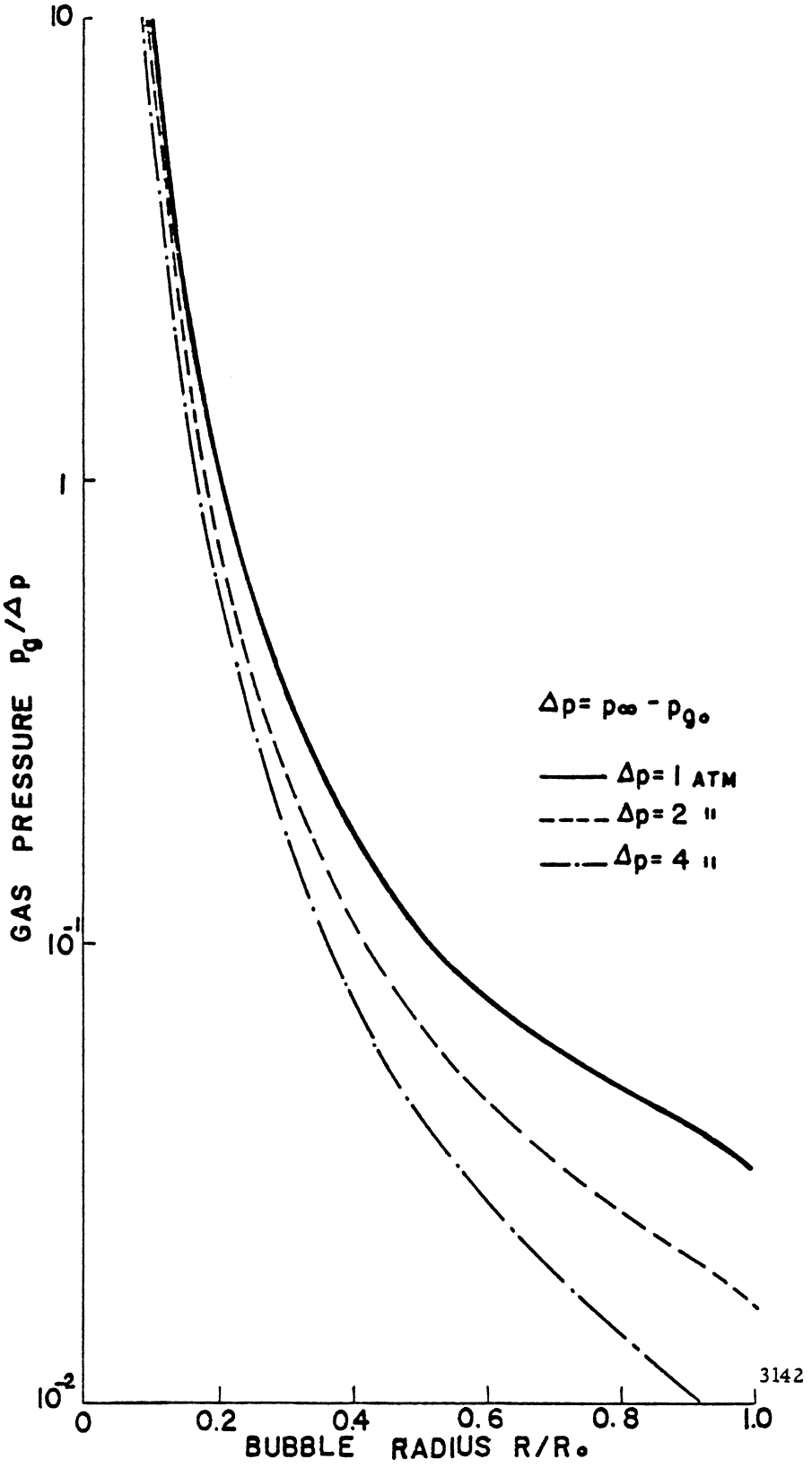

Figure 43. Effect of Overpressure (Δp) on the Dimensionless Internal (Gas + Vapor) Pressure History of Collapsing Bubbles, $R_o = 50 \times 10^{-3}$ in., $T_o = 537^oR$, $p_{i_o} = 10^{-3}$ atm., $p_{v_o} = .0277^o$atm., $\alpha = 0.1$

Mitchell thesis

Fig. 38

3) Increased NPSH causes a strong increase of age in this type of facility up to at least 4 atm. H. Obviously, damage must maximize at some higher H and then decrease to near zero, since the number size of bubbles decreases with increasing NPSH ough their collapse violence increases), reaching at sufficiently high NPSH, depending upon facility quency and amplitude.

owledgements

Financial support provided by: National Science dation, Grant No. GK 1889, Westinghouse Electric oration, and Worthington Pump International.

rences

. G. Hammitt and D. O. Rogers, "Effects of Pres-ure and Temperature Variation in Vibratory Cavita-ion Damage Test", Journal Mech. Engr. Sci., 12, 6, 970, 432-439.

2. R. Garcia, "Comprehensive Cavitation Damage Data for Water and Various Liquid Metals Including Correlations with Material and Fluid Properties", Ph.D Thesis, Nucl. Engr. Dept., University of Mich., Aug. 1966; see also Garcia-Hammitt, Trans, ASME, J. Basic Engr., 89, 1967.

3. F. G. Hammitt, discussion of Reference 4.

4. S. G. Young and J. R. Johnston, "Effect of Temperature and Pressure on Cavitation Damage in Sodium", ASTM STP 474, 67-103, 1967.

5. J. M. Hobbs and A. Laird, "Pressure, Temperature and Gas Content Effects in the Vibratory Cavitation Erosion Test", 1969 Cavitation Forum, ASME pp. 3-4.

Ref. 75

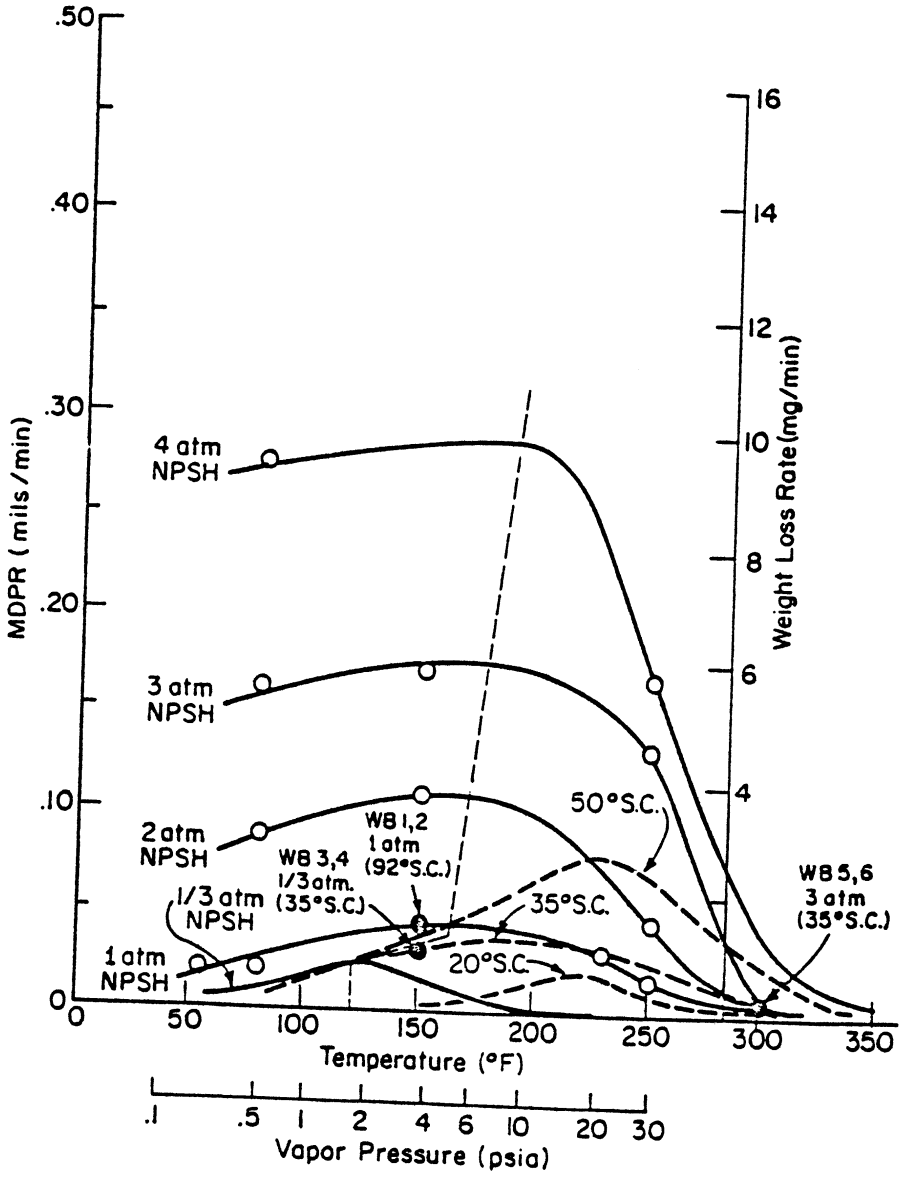

Figure 39 Maximum MDPR Versus Temperature and Vapor Pressure for Bearing Brass (SAE-660)

Hammitt, Bhatt

Cavitation Forum 1972

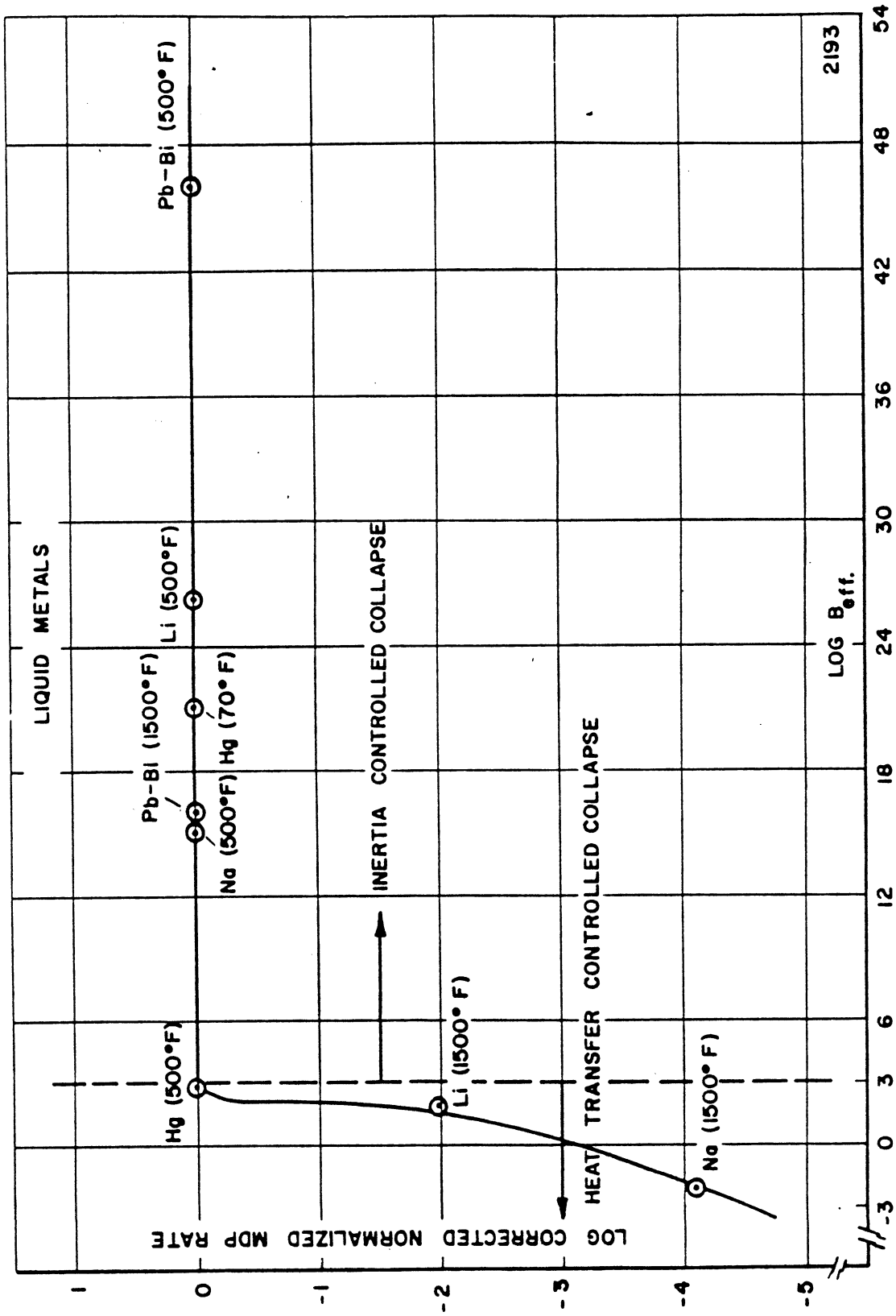

Fig. 40

Fig. 82.--Effect of thermodynamic parameter on cavitation damage - liquid metals

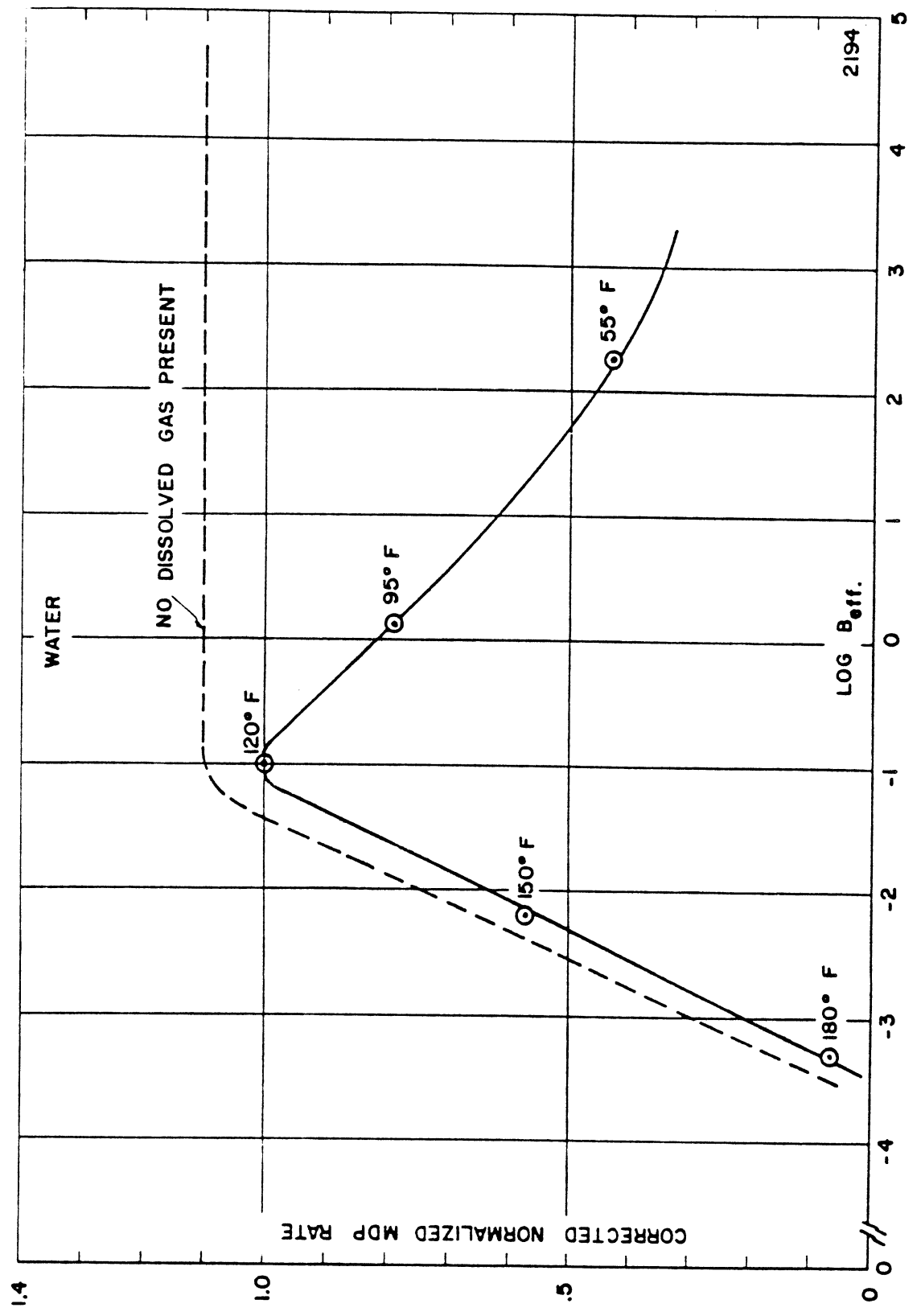

Fig. 83.--Effect of thermodynamic parameter on cavitation damage - water.

Garcia thesis

Fig. 41

Ruggeri - Penn State 1970

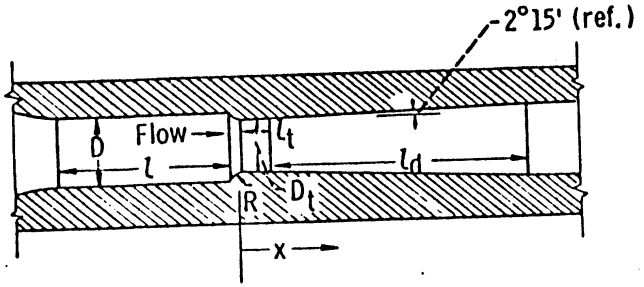

	Venturi scale	
	1.0	0.7
Free stream diameter, D	1.743	1.232
Throat diameter, D_t	1.377	0.976
Radius of curvature, R	0.183	0.128
Approach section length, l	4.198	2.964
Throat length, l_t	0.75	0.52
Diffuser length, l_d	4.66	3.26

Fig. 2 - Venturi Test Sections. All dimensions in inches.

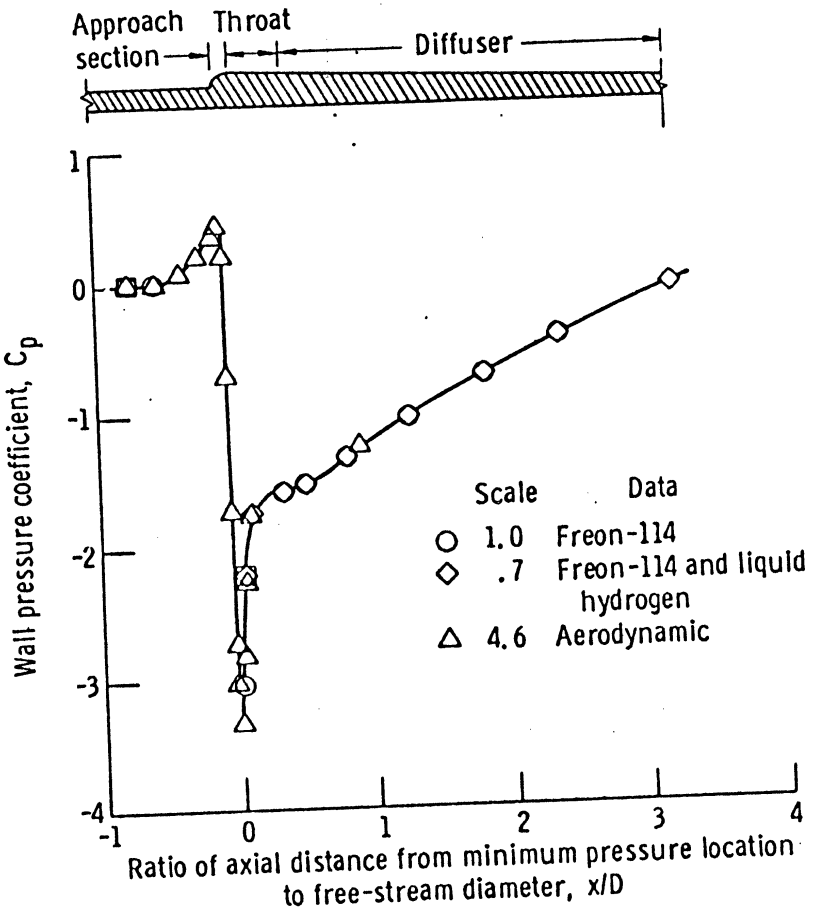

Fig. 3 - Wall Pressure Distribution for Venturis.

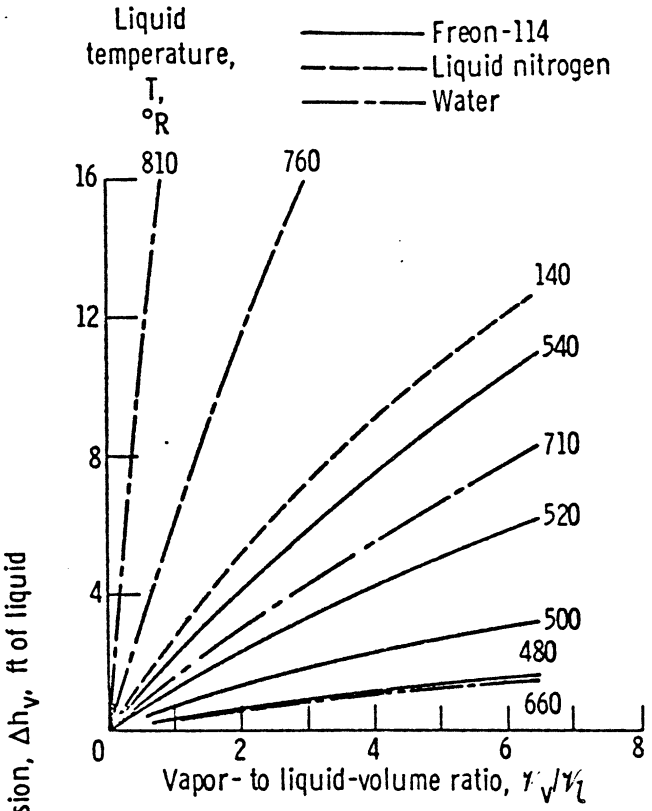

(a) Water, Liquid Nitrogen, and Freon-114.

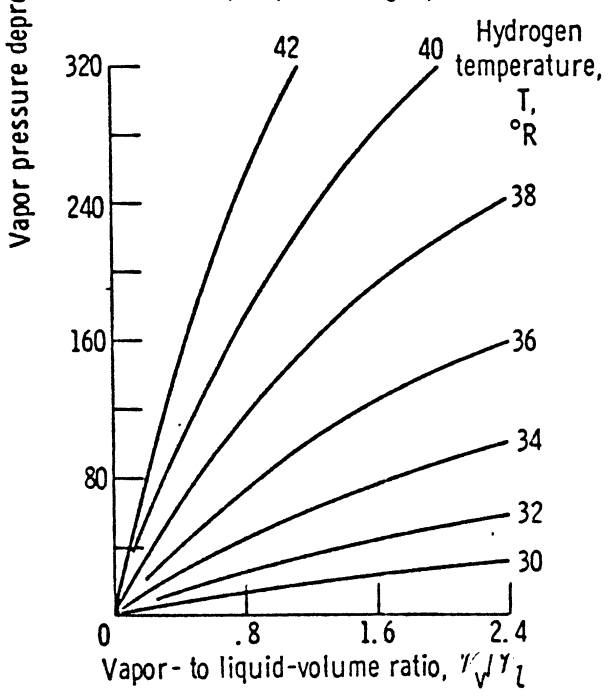

(b) Liquid hydrogen.

Fig. 1 - Vapor Pressure Depressions for Various Liquids and Liquid Temperatures.

Ruggeri Penn State 1970

F. 9.43 Chap 4

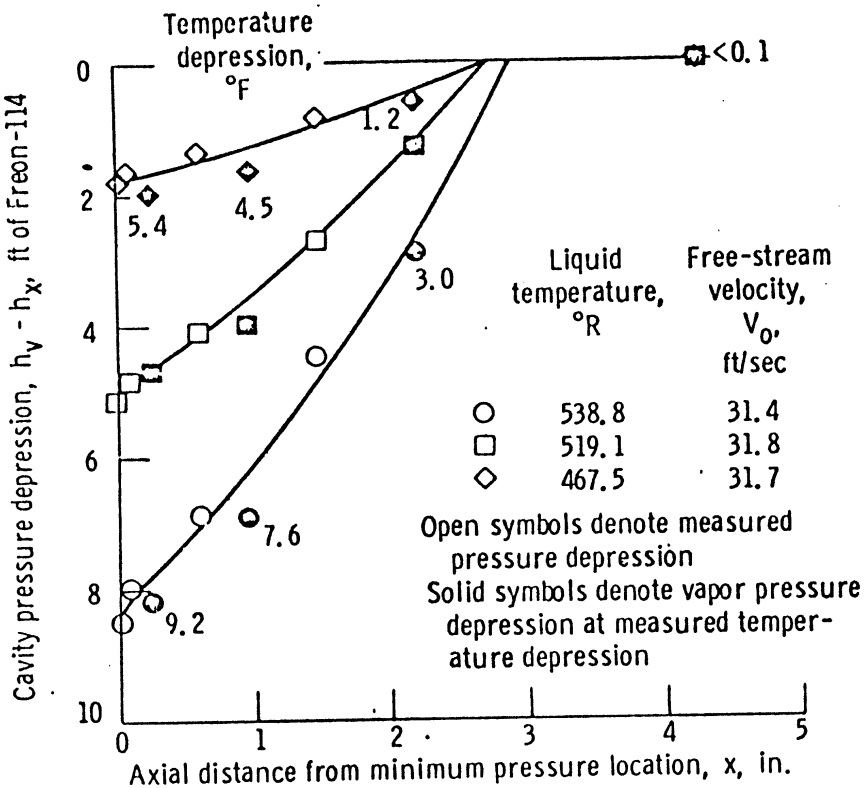

Fig. 6 - Effect of Free Stream Liquid Temperature on Cavity Pressure and Temperature Depressions. Freon-114; 1.0-Scale Venturi; Nominal Cavity Length, $2\frac{3}{4}$ Inches.

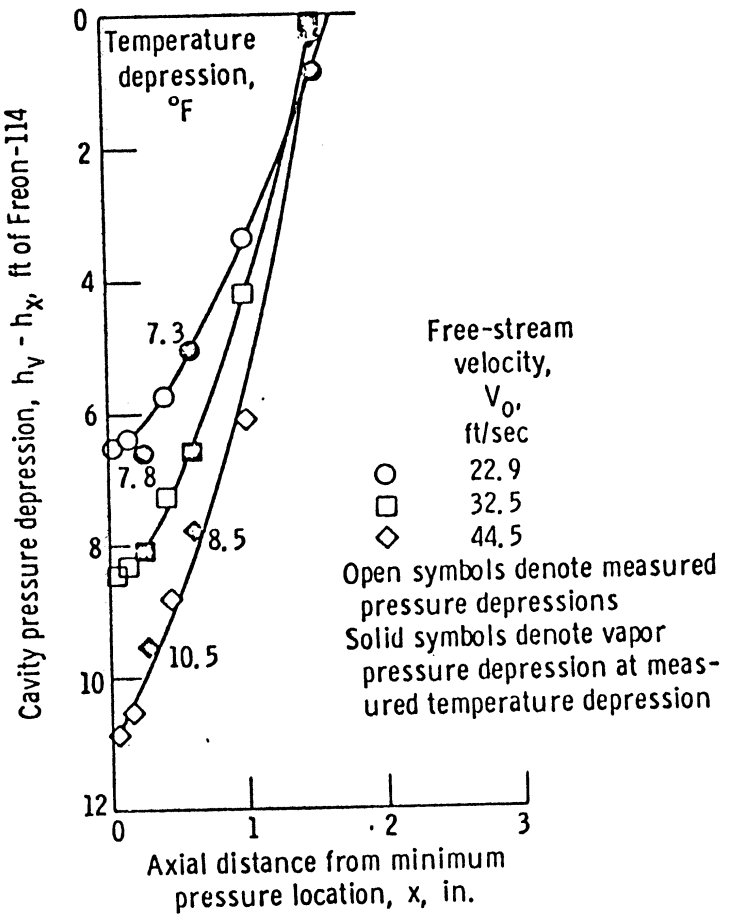

Fig. 7 - Effect of Free-Stream Velocity on Pressure and Temperature Depressions Within Cavitated Regions of Freon-114. Venturi Scale, 0.7; Liquid Temperature, 540° R; Nominal Cavity Length, 1.6 Inches.

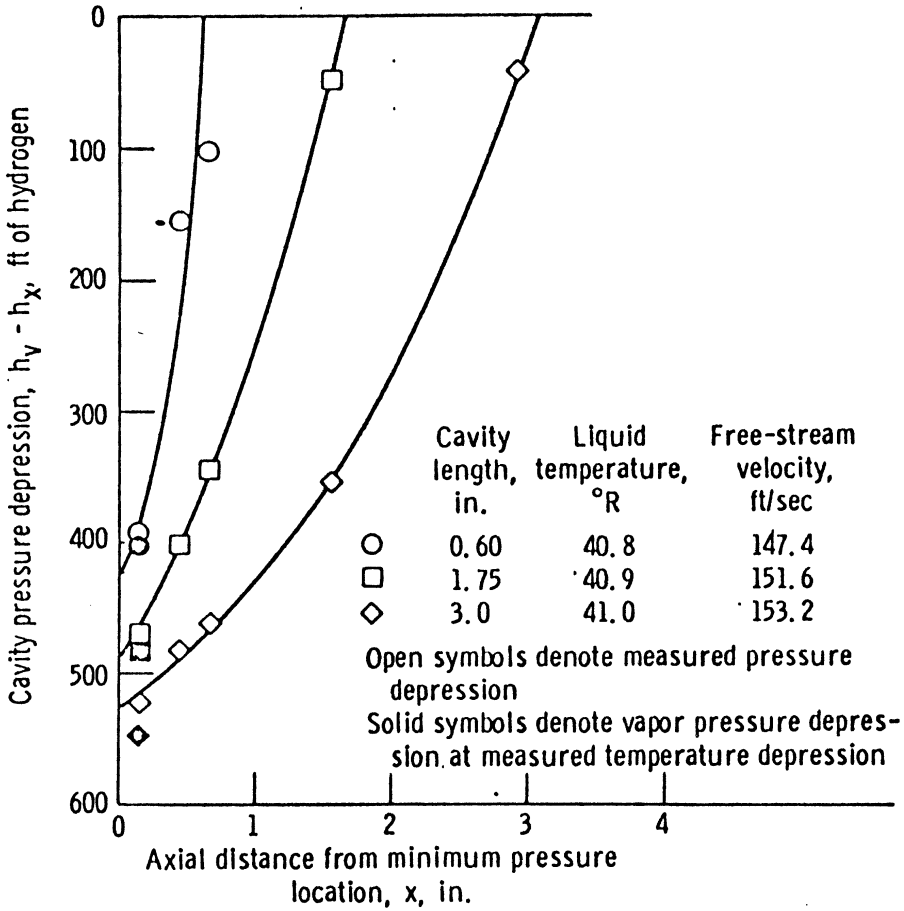

Fig. 8 - Effect of Cavity Length on Cavity Pressure Depression. Liquid Hydrogen; 0.7-Scale Venturi.

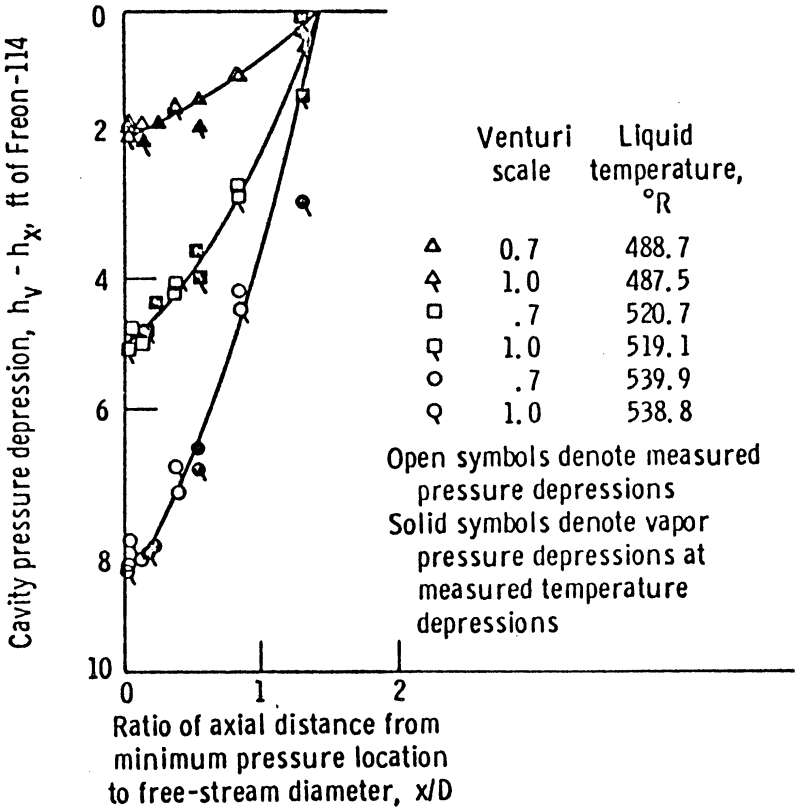

Fig. 9 - Effect of Venturi Scale on Pressure and temperature Depressions Within Cavitated Regions of Freon-114. Cavity Length, 1.4 Free-Stream Diameters.

Fig 45 Chap IV

Sodium MP 97.5 C
BP 1020°C @ 3

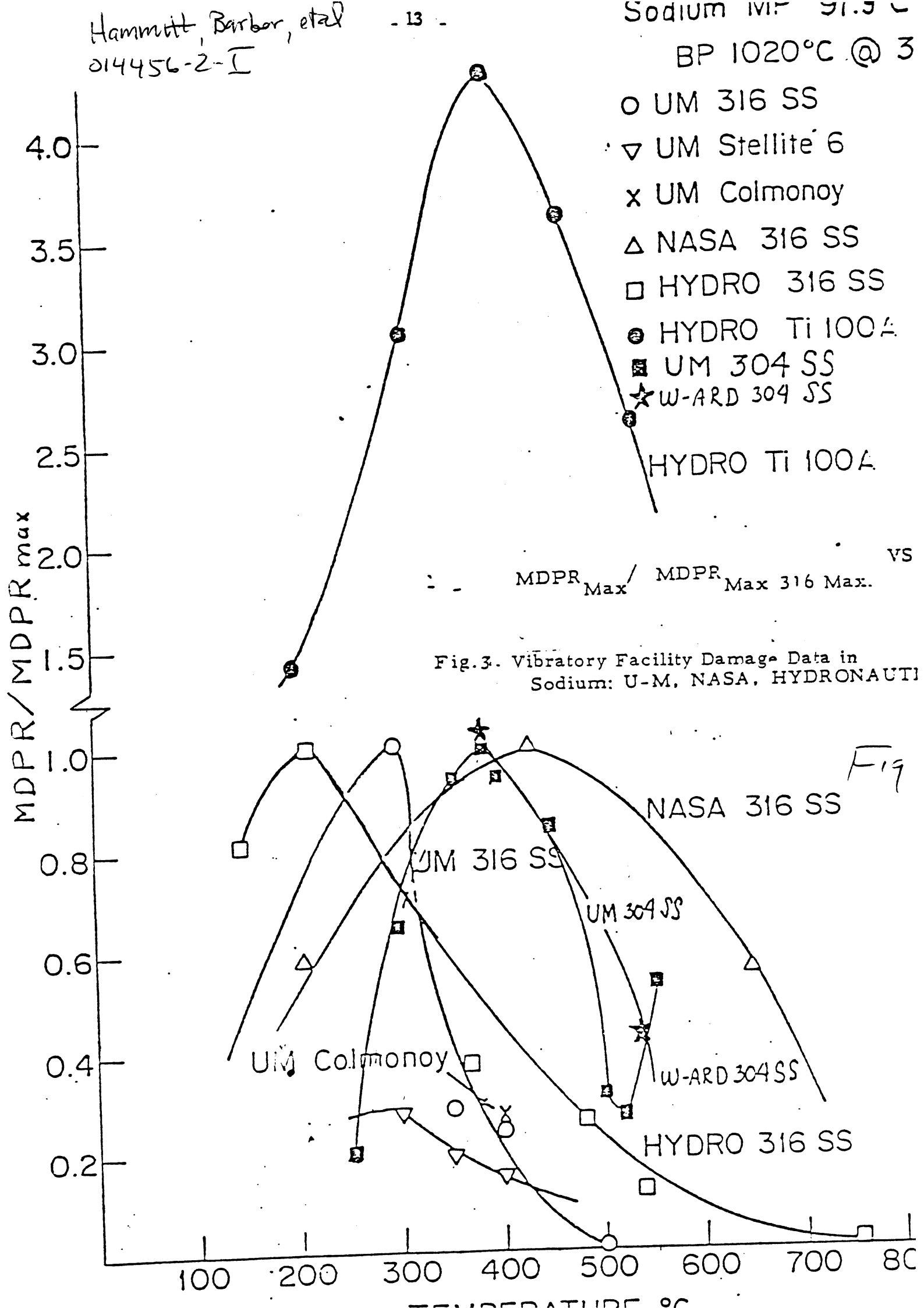

vs

$MDPR_{Max}$ / $MDPR_{Max\ 316\ Max.}$

Fig.3. Vibratory Facility Damage Data in Sodium: U-M, NASA, HYDRONAUTI

Fig

Figure 4

WEIGHT LOSS VS TEMPERATURE

for SODIUM

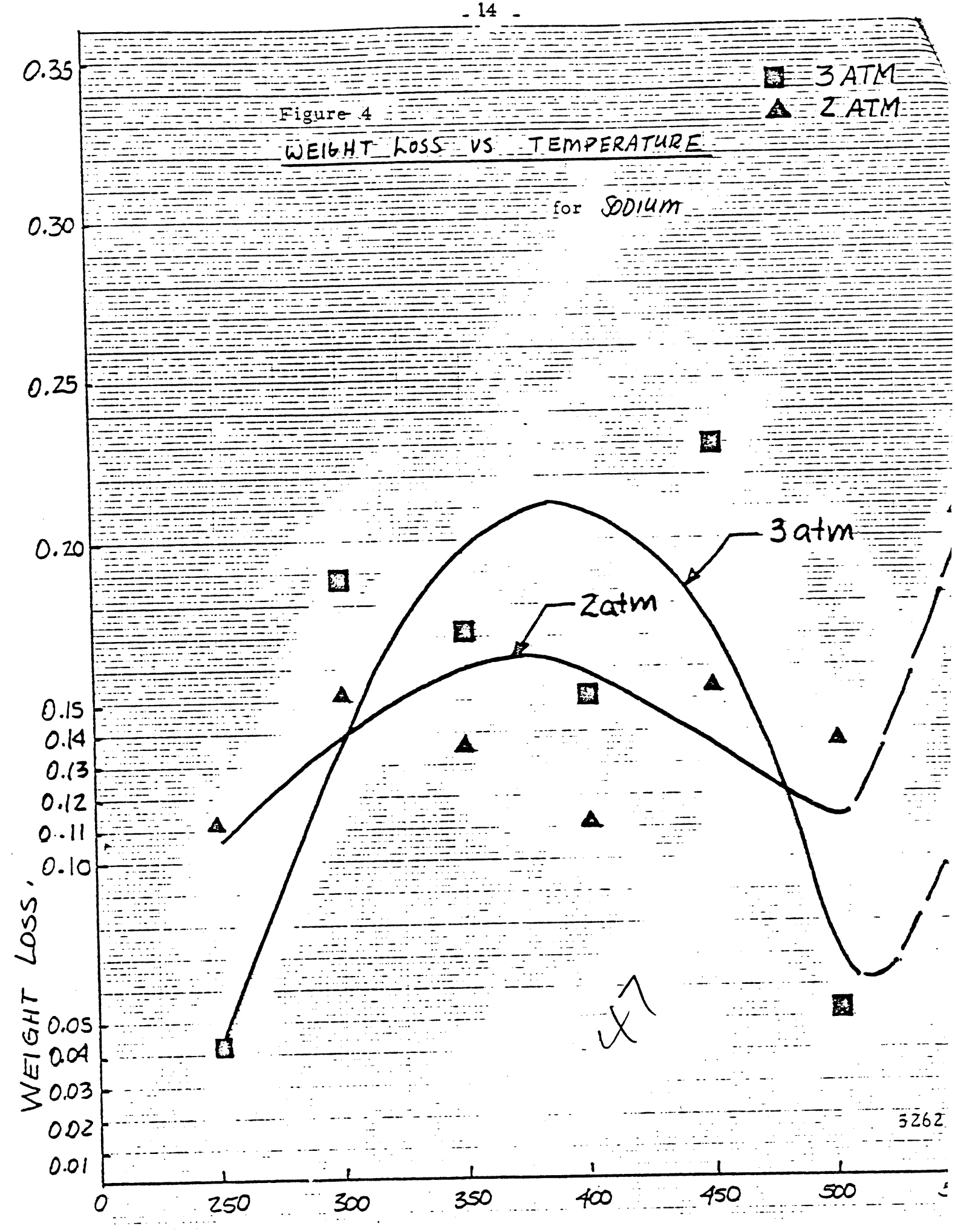

Hammett Barber, et al

014456-2-I

Fig. 5 - Ultimate Resilience (UR) x Volume Loss Rate (VLR) vs. Test Temperature.

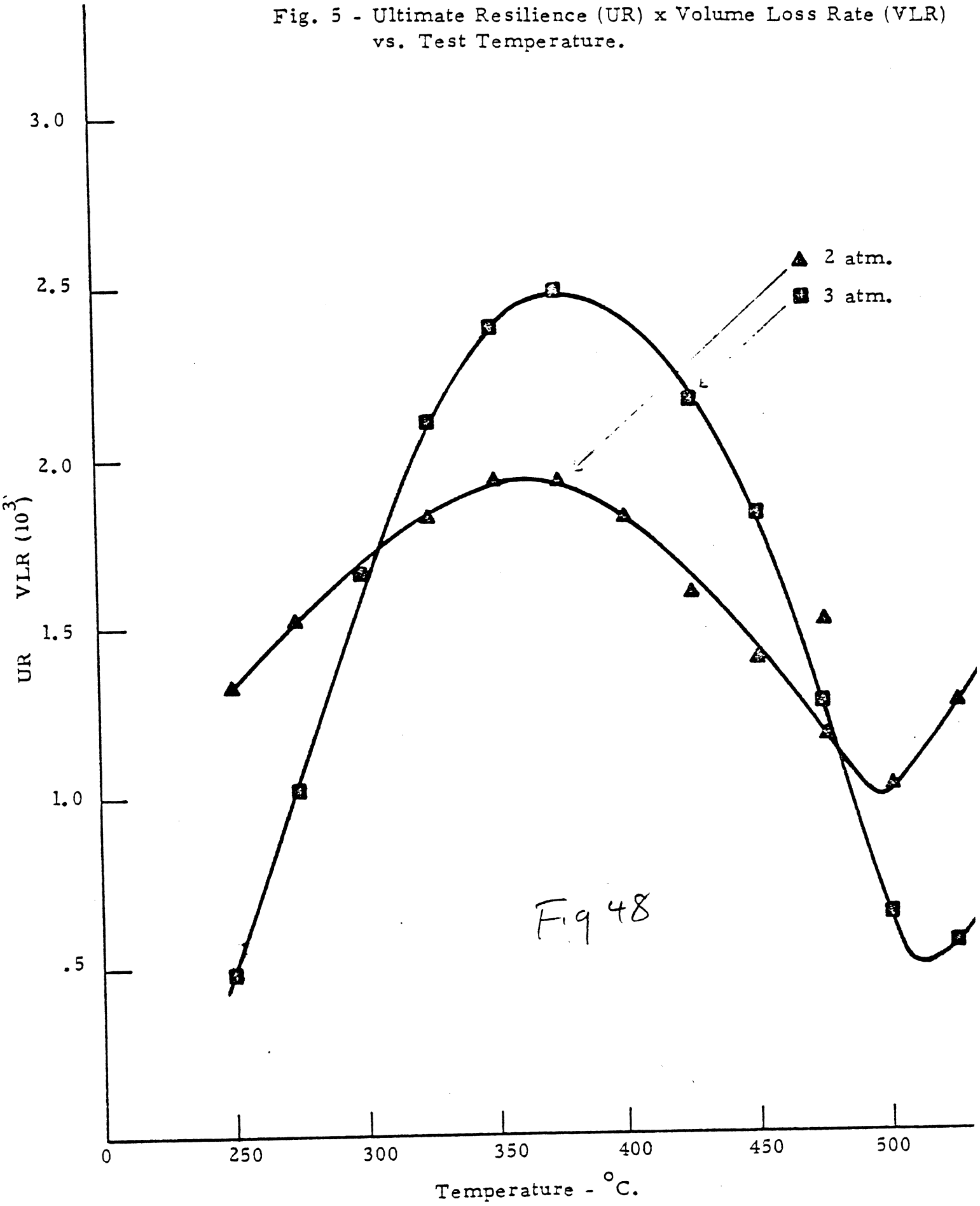

Fig 48

Hammett, Barber, etal
014456-2-I